LBL-1547 c.1

PROPERTIES OF THE $B^+(1235)$ MESON PRODUCED IN π^+p INTERACTIONS AT 7.1 GeV/c

Ronald Laurence Ott
(Ph. D. Thesis)

September 15, 1972

For Reference

Not to be taken from this room

Prepared for the U.S. Atomic Energy Commission
under Contract W-7405-ENG-48

DISCLAIMER

This document was prepared as an account of work sponsored by the United States Government. While this document is believed to contain correct information, neither the United States Government nor any agency thereof, nor the Regents of the University of California, nor any of their employees, makes any warranty, express or implied, or assumes any legal responsibility for the accuracy, completeness, or usefulness of any information, apparatus, product, or process disclosed, or represents that its use would not infringe privately owned rights. Reference herein to any specific commercial product, process, or service by its trade name, trademark, manufacturer, or otherwise, does not necessarily constitute or imply its endorsement, recommendation, or favoring by the United States Government or any agency thereof, or the Regents of the University of California. The views and opinions of authors expressed herein do not necessarily state or reflect those of the United States Government or any agency thereof or the Regents of the University of California.

TABLE OF CONTENTS

Abstract v
I. Introduction 1
II. Experimental Method 4
A. Primary and Secondary Beam Structure 4
B. Secondary Beam Configuration 4
C. Pathlength 7
III. Experimental Analysis 8
A. Scanning 8
B. Measurement 9
C. Computer Analysis 9
D. Detection Efficiencies 11
1. Scanning Efficiency 11
2. Measurement Efficiency 13
IV. The Reaction $\pi^+ p \rightarrow \pi^+\pi^+ p\pi^-\pi^0$ 15
A. Investigation of the $\omega(784)$ Dalitz Plot Anomaly . 16
B. Investigation of a Possible $\omega(784)\pi$ Kinematic Enhancement 18
C. $\pi^+ p \rightarrow \Delta^{++}(1236)\pi^+\pi^-\pi^0$ Production Channel Effects 19
D. Sample of Events for Analysis 22
V. Determination of the Properties of the $B^+(1235)$ Meson 23
A. Spin-Parity Analysis 23
B. Isospin, G-Parity, and Charge Conjugation Eigenvalue 30
C. Mass, Width, and D/S Ratio 30
1. Basic Hypothesis 33
2. Results 35
D. Production Cross Section 41
E. Branching Ratios 45
VI. Discussion 47

Acknowledgements 50
Appendix A 51
Appendix B 56
Appendix C 59
Appendix D 61
Footnotes and References 64

PROPERTIES OF THE $B^+(1235)$ MESON PRODUCED IN π^+ p INTERACTIONS AT 7.1 GEV/C

Ronald Laurence Ott

Lawrence Berkeley Laboratory
University of California
Berkeley, California

15 September 1972

ABSTRACT

The mass, width, D/S ratio, production cross section and branching ratios of the $B^+(1235)$ meson are determined from the reaction $\pi^+ p \rightarrow B^+(1235) p$ at 7.1 GeV/c. Chung and Berman-Jacob analyses of the $\omega\pi$ decay angular distributions show that the spin-parity of the B(1235) is $J^P = 1^+$ or 2^+, 3^-, ... The mass, width, and D/S ratio, determined from an analysis of the mass and decay angular distributions assuming that the spin-parity of the B(1235) is $J^P = 1^+$, are found to be $E_R = 1.252 \pm 0.006$ GeV, $\Gamma^R = 0.156^{+0.021}_{-0.018}$ GeV, and $\Gamma^R_2/\Gamma^R_0 = 0.00^{+0.06}_{-0.00}$ which indicates that the decay is entirely S-wave. The B(1235) production cross section is found to be 42^{+4}_{-7} μb at this momentum and upper limits for the branching ratios for the decay of the B(1235) into other possible channels relative to $\omega\pi$ were determined to be $\pi\pi/\omega\pi < 0.15$, $\eta\pi/\omega\pi < 0.15$, $K\bar{K}/\omega\pi < 0.08$, and $\phi\pi/\omega\pi < 0.025$ with 90% confidence level.

I. INTRODUCTION

In 1937 Yukawa proposed that the fundamental interaction between nucleons is the exchange of a virtual quantum whose mass could be related to the range of the interaction. It is this distance and the strength of the interaction which have prevented the development of a quantitative theory of strong interactions. Attempts to understand the interactions between hadrons have been in two directions: (1) the comprehension of the dynamics of these interactions, and (2) the discovery of symmetry relations among the particles. Knowledge of the properties and quantum numbers of the known elementary particles is germane and, in fact, crucial to the development of any comprehensive theory of high energy physics.

In this thesis we attempt to determine the properties and quantum numbers of the B(1235) meson produced in the reaction $\pi^+ p \rightarrow B^+(1235)\, p$ at an incident pion momentum of 7.1 GeV/c. At this momentum the data differ from those of other experiments primarily in (a) the absence of anomalies and interference effects found in $\pi^\pm p$ interactions at 3 to 4 GeV/c, (b) a larger B(1235) signal to $\omega\pi$ background ratio, and-or (c) a greater number of B(1235) events above background because of larger statistics.

The analysis is limited to a determination of the inherent properties of the B(1235) and does not attempt to resolve the question of its production mechanism in this reaction. These properties include its mass, width, and spin-parity assignment. If the spin-parity of the B(1235) is $J^P = 1^+$ the two-particle $\omega\pi$ decay mode

can have relative orbital angular momentum $\ell_J = 0$ or 2 (S-wave or D-wave), each of which can be considered a separate decay channel with partial widths Γ_0^R and Γ_2^R at resonance. The quotient Γ_2^R/Γ_0^R is referred to as the D/S ratio.

The B(1235) meson has been studied previously in $\pi^\pm p$, $p\bar{p}$, KD, and γp interactions with results for its mass and width which differ by several standard deviations and with uncertainty remaining in its spin-parity assignment. Its only confirmed decay mode is $B(1235) \rightarrow \omega(784)\pi$ and upper limits have been determined for several other possible decay channels such as $\pi\pi$, $K\bar{K}$, $\eta\pi$, and $\phi\pi$.[1] The $\pi^\pm p \rightarrow B^\pm(1235)\, p$ productions cross section does not decrease rapidly with energy, and at this momentum the cross section is in the range 20 to 50 μb.[2]

Values obtained for the mass of the B(1235) vary from 1.200 to 1.260 GeV with weighted average $E_R = 1.233 \pm 0.007$ GeV, while values for its width range from 0.078 to 0.203 GeV with weighted average $\Gamma^R = 0.104 \pm 0.009$ GeV.[1] There is an apparent discrepancy between the width of the B(1235) found from an analysis of $\pi^\pm p$ interactions and that determined from $p\bar{p}$ annihilations at rest.[3,4] This is probably the result of uncertainty in the very large $\omega\pi$ background in the reaction $p\bar{p} \rightarrow \omega\pi^+\pi^-$ which is also complicated by crossing ω bands.

Several attempts have been made to determine the intrinsic spin-parity of the B(1235).[3,5,6,7] Ascoli <u>et al</u> find either $J^P = 1^+$ or $J^P = 2^+, 3^-, \ldots$ where the oberved polarization of the B(1235) indicates that $J^P = 1^+$ is more probable.[5] From an analysis of the

production Dalitz plot Bizzari et al find that $J^P = 1^+$ and $J^P = 1^-$ are equally probable while other spin-parity assignements give unsatisfactory results.[3] The results of Carmony et al support the $J^P = 1^-$ assignment although statistical limitations and background do not allow the elimination of other possibilities.[6] Werbrouck et al find that $J^P = 1^+$ is the most satisfactory spin-parity assignment with $J^P = 2^+, 3^-, \ldots$ improbable.[7] In addition, it was determined that the ratio of the magnitude of the D-wave amplitude to the magnitude of the S-wave amplitude is 0.4 ± 0.2 and that the relative phase between these amplitudes is less than 45°.

In Section II we describe the bunched structure of the primary electron beam and the secondary beam optics configuration. Section III is a discussion of the data reduction and experimental detection efficiencies. In Section IV we discuss the reaction $\pi^+ p \rightarrow \pi^+\pi^+ p\pi^-\pi^0$ for $M(4\pi) < 1.750$ GeV including the ω Dalitz plot anomaly, a possible $\omega\pi$ kinematic enhancement at $M(\omega\pi) \simeq 1.2$ GeV, and production channel interference effects from the reaction $\pi^+ p \rightarrow \Delta^{++}(1236)\pi^+\pi^-\pi^0$. The B(1235) spin-parity analysis, mass, width, and D/S ratio determination, production cross section, and branching ratios are presented in Section V. In Section VI we discuss and summarize our results.

II. EXPERIMENTAL METHOD

Events used in the analysis of the B(1235) meson were produced in the Stanford Linear Accelerator Center 82 inch hydrogen bubble chamber which was exposed to an RF separated π^+ beam of momentum 7.1 GeV/c.

A. PRIMARY AND SECONDARY BEAM STRUCTURE

The Stanford linear accelerator is a disk-loaded waveguide operating at a frequency of 2856 MHz. Consequently the emerging electron beam is structured in time. Electrons are emitted from the accelerator in approximately 2 μsecond bursts, each containing many pulses separated by the RF period and roughly 1/36 of the RF period in width (Fig. 1). At the electron target secondary particles are produced with this same structure in time but, of course, they are not monochromatic and secondaries of the same momentum will separate in space-time because of mass differences. Pulses of equal mass secondary particles will broaden due to momentum differences, and if the momentum bite is too large RF separation of pions and kaons will be less effective and proton contamination will increase. The bunched structure of the secondary beam allows one to use a single RF separator instead of two which would be necessary with a continuous, high energy beam.

B. SECONDARY BEAM CONFIGURATION

A diagram of the secondary beam configuration from the electron target to the hydrogen bubble chamber is shown in Fig. 2.[8] B60 is a vertical bending magnet which levels the 18 GeV primary electron

beam and steers the electrons in the vertical plane. Q60,61 is a quadrupole doublet which focuses the electron beam onto the target while B61 is a horizontal bending magnet which steers the electrons in the horizontal plane. The electron target consists of a beryllium rod approximately one radiation length long (0.25" x 0.25" x 12.0") suspended by thin wires from an insulated cage. A ZnS screen used for monitoring the position of the electron beam is placed between the target and the beam dump, a water-cooled cylinder. The secondary beam optics are designed to accept secondary particles produced at about 1° from the primary electron beam direction where the pion flux is at a maximum. The secondary beam optics can be divided into three main parts: (a) momentum analysis, (b) RF separation, and (c) beam dispersion for position-momentum correlation in the chamber.[9]

Quadrupole doublet Q1,2 (horizontal magnification $\simeq$ 1/2 and vertical magnification $\simeq$ 2) focuses the target source onto a three-foot Fe collimator F1 with a vertical opening of 1/2" and a horizontal opening of 5/8". Dipole D1 (horizontal bend of 1.3°) provides dispersion at F1 so that collimation in the horizontal plane allows a momentum bite of $\Delta p/p \simeq 5\%$ while collimation in the vertical plane at F1 narrows the vertical image at F2. Q3,4 is a quadrupole doublet which focuses the beam at F1 onto collimator F2. It is adjusted so that the magnifications in both planes from the target to F2 is approximately one. D2 is a dipole (horizontal bend of 3°) which removes from the beam the dispersion introduced for momentum selection at D1. A Pb vertical collimator C4 is positioned so that the beam does not hit the irises of the RF separator and a small bending

magnet D2.1 steers the beam in the vertical direction so that it will hit the bubble chamber which is higher in elevation than the electron target.

The distance from the electron target to the RF separator is chosen such that the difference in time at which the pions and kaons arrive at the separator is one-half the RF period. This allows maximum separation of pions and kaons while protons, which have spread across the RF cycle because of the momentum bite at F1, will be rejected at F2 during three-fourths of the RF cycle. Only one RF separator is needed because of the bunched structure of the SLAC beam in comparison with the use of two separators with continuous, high energy beams. The separator, a 12 foot long, disk-loaded waveguide which operates at the same frequency at the electron accelerator, can be phased to deflect kaons upward ($\simeq$ 2 mr.) and pions downward ($\simeq$ 2 mr.). The kaons are stopped at F2, a three-foot Fe collimator with a vertical opening of 5/8" and a horizontal opening of 1/2", while the pions and approximately one-fourth of the protons go through. A proton telescope consisting of scintillators S1, S2, and a nitrogen Cerenkov counter C (at 240 PSIA) is placed behind collimator F2 to detect protons.

Two bending magnets D3 and D4 (horizontal bend of 4° each) provide dispersion in the bubble chamber for position-momentum correlation. Q5,6 is a quadrupole doublet which parallels the beam before D1 and Q7,8 is a second quadrupole doublet which focuses the beam onto the chamber and adjusts the magnification from F2 to the bubble chamber to be about 1.5 in both planes. BC is the 82 inch

hydrogen bubble chamber which was pulsed at 2 pps. The primary electron beam intensity was adjusted so that there were 10 to 15 beam tracks in the chamber for each beam burst.

Kaon contamination of the beam is negligible while proton contamination is less than 1% and muon contamination from pions decaying in flight has been estimated to be less than a few percent.

C. PATHLENGTH

The pathlength, which is a measure of the total flux of π^+ particles which went through the chamber, has been determined using two different methods.[10] Using the total number of beam tracks, the fiducial length, and corrections for bad film frames and beam scatters at the entrance to the chamber, the pathlength was determined to be $\lambda = 44.8 \pm 0.7$ events/μb. An independent calculation using the known total cross section and a determination of the total number of interactions with corrections for detection inefficiencies gave $\lambda = 42.8 \pm 1.0$ events/μb which we shall use in the determination of cross sections. The discrepancy is the result of muon contamination of the beam which was not accounted for in the first calculation and which would tend to increase the pathlength.

III. EXPERIMENTAL ANALYSIS

A. SCANNING

The $B^+(1235)$ meson, produced in the reaction

$$\pi^+ p \rightarrow B^+(1235)\, p \qquad (1)$$

decays through strong interactions into $\omega\pi$ which is the only confirmed decay mode:

$$B^+(1235) \rightarrow \omega(784)\pi^+ \qquad (2)$$

However, there may be several other decay channels including

$$B^+(1235) \rightarrow \eta(548)\pi^+ \qquad (3)$$

$$B^+(1235) \rightarrow \phi(1019)\pi^+ \qquad (4)$$

$$B^+(1235) \rightarrow \pi^+\pi^0 \qquad (5)$$

and

$$B^+(1235) \rightarrow K^+ \bar{K}^0 \qquad (6)$$

Reactions (2,3,4) may appear in the chamber as four-prongs while reaction (5) may appear as a two-prong. Reaction (6) may be seen as a vee two-prong since the $\bar{K}^0$ is required to decay visibly in the chamber. More than 700 000 pictures were taken of an exposure of the SLAC 82 inch hydrogen bubble chamber to the RF separated π^+ beam.

Scanners were required to record events for all topologies within a well-defined fiducial volume except those which occurred on bad film frames and those which could be associated with an incident track which was non-beam.[11] In addition, scanners were required to recognize events with one or more positive tracks which were heavily ionizing in all three views and which did not decay. These events are called HEAVY while all others are called

LIGHT. In this way most of the events with momentum transfer squared to the proton less than 1 $(GeV/c)^2$ could be identified without measurement and fitting. The number of events of each topology which were found is approximately:

TWO-PRONG	437 700 EVENTS
FOUR-PRONG	445 900 EVENTS
VEE TWO-PRONG	29 000 EVENTS

All of the film was scanned once and a fraction depending upon topology was rescanned and conflicted.[12] Although several topologies have been scanned more than twice, the sample of events used in this analysis was derived from those events found in the first and second scans.

B. MEASUREMENT

All events were measured at least once on a Spiral Reader. Four-prong and vee two-prong events which failed to fit any kinematic hypothesis of the first measurement were remeasured on a Spiral Reader or on a Franckenstein. In order to maximize the number of vee two-prongs some of the twice-failing events of this topology were measured a third time. Only a small sample of the two-prong events, including both passing and failing events on the first measurement, was remeasured to determine the measurement efficiency and measurement ambiguities for this topology.

C. COMPUTER ANALYSIS

Measurements were analyzed using the Alvarez Group standard programs which use the measuring machine output to geometrically reconstruct the tracks in three dimensions and perform a chi-square

fit to several reaction hypotheses according to the event topology using conservation of energy and three-momentum. In addition to the three-dimensional track reconstruction information from ionization density[13], range-momentum relations for stopping particles, momentum-position and angle-position correlation in the chamber (beam averaging) is used.[9]

Four-prong events are fitted to reaction hypotheses which include

$$\pi^+ p \rightarrow \pi^+\pi^+ p\pi^-\pi^0 \qquad (7)$$

and

$$\pi^+ p \rightarrow \pi^+\pi^+\pi^+\pi^- n \qquad (8)$$

Vee two-prong events are fitted to reaction hypothese which comprise

$$\pi^+ p \rightarrow K^+ p \bar{K}^0 \qquad (9)$$

while two-prong events are fitted to reaction hypotheses which include

$$\pi^+ p \rightarrow \pi^+ p\pi^0 \qquad (10)$$

and

$$\pi^+ p \rightarrow \pi^+\pi^+ n \qquad (11)$$

The kinematic confidence level of a constrained fit is required to be greater than 10^{-5}.[14]

Events from reaction (7) were selected from the sample of passing four-prongs; a fraction $f = 20 \pm 1\%$ of this topology had been second-scanned and conflicted, and events which failed on the first measurement were remeasured. Events which fit the reaction $\pi^+ p \rightarrow \pi^+\pi^+ p\pi^-\pi^0$ were selected for analysis if (a) there were no four-constraint fits with kinematic confidence level greater than 10^{-5}, (b) the kinematic confidence level of the fit to reaction (7) was greater than 10^{-3}, (c) the chi-square calculated from ionization

density information for this hypothesis was less than five plus the minimum ionization density chi-square for all hypotheses of this event, (d) the sum of the kinematic and ionization density chi-squares was a minimum for all constrained fits, and (e) the corresponding zero-constraint missing mass calculation satisfied $-0.10 \leq (\text{Missing Mass})^2 \leq 0.15\ \text{GeV}^2$.[15]

Reaction (9) is a seven-constraint hypothesis while reactions (7,8,10,11) have only one kinematic constraint.

D. DETECTION EFFICIENCIES

To determine the number of events in each decay channel of the B(1235) one must correct the apparent number of events for detection inefficiencies and selection cuts. We found that the detection efficiencies for four-prong events with small momentum transfer squared to the proton, where resonance production is most likely to occur, are the same as those for all HEAVY four-prong events.

1. SCANNING EFFICIENCY

The sample of events used for analysis was obtained from events found in the first and second scans of the film. The scanning efficiency was computed for the entire sample using events from a fraction f of the film which had been scanned twice and conflict scanned.[12] The efficiency for each scan was determined from this fraction of the film using the Geiger-Werner method, which assumes that the probebility of an event being found is the same for all events of a given topology and that the scans are independent.[16] The efficiency E_1 of the first scan is given by

$$E_1 = N_A/(N_A + N_C + N_D) \tag{1}$$

and the efficiency E_2 of the second scan is given by

$$E_2 = N_A/(N_A + N_B + N_D) \tag{2}$$

where N_X is the number of events given efficiency X by the conflict scanner. These assigned efficiencies are defined as

(A) The event was found correctly on both scans.

(B) The event was found correctly on the first scan but not found or incorrectly identified on the second scan.

(C) The event was found correctly on the second scan but not found or incorrectly identified on the first scan.

(D) The event was not found or incorrectly identified on both scans.

The scanning efficiency for the entire sample is, therefore, given by

$$E_S = E_1 + f(1 - E_1)E_2 \tag{3}$$

where f is the fraction of the film which was second-scanned. Although the scans are not independent this method is useful when the scanning efficiencies are high. Only passing events were used to determine the scanning efficiency since many of the failing events were incorrectly identified by the scanner and did not belong to the sample. A small correction has been made to the number of events N_C which were found on the second scan and not

found or incorrectly identified on the first scan; some of these events which failed on the first measurement have not been remeasured while other failing events have been measured twice. The correction was based on the second measurement passing rate for events of the same topology. Table (1) shows the scanning efficiencies and statistical errors for each topology.

2. MEASUREMENT EFFICIENCY

The measurement efficiency E_M of the sample is defined by

$$E_M = \frac{\text{NUMBER OF PASSING EVENTS}}{\text{NUMBER OF MEASURABLE EVENTS}} \qquad (4)$$

where the number of measurable events is the number of recorded events minus the number of unmeasurable events. An unmeasurable event is one which has either been misidentified by the scanner or else identified correctly according to the scanning instructions but (usually) the result of an incident non-beam track. The number of unmeasurable events was determined by looking at twice-failing events of each topology on a scanning table. It was found that $3\pm1\%$ of the recorded two-prongs, $5\pm1\%$ of the recorded four-prongs, and $8\pm1\%$ of the recorded vee two-prongs are unmeasurable events. These unmeasurable events, which are not part of the experimental sample, are also excluded in the pathlength determination.

Events which are assigned a vee two-prong primary event type by the scanner may degenerate into a two-prong secondary event type if the vee is found to be unassociated with the vertex, for example. However, not all of the two-prong events which have been given

incorrectly a vee two-prong event type will degenerate into a two-prong event type; some of these two-prongs will still pass as vee two-prongs. Since it is not known how many of the vee two-prongs are actually two-prongs one cannot correct the measurement efficiency for this contamination, but one can try to estimate it. One can compute the measurement efficiency of the total vee two-prong sample which includes for vee two-prongs and two-prongs. This will be a good estimate of the actual vee two-prong measurement efficiency if the difference between the vee two-prong and the two-prong measurement efficiency is not large, and the sign of the bias of this estimate can be determined by noting whether the actual two-prong measurement efficiency is larger or smaller than this estimate. Table (2) gives the measurement efficiencies and statistical errors for each topology according to measurement number.

IV. THE REACTION $\pi^+ p \rightarrow \pi^+\pi^+ p\pi^-\pi^0$

The decay of the $B^+(1235)$, produced in the reaction $\pi^+ p \rightarrow \pi^+\pi^+ p\pi^-\pi^0$, may be affected by final state interactions. Indeed, reaction (7) for events with $M(4\pi) \leqslant 1.750$ GeV is characterized by the production of $\Delta^{++}(1236)$ and several meson resonances. An enhancement can be seen in the region of the $\rho(765)$ in the $(\pi^+\pi^-)$, $(\pi^+\pi^0)$, and $(\pi^-\pi^0)$ mass distributions above a large $\pi\pi$ background (Figs. 3a,b,c). The $\eta(548)$ and $\omega(784)$ are clearly observed in the $(\pi^+\pi^-\pi^0)$ mass distribution (Fig. 4a) for $M(3\pi)^0 \leqslant 1.0$ GeV; at the peak of the ω the signal to noise ratio is approximately 8.5 to one. There are 227 events with both pion triplets in the ω mass region $0.765 \leqslant M(\pi^+\pi^-\pi^0) \leqslant 0.805$ GeV where more than 5200 events have at least one pion triplet in the ω mass region. In the analysis, events with both pion triplets in the ω mass region are given weight one-half and counted as separate events. The (4π) mass distribution (Fig. 5a) shows an enhancement in the region of the B(1235) above a large 4π background, and an improvement in the signal to noise ratio can be obtained by choosing events with at least one $(3\pi)^0$ triplet in the ω mass region as shown in Fig. (5b). A background complication is introduced by $\Delta^{++}(1236)$ production; Fig. (6a), which shows the $(\pi^+ p)$ mass distribution, indicates that $\pi^+ p \rightarrow \Delta^{++}(1236)\pi^+\pi^-\pi^0$ is a strong production channel for reaction (7) at 7.1 GeV/c. If one selects events with at least one $(\pi^+_a\pi^-\pi^0)$ triplet in the ω mass region, approximately 28% of these events have a $(\pi^+_b p)$ mass less than 1.4 GeV (Fig. 6b); the

total number of events has decreased because of the $(3\pi)^0$ mass cut, but the Δ^{++} signal to noise ratio has increased. A Dalitz plot of $M^2(\pi^+_b p)$ versus $M^2(\omega\pi^+_b)$ is shown in Fig. (9). Further improvement in the B(1235) signal is possible by removing events with at least one $(\pi^+ p)$ combination in the Δ^{++} mass region $M(\pi^+ p) = 1.236 \pm 0.120$ GeV, as shown in Fig. (5c); the removal of Δ^{++} reduces the background above the B(1235) considerably. In Section C we will discuss the effects of $\Delta^{++}(1236)$ production. The $(\pi^0 p)$ and $(\pi^- p)$ mass distributions (Figs. 6c,d) indicate that $\Delta^+(1236)$ and $\Delta^0(1236)$ production are negligible in this reaction. Fig. (5d) shows the $(\omega\pi^+)$ mass distribution for events with both pion triplets in the ω mass region which peaks at low $(\omega\pi^+)$ mass.

A. INVESTIGATION OF THE $\omega(784)$ DALITZ PLOT ANOMALY

An anomaly concerning B(1235) production and the ω Dalitz plot was reported by Goldhaber et al in an analysis of the reactions $\pi^\pm p \rightarrow \pi^\pm\pi^+ p\pi^-\pi^0$ at 3.65 and 3.7 GeV/c.[17] The $\omega(784)$ decay matrix element squared is proportional to the parameter[18]

$$\lambda = \left| \frac{\bar{P}_+ \times \bar{P}_-}{Q^2 + 2QM} \right|^2 \qquad (5)$$

where $\bar{P}_+$ and $\bar{P}_-$ are the three-momenta of the π^+ and π^- respectively and Q is the total kinetic energy of the three pions in their center of mass, and M is the sum of the rest masses of the three pions. A contour λ = a constant can be defined which divides the $J^P = 1^-$ decay Dalitz plot into an inner and an outer region which contain equal numbers of events from the decay. If there is an isotropic

phase space background from unassociated $(3\pi)^0$ the contribution of these events is divided in proportion to the area in each region. Approximately 29% of the total area is contained in the inner region while the remainder is in the outer region. The normalized Dalitz plot is shown in Fig. (7a) for events with Δ^{++} removed. The Dalitz plot variables X and Y are defined by

$$X = (T_+ - T_-)/\sqrt{3}\,Q \qquad (6a)$$

and

$$Y = T_0/Q \qquad (6b)$$

where T_+, T_-, and T_0 are the kinetic energies of the π^+, π^-, and π^0 respectively in their center of mass. The inner and outer regions are shown separately in Figs. (7b,c) for $\lambda = 0.006$, and the resulting $(\pi^+\pi^-\pi^0)$ mass distributions are shown in Fig. (4b) for the inner region ($\lambda \geqslant 0.006$) and in Fig. (4c) for the outer region ($\lambda \leqslant 0.006$). The ω enhancements are about the same for both regions while there is a considerable difference in $(3\pi)^0$ backgrounds. Since the Dalitz plot for the η decay peaks at low pion kinetic energies, the η signal is large in the outer region (Fig. 4c) and small in the inner region (Fig. 4b) $(3\pi)^0$ mass distribution.

Goldhaber et al found that when one selected pion triplets in the ω mass region the resulting $(4\pi)^{\pm}$ mass distributions showed a B(1235) enhancement for pion triplets from the outer $(3\pi)^0$ Dalitz plot region while the distributions for events from the inner region, which has a better ω signal to noise ratio, did not show

a significant peak in the region of the B(1235). The $(\omega\pi^+)$ mass distribution, with Δ^{++} removed, for the inner and outer $(3\pi)^0$ Dalitz plot regions (Figs. 8a,b) do not give any evidence for this effect at 7.1 GeV/c; strong B(1235) signals are clearly seen for both regions. There are 926 (871) events with $M(\omega\pi^+) \leqslant 1.4$ GeV for $\lambda \geqslant 0.006$ ($\lambda \leqslant 0.006$).

B. INVESTIGATION OF A POSSIBLE $\omega(784)\pi$ KINEMATIC ENHANCEMENT

A second effect was reported by Chung et al, in an analysis of the reaction $\pi^- p \rightarrow \pi^+ p \pi^- \pi^0$ at 3.2 and 4.2 GeV/c, who found that the B(1235) was consistent with the hypothesis of a kinematic enhancement.[19] Evidence for this hypothesis was (a) the B(1235) enhancement was strongly correlated with nucleon isobar production, and (b) angular distributions were consistent with a ρ-exchange model by Deck, Maor, and O'Halloran which resulted in a broad enhancement in the region $M(\omega\pi^-) \simeq 1.2$ GeV.

Peaking of the proton-proton scattering angle in the N^* rest frame in the forward direction was shown by Chung et al to be consistent with ρ-exchange production of $N^*(1520)$ and $N^*(1680)$ resonances. In addition, the B(1235) enhancement was shown to be associated with the production of $N^*(1520)$ and $N^*(1680)$ and peaking of the proton-proton scattering angle. Therefore, if ρ-exchange was responsible for N^* production, the B(1235) could be the result of a broad kinematical enhancement which was a consequence of the peripheral N^* production mechanism. We find that neither of these observations is consistent with data from reaction (7) at 7.1 GeV/c.

A Dalitz plot of $M^2(\pi^+_b p)$ against $M^2(\omega\pi^+_b)$ shows (Fig. 9) that

in this reaction B(1235) production occurs independently of any baryon resonance in contrast with the striking interference effect found at lower energy in $\pi^{\pm}$ p interactions. Although there is some simultaneous production of both B(1235) and $\Delta^{++}(1236)$, the crossing Dalitz plot bands constitute only a few percent of the B(1235) region. The distribution of momentum transfer squared from the target to the outgoing proton for events with at least one pion triplet in the ω mass region, with Δ^{++} removed, is shown in Figs. 10a,b,c) for the Lower ($M(\omega\pi^{+}) \leqslant 1.085$ GeV), Central ($1.085 \leqslant M(\omega\pi^{+}) \leqslant 1.385$ GeV), and Upper ($1.385 \leqslant M(\omega\pi^{+}) \leqslant 1.535$ GeV) ($\omega\pi^{+}$) mass regions. If one assumes that the differential cross section is given by the usual e^{At} peripheral matrix element squared, one finds that the slope

$$A = -\frac{1}{N}\frac{dN}{dt}$$

is in the range $A = 3$ to 5 $(\mathrm{GeV}/c)^{-2}$ for both the B(1235) signal and the $\omega\pi$ background.[20]

C. π^{+} p $\rightarrow \Delta^{++}(1236)\pi^{+}\pi^{-}\pi^{0}$ PRODUCTION CHANNEL EFFECTS

The decay of the B(1235) meson is a two-step process in which the decay of the B(1235) into $\omega\pi$ is followed by the decay of the ω into $\pi^{+}\pi^{-}\pi^{0}$. Let Θ and ϕ be the polar and azimuthal angles of the ω momentum direction in the Jackson rest frame of the B(1235) and let β and α be the polar and azimuthal angles of the normal to the ω decay plane in the ω helicity rest frame as shown in Fig. (11) (See also Appendix A). It will be shown that $\Delta^{++}(1236)$ production does not appreciably distort the $\cos\beta$ and α distributions used to determine the mass, width, and D/S ratio of the B(1235) and that a simple (π^{+} p) mass cut will remove the Δ^{++} in a known manner.

The distribution of $\cos\Theta$, ϕ, $\cos\beta$, and α for the Lower, Central, and Upper ($\omega\pi^{+}$) mass regions is shown in Figs. (12a,b,c) through (15a,b,c). The production of Δ^{++} can distort these angular distributions, especially if there are interference effects between the $\Delta^{++}(1236)\pi^{+}\pi^{-}\pi^{0}$ and $B^{+}(1235)$ p production channels of reaction (7). Since Δ^{++} production is significant in this reaction one must determine to what extent this production affects the B(1235) decay angular distributions and correct for this distortion in the analysis. Figs. (12d,e,f) through (15d,e,f) show these same angular distributions for events which, in addition, have Δ^{++} removed.

The distribution of $\cos\Theta$ for events with at least one pion triplet in the ω mass region is shown in Figs. (16a,b) for $M(\pi^{+}_{b}\,p) \lesssim 1.4$ GeV, where π^{+}_{b} is the pion which is not in the ω and which will be referred to as the bachelor pion. The distribution indicates that Δ^{++} is produced with nearly all of the π^{+}_{b} going backward in the $\omega\pi^{+}_{b}$ center of mass. This is not unuaual kinematically since the polar axis is along the incident π^{+} beam direction and the target proton momentum is highly peaked in the backward direction because the B(1235) is produced with relatively low kinetic energy. Therefore, the outgoing proton, which is peripheral in this reaction, and the bachelor pion both are moving backward in this reference frame, a condition which does not contradict the low (π^{+}_{b} p) mass enhancement at the $\Delta^{++}(1236)$.

We can use this property of the $\cos\theta$ distribution to determine the effect of Δ^{++} production on the $\cos\beta$ and α angular distributions. Instead of making a selection cut on the $(\pi^+ p)$ mass to remove Δ^{++}, one could select events with $\cos\theta < 0$; although this reduces the B(1235) signal more than does a $(\pi^+ p)$ mass cut, it has the distinct advantage that one can readily calculate the distribution of $\cos\beta$ and α for $B^+(1235)$ p events with little $\Delta^{++}(1236)\pi^+\pi^-\pi^0$ ambiguity. Integrating the decay angular distribution (See Appendix A) over the backward hemisphere and renormalizing one finds that

$$I'(\hat{n}) = 2\int_{-1}^{0}\int_{0}^{2\pi} W(\beta,\alpha;\theta,\phi)\,\sin\theta\,d\theta\,d\phi \qquad (7)$$

$$= I(\hat{n})$$

The distribution of $\cos\beta$ and α for events with $\cos\theta < 0$ is the same as that for events with no selection on $\cos\theta$, and one has avoided distortion of the $\cos\beta$ and α angular distributions as a result of Δ^{++} production which occurs almost entirely for $\cos\theta > 0$ at this momentum. The distribution of $\cos\beta$ for events with $\cos\theta < 0$ (Figs. 17a,b,c) indicates that Δ^{++} production does not appreciably distort the $\cos\beta$ distribution (Figs. 14a,b,c) and that a $(\pi^+ p)$ mass cut to remove Δ^{++} does not introduce substantial systematic errors (Figs. 14d,e,f).

Production of $\Delta^{++}(1236)$ does affect the $\cos\theta$ distribution which is used in the spin-parity analysis. However, there is evidence that Δ^{++} production does not interfere with B(1235) production, and only

a small amount of background is found under the $\Delta^{++}(1236)$. Consequently, we assume that a $(\pi^+ p)$ mass cut to remove Δ^{++} does not appreciably affect the B(1235) decay angular distributions.

In conclusion, we find no anomalies or interference effects associated with the B(1235) which have been reported at lower energies or in other interactions.

D. SAMPLE OF EVENTS FOR ANALYSIS OF THE B(1235)

The intrinsic spin-parity, mass, width, and D/S ratio of the B(1235) were determined using events from reaction (7) with at least one pion triplet in the ω mass region and with $\Delta^{++}(1236)$ removed.[21] The result of this selection was a sample of events with an excellent B(1235) signal to $\omega\pi$ background ratio which is imperative in the spin-parity analysis and desireable in the mass and width determination. Fig. (5c) shows the $(\omega\pi^+)$ mass distribution and Figs. (23a,b,c,d) show the m = 0 moments of the $I(\beta,\alpha)$ angular distribution for these events.

V. DETERMINATION OF THE PROPERTIES OF THE $B^+(1235)$ MESON

The following properties of the $B^+(1235)$ meson were determined from an analysis of the decay $B^+(1235) \rightarrow \omega(784)\pi^+$ using a sample of events from reaction (7):

(a) Intrinsic spin-parity

(b) Isospin, G-parity, and charge conjugation eigenvalue C_n of the $B^0(1235)$

(c) Mass and width

(d) Production cross section in the reaction $\pi^+ p \rightarrow B^+(1235)\, p$ at 7.1 GeV/c

We also attempt to determine upper limits for the branching ratios of several other possible decay channels, including $\pi\pi$, $\eta\pi$, $K\bar{K}$, and $\phi\pi$ relative to the $\omega\pi$ decay mode.

A. SPIN-PARITY ANALYSIS

The Chung spin-parity analysis for boson resonances which decay into a spin-1 and a spin-0 particle is described in Appendix B, and the Berman-Jacob spin-parity analysis of two-step decay processes is described in Appendix C. The parameter

$$R_M^2 = \sqrt{3/8}\ \frac{\varepsilon\, J(J+1)}{J(J+1) - 3} \qquad (8)$$

where ε is the relative ω-B parity is plotted in Fig. (21) for J^P normal (dashed curve) and J^P abnormal (solid curve). If the spin-parity of the resonance is known, the sign of R_M^2 indicates whether $J(J+1)$ is larger or smaller than three. A chi-square can be calculated for

various hypotheses of spin-parity (See Appendix D) which can be used to determine how well each J^P assignment describes the data if one spin-parity is dominant.

Although the Chung and Berman-Jacob analyses are expressed in different notation it can be shown that these analyses, in fact, give the same information if $L_{max} = 2$ and have the same spin-parity ambiguities. In the Chung analysis (with L = 2) if $J^P = 1^+$ (1^-) is a solution of Eqn. (B-5) then $J^P = 2^+$ (2^-) is also a solution, while in the Berman-Jacob analysis $R_M^2 = -1.22$ (+1.22) for $J^P = 1^+$ (1^-) <u>and</u> 2^+ (2^-). Therefore, one must determine the spin-parity of the decaying resonance independently of Eqns. (B-5) and (C-7).

We found that we could not determine a spin-parity series for the B(1235) using Eqns. (B-3,4) which relate several $G(\ell m; LM)$ functions. Instead, polarization information from the ω decay might be used to resolve this problem. In terms of the helicity amplitudes g_λ (See Appendix A) the distribution of $\cos\beta$ is given by

$$I(\beta) = 3/2\left[|g_0|^2\cos^2\beta + |g_1|^2\sin^2\beta\right] \qquad (9)$$

If the ω is longitudinally polarized ($g_0 \neq 0$) then $J^P \neq 1^-, 2^+, 3^-, \ldots$ since $g_0 = 0$ for this series, while the absence of longitudinal polarization implies only that $J^P \neq 0^-$ since g_0 could be small for $J^P = 1^+, 2^-, 3^+, \ldots$.

In a Chung analysis one must first determine whether or not the spin J of the resonance is non-zero using the properties of the

$G(\ell m;LM)$ functions. If $J = 0$ then $G(20;00) = -\sqrt{2/3}$ and $G(\ell m;LM)$ vanishes for $L > 0$. Fig. (18a) shows that $G(20;00) \neq -\sqrt{2/3}$ in the region of the B(1235) and, in fact, it is positive. In addition, $G(00;22)$ and $G(20;20)$ are non-zero in this region by two to three standard deviations (Figs. 18b,c). The $G(\ell m;LM)$ are consistent with zero for $\ell = 0$ and 2 (the only possible values) and $L > 2$ so that $G(\ell m;LM) = 0$ for $L > 2J$ if $J = 1$.

The $(\omega\pi^+)$ mass distribution was divided into six 120 MeV intervals from threshold to 1.655 GeV and an analysis was completed of each interval. The distribution of chi-square is shown in Figs. (19a-f) for J^P normal (corresponding to $\eta = -1$) and in Figs. (20a-f) for J^P abnormal (corresponding to $\eta = 1$) as a function of $J(J+1)$ in the Chung analysis (with $L = 2$), and in Figs. (22a-f) as a function of R_M^2 in the Berman-Jacob analysis for each $(\omega\pi^+)$ mass interval.

We divide the discussion into three parts - (a) Region I ($M(\omega\pi^+) \leqslant 1.175$ GeV), the background region below the B(1235), (b) Region II ($1.175 \leqslant M(\omega\pi^+) \leqslant 1.295$ GeV), the B(1235) region, and (c) Region III ($1.295 \leqslant M(\omega\pi^+) \leqslant 1.655$ GeV), the background region above the B(1235). In the analysis we look for minima in the chi-square distributions near integral values of spin J. The spin-parity series was determined from ω-polarization information whenever possible. However, the analysis is not meaningful if one spin-parity is not dominant in each mass interval.

<u>Region I</u>: The chi-square distributions for the region $M(\omega\pi^+) \leqslant 1.175$ GeV as a function of $J(J+1)$ in the Chung analysis are shown in Figs.

(19a,b) and (20a,b). In the interval $M(\omega\pi^+) \leqslant 1.055$ GeV one might expect an abnormal spin-parity state since $\ell_J = 0$ usually dominates at threshold due to the orbital angular momentum potential barrier. There is a minimum in the chi-square distribution for J^P abnormal near $J(J+1) \simeq 1/2$ and a broad minimum for large $J(J+1)$, while a maximum in the chi-square distribution for J^P normal occurs for $J(J+1) \simeq 3$ and a broad minimum for large $J(J+1)$ (Figs. 19a,20a). In the Berman-Jacob analysis a minimum in the chi-square distribution for this interval (Fig. 22a) occurs for $R_M^2 = 0.04^{+0.63}_{-0.50}$, where the errors are defined by the chi-square interval $\chi^2_{min}+1$, which allows solutions for $J \leqslant 1$ and for large J in both spin-parity series (Fig. 21). However, in this interval $G(20;00) \neq -\sqrt{2/3}$ which shows that spin $J = 0$ is not a solution.

If the ω is not longitudinally polarized ($g_0 = 0$) then

$$I(\beta) = 3/2 \sin^2\beta \tag{10a}$$

and

$$\langle Y_2^0(\beta,\alpha)\rangle = \int I(\beta)\, Y_2^0(\beta,\alpha)\, d\cos\beta = -1/\sqrt{20\pi} \tag{10b}$$

The $\langle Y_2^0(\beta,\alpha)\rangle$ moments, which are shown in Fig. (23b) as a function of $(\omega\pi^+)$ mass, differ from this expected value by two to four standard deviations in this region which indicates that the ω is longitudinally polarized and, therefore, the spin-parity is abnormal. Although the minimum chi-square in the Chung analysis for J^P abnormal occurs for $J(J+1) \simeq 1/2$ it has been shown that $J = 0$ is not a solu-

tion and we conclude that $J^P = 1^+$ if there is one dominant spin-parity in this interval.

The chi-square distributions for the interval $1.055 \leqslant M(\omega\pi^+) \leqslant 1.175$ GeV as a function of J(J+1) in the Chung analysis are shown in Figs. (19b,20b). There is a minimum in the chi-square distribution for J^P abnormal near J(J+1) = 2, while there is a maximum in the chi-square distribution for J^P normal for J(J+1) ≃ 2 and a broad maximum for large J(J+1). The minimum chi-square in the Berman-Jacob analysis occurs for $R_M^2 = -3.20^{+2.39}_{-\infty}$ (Fig. 22b) which allows $J^P = 1^+$ or 2^+, 3^-, ... if one spin-parity is dominant.

Polarization information for this interval indicates that the ω is longitudinally polarized. However, there is a large resonance contribution to the amplitude in this interval so that polarization information may not be useful if the resonance does not also have abnormal spin-parity.

Region II: The chi-square distributions for the region $1.175 \leqslant M(\omega\pi^+) \leqslant 1.295$ GeV are shown in Figs. (19c,20c) as a function of J(J+1) in the Chung analysis, and in Fig. (22c) as a function of R_M^2 in the Berman-Jacob analysis. Using the properties of the $G(\ell\, m;LM)$ functions we have shown that the spin J of the B(1235) cannot be zero.

In the Chung analysis the minimum chi-square for J^P abnormal (Fig. 20c) is near J(J+1) = 2, while the chi-square distribution for J^P normal (Fig. 19c) has a maximum for J(J+1) ≃ 2 and a broad minimum for large J(J+1). In the Berman-Jacob analysis the chi-square distribution (Fig. 22c) has a minimum for $R_M^2 = -0.69^{+0.13}_{-0.21}$, where

$R_M^2 = 1.22$ for $J^P = 1^+$. Therefore, the Chung and Berman-Jacob analyses allow $J^P = 1^+$ or 2^+, 3^-, ... if there is one dominant spin-parity in this region.

If the spin-parity of the B(1235) were J^P normal then $g_0 = 0$ and the ω cannot be longitudinally polarized, which implies that

$$I(\beta) = 3/2 \sin^2\beta$$

and

$$\langle Y_2^0(\beta,\alpha)\rangle = -1/\sqrt{20\pi}$$

The $\langle Y_2^0(\beta,\alpha)\rangle$ moments (Fig. 23b) differ from this expected result by three to four standard deviations in this region which indicates that the ω is longitudinally polarized. If this polarization were the result of the abnormal spin-parity of the B(1235) alone then we could conclude that $J^P = 1^+$. However, there is enough background in this region to account for this polarization so that $J^P = 2^+$, 3^-, ... cannot be eliminated.

Region III: The chi-square distributions for the region $1.295 \leqslant M(\omega\pi^+) \leqslant 1.655$ GeV are shown in Figs. (19d,e,f) and (20d,e,f) as a function of J(J+1) in the Chung analysis and in Figs. (22d,e,f) as a function of R_M^2 in the Berman-Jacob analysis. In the region above the B(1235) there is an increasing probability of other ℓ_J-waves and also resonances in the R-region. It is not as likely, therefore, that one spin-parity is dominant in each interval and, consequently, polarization information would be less useful.

The chi-square distributions for the intervals $1.295 \leqslant M(\omega\pi^+)$

$\leqslant$ 1.415 GeV and 1.535 $\leqslant M(\omega\pi^+) \leqslant$ 1.655 GeV in the Chung analysis for J^P abnormal (Figs. 19d,f and 20d,f) have minima near J(J+1) = 2, while the chi-square distributions for J^P normal have maxima for J(J+1) $\simeq$ 2 and broad minima for large J(J+1) which is not unlike the chi-square distributions in Regions I and II. In the Berman-Jacob analysis for these intervals there are minima in the chi-square distributions for $R_M^2 < 0$ so that $J^P = 1^+$ or 2^+, 3^-, ... would be allowed if one spin-parity were dominant.

In the interval 1.415 $\leqslant M(\omega\pi^+) \leqslant$ 1.535 GeV, however, there is a minimum in the chi-square distribution in the Chung analysis for J^P normal near J(J+1) = 2, while a maximum appears in the chi-square distribution for J^P abnormal for J(J+1) $\simeq$ 2 and a broad minimum for large J(J+1). This is just the opposite of the general features of the chi-square distributions for all other intervals. In the Berman-Jacob analysis the minimum chi-square occurs for $R_M^2 > 0$ (Fig. 22e) so that $J^P = 1^-$ or 2^-, 3^+, ... would be allowed if one spin-parity were dominant in this interval.

The possible $\omega\pi$ decay mode of the g(1680) can be seen in Fig. (5c) above a large background. Both mass-width (E_R = 1.682 GeV and Γ^R = 0.157 GeV) and spin-parity ($J^P = 3^-$) assignments of the g(1680) were determined from an analysis of the $\pi\pi$ decay mode[25], while results from a study of other decay modes, such as $\omega\pi$, indicate there may be more than one resonant state in this region because of the discrepancies of branching ratios, masses, and widths.[26]. Because of the large amount of background under the g(1680) it is not possible to measure its spin-parity directly without some

improvement in the signal to noise ratio.

B. ISOSPIN, G-PARITY, AND CHARGE CONJUGATION EIGENVALUE

The B(1235) decays into $\omega\pi$ and, therefore, it must have isospin and G-parity $I^G = 1^+$.

The charge conjugation operator C changes a particle state into its antiparticle. Therefore, particles which are eigenstates of the charge conjugation operator must have baryon number B = 0, charge Q = 0, and hypercharge Y = 0. The charge conjugation eigenvalue of such a neutral system is given by

$$C = (-1)^I G \tag{11}$$

Thus the charge conjugation eigenvalue of the $B^0(1235)$, which decays into $\omega\pi^0$, is $C_n = -1$ since I = 1 and G = +1.

C. MASS, WIDTH, AND D/S RATIO

The mass, width, and D/S ratio were determined by fitting the amplitudes for the two-step B(1235) decay simultaneously to the mass and angular distributions assuming that its intrinsic spin-parity is $J^P = 1^+$. Explicit dependence on the production mechanism is eliminated by integrating the angular distribution (Eqn. A-9) over angles θ, ϕ, and α and using the trace normalization of the density matrix $\rho_{M,M'}$ to obtain

$$I(\beta) = 3/2\, |f_0|^2 \sum_\lambda |g_\lambda|^2 \left[d^{(1)}_{\lambda,0}(\beta)\right]^2$$

which is independent of $\rho_{M,M'}$. The helicity amplitudes g_λ can be

expressed in terms of partial wave amplitudes a_ℓ using the relation

$$g_\lambda = \frac{\sum_\ell (2\ell + 1)^{\frac{1}{2}} a_\ell \, (\ell \; 0 \; 1 \; \lambda | J \; \lambda)}{\left[(2J + 1)\left(\sum |a_\ell|^2\right)\right]^{\frac{1}{2}}} \qquad (12)$$

where $(\ell_1 \, m_1 \, \ell_2 \, m_2 | \; J \; M)$ is the usual Clebsch-Gordon coefficient. Assuming that the total angular momentum of the $\omega\pi$ system is $J = 1$ over the mass region of interest, the helicity amplitudes become

$$g_0 = \frac{a_0 - \sqrt{2}\, a_2}{\sqrt{3}\left[|a_0|^2 + |a_1|^2 + |a_2|^2\right]^{\frac{1}{2}}} \qquad (13)$$

and

$$g_{\pm 1} = \frac{a_0 \mp \sqrt{3/2}\, a_1 + \sqrt{1/2}\, a_2}{\sqrt{3}\left[|a_0|^2 + |a_1|^2 + |a_2|^2\right]^{\frac{1}{2}}} \qquad (14)$$

and therefore

$$I(\beta) = \qquad (15)$$

$$\frac{|a_0|^2 + 3/2\,|a_1|^2(1-\cos^2\beta) + 1/2\,|a_2|^2(1+3\cos^2\beta) + \sqrt{2}\,\mathrm{Re}(a_0 a_2^*)(1-3\cos^2\beta)}{2\left[|a_0|^2 + |a_1|^2 + |a_2|^2\right]}$$

The mass distribution is given by

$$\frac{dN}{dM} = |a_0|^2 + |a_1|^2 + |a_2|^2 \qquad (16)$$

where M is the $(\omega\pi^+)$ mass and $|f_0|^2$, which is a coupling constant,

has been set equal to one arbitrarily.

The m = 0 moments of the angular distribution are defined by

$$\langle Y_\ell^0(\beta,\alpha)\rangle = \int I(\beta)\, Y_\ell^0(\beta,\alpha)\, d\cos\beta \qquad (17)$$

Substituting $I(\beta)$ into this expression one finds that

$$\langle Y_\ell^0(\beta,\alpha)\rangle = 0 \text{ for } \ell \neq 0 \text{ or } 2 \qquad (18a)$$

and

$$\langle Y_2^0(\beta,\alpha)\rangle = \frac{-|a_1|^2 + |a_2|^2 - 2\sqrt{2}\,\mathrm{Re}(a_0 a_2^*)}{\sqrt{20\pi}\left[|a_0|^2 + |a_1|^2 + |a_2|^2\right]} \qquad (18b)$$

The m = 0 moments (Eqn. 17) are shown in Figs. (23a-d) for $\ell = 1$, 2, 3, 4 as a function of $(\omega\pi^+)$ mass for events with at least one pion triplet in the ω mass region and with Δ^{++} removed.[21] Within statistical errors the moments are zero for $\ell \neq 0$ or 2 for $M(\omega\pi^+) \leqslant 1.535$ GeV, and since $\langle Y_2^0(\beta,\alpha)\rangle < 0$ in this region there must be P-wave or S-wave - D-wave interference contributing to the amplitude (Eqn. 18b). The distortion of the $\cos\beta$ distribution introduced by the $(\pi^+ p)$ mass cut to remove Δ^{++} can be assessed by calculating the m = 0 for events with $\cos\theta < 0$ instead, as shown in Figs. (24a-d). The moments are very similar, differing by a slight shift of the $\langle Y_2^0(\beta,\alpha)\rangle$ moments toward more positive values in the background regions above and below the B(1235).

To determine the mass, width, and D/S ratio the region $M(\omega\pi^+) \leqslant 1.535$ GeV was divided into intervals and the amplitudes given by Eqns. (15 and 16) were fitted simultaneously to the $(\omega\pi^+)$ mass

distribution (Fig. 5c - 10 MeV intervals) and to $\langle Y_2^0(\beta,\alpha)\rangle$ (Fig. 23b - 50 MeV intervals) for events with at least one pion triplet in the ω mass region and with Δ^{++} removed.[20] Several hypotheses which differed primarily in ℓ_J-wave background were attempted.

1. Basic Hypothesis

The basic hypothesis is that of a $J^P = 1^+$ resonance with mass E_R and total width Γ^R at resonance which decays into both S-wave and D-wave $\omega\pi$ channels with S-, P-, and D-wave background. The D/S ratio is defined by

$$\text{D/S RATIO} = \Gamma_2^R/\Gamma_0^R \tag{19}$$

where Γ_0^R and Γ_2^R are the S-wave and D-wave partial decay widths at resonance and where the total width $\Gamma = \Gamma_0 + \Gamma_2$.

An ℓ_J-wave Breit-Wigner amplitude can be written

$$A_\ell^{BW}(M) = 1/2 \; \frac{\sqrt{\Gamma_p \, \Gamma(M)}}{E_R - M - i\,\Gamma(M)/2} \tag{20}$$

where Γ_p is the total width for resonance production (assumed to be S-wave), $\Gamma(M)$ is the partial width for decay into the ℓ_J-wave channel, E_R is the resonance mass, and $\Gamma(M)$ is its total width. The ℓ_J-wave partial width, which depends on the orbital angular momentum potential and phase space, is given by

$$\Gamma_\ell(M) = \frac{\left[\dfrac{q^2}{q^2 + x^2}\right]^\ell \dfrac{q}{M}}{\left[\left[\dfrac{q^2}{q^2 + x^2}\right]^\ell \dfrac{q}{M}\right]_R} \Gamma_\ell^R \tag{21}$$

where q is the $\omega\pi$ center of mass momentum

$$q^2 = \frac{\left[M^2 - (M_\omega + M_\pi)^2\right]\left[(M^2 - (M_\omega - M_\pi)^2\right]}{4M^2}$$

R denotes the value of the subscripted (superscripted) quantity at $M = E_R$ and x represents the reciprocal of the radius of interaction which was taken to be $x = 0.100$ GeV/c. The total resonance width is given by $\Gamma(M) = \sum_n \Gamma_n(M)$, where the sum is over all channels and partial waves. With these assumptions the partial wave amplitudes can be written

$$a_0 = 1/2 \; \frac{\sqrt{\Gamma_p \, \Gamma_0(M)}}{E_R - M - i\,\Gamma(M)/2} + B_0 \left[\frac{q\, E_R\, Q}{M\, q_R\, Q_R}\right]^{\frac{1}{2}} \tag{22a}$$

$$a_1 = B_1 \left[\frac{q\, E_R\, Q}{M\, q_R\, Q_R}\right]^{\frac{1}{2}} \tag{22b}$$

and

$$a_2 = 1/2 \; \frac{\sqrt{\Gamma_p \, \Gamma_2(M)}}{E_R - M - i\,\Gamma(M)/2} + B_2 \left[\frac{q\, E_R\, Q}{M\, q_R\, Q_R}\right]^{\frac{1}{2}} \tag{22c}$$

where $B_\ell = |B_\ell| \, e^{i\delta_\ell}$ represents the ℓ_J-wave background amplitude divided by the square root of three-body phase space, and Q is the B-p center of mass momentum

$$Q^2 = \frac{\left[S - (M_p + M)^2\right]\left[S - (M_p - M)^2\right]}{4S}$$

where S is the total center of mass energy squared. A parameter

$0 \leqslant K_\ell \leqslant 1$ multiplying the cross terms is allowed to vary to determine the coherence of the $\ell_J = 0$ and 2 backgrounds with respect to the phase of the resonance when the amplitudes are squared. The background amplitude magnitudes $|B_\ell|$ ($\ell = 0, 1, 2$) are linear functions of the $(\omega\pi^+)$ mass and the phases δ_ℓ ($\ell = 0$ and 2) are constants. There are, therefore, a total of fourteen parameters to be determined: mass, width, D/S ratio, background amplitude magnitudes (6), phases (2), and coherence (2), and production partial width (a normalization constant). This represents a minimum number of unknowns consistent with the physical assumptions.

The mass resolution (Fig. 25) has been shown to accurately represent the uncertainties introduced by multiple scattering and measurement error.[27]

The parameters were determined by finding a minimum value of chi-square given by

$$\chi^2 = \frac{\sum_{i=1}^{60} \left[\left(\frac{\Delta N}{\Delta M}\right)_i^{exp} - \left(\frac{\Delta N}{\Delta M}\right)_i^{th}\right]^2}{\left(\frac{\Delta N}{\Delta M}\right)_i^{exp}} + \frac{\sum_{i=1}^{12} \left[\langle Y_2^0(\beta,\alpha)\rangle_i^{exp} - \langle Y_2^0(\beta,\alpha)\rangle_i^{th}\right]^2}{\sigma^2\left[Y_2^0(\beta,\alpha)\right]} \qquad (23)$$

2. RESULTS

For purposes of reference and comparison with other experiments we fitted the $(\omega\pi^+)$ mass distribution (Fig. 5c) to an S-wave

Breit-Wigner resonance with a non-interfering quadratic background. From a chi-square fit with $\chi^2_{min} = 39.52$ and 53 degrees of freedom, the mass and width were determined to be

$$E_R = 1.243 \pm 0.006 \text{ GeV}$$

and

$$\Gamma^R = 0.134^{+0.023}_{-0.026} \text{ GeV}$$

We found four related solutions to Eqns. (17,18b) using the parameterization given by Eqns. (22a,b,c). The mass E_R depends on the relative resonance-background phase in the S-wave while an ambiguity in the D/S ratio is a consequence of the behavior of Eqn. (18b) as a function of D/S. The width Γ^R was found to be somewhat independent of these uncertainties. We will describe the solutions and argue for the elimination of three of them in the discussion.

<u>Solution I</u>: The mass, width, and D/S ratio were determined to be

$$E_R = 1.235 \pm 0.005 \text{ GeV}$$

$$\Gamma^R = 0.147 \pm 0.021 \text{ GeV}$$

and

$$\Gamma^R_2/\Gamma^R_0 = 0.00^{+0.05}_{-0.00}$$

from a fit with $\chi^2_{min} = 45.95$ and 58 degrees of freedom, which corresponds to a confidence level greater than 80%, where the

errors were found by determining the fourteen-parameter $\chi^2_{min}+1$ surface. Several terms in the amplitude squared are shown in Figs. (26a), the total amplitude squared; (26b), S-wave resonance squared; (26c), P-wave background squared; (26d), D-wave background squared; and (e), S-wave resonance and D-wave background interference. The solution parameters are summarized in Table (4).

The S-wave background was found to vanish in this solution while the P-wave and D-wave backgrounds, which are primarily determined by $\langle Y_2^0(\beta,\alpha)\rangle$, cannot also vanish. The phase of the D-wave background is close to 110° so that the S-wave resonance and D-wave background interference peaks above the mass of the resonance to account for the minimum in the $\langle Y_2^0(\beta,\alpha)\rangle$ distribution (Fig. 23b).

Solution II: From a study of Eqns. (17,18b) and the properties of the first solution it was found that a second solution was possible by interchanging the S-wave and P-wave background amplitudes of the first solution. The D-wave background magnitude, phase, and coherence were not changed while the S-wave background phase was chosen so that the S-wave and D-wave background interference was negative to compensate for the absence of P-wave background in Eqn. (18b). The S-wave coherence was set equal to one since the P-wave background of the first solution was large.

Using these initial condition the mass, width, and D/S ratio were determined to be

$$E_R = 1.252 \pm 0.006 \text{ GeV}$$

$$\Gamma^R = 0.156^{+0.021}_{-0.018} \text{ GeV}$$

and

$$\Gamma^R_2/\Gamma^R_0 = 0.00^{+0.06}_{-0.00}$$

from a fit with $\chi^2_{min} = 42.95$ and 58 degrees of freedom, which corresponds to a confidence level of approximately 90%. Several terms in the amplitude squared are shown in Figs. (27a), the total amplitude squared; (27b), S-wave resonance squared; (27c), S-wave resonance-background interference; (27d), S-wave background squared; (27e), P-wave background squared; (27f), D-wave background squared; (27g), S-wave resonance and D-wave background interference; and (27h), S-wave and D-wave background interference. The solution parameters are summarized in Table (4).

The P-wave background is small but non-vanishing because the S-wave and D-wave background interference cannot be large enough to compensate for the D-wave background squared in Eqn. (18b). In this solution the S-wave resonance-background interference, which contributes to the mass distribution (Eqn. 17), peaks below the mass of the resonance and requires the resonance mass to increase, while the S-wave resonance and D-wave background interference, which contributes only to $\langle Y_2^0(\beta,\alpha)\rangle$, peaks above the mass of the resonance. No up-down ambiguity in the sign of the relative S-wave background - D-wave background phase was allowed by this solution.

Solution III: A third (and fourth) solution follows from the behavior of $\langle Y_2^0(\beta,\alpha)\rangle$ as a function of the D/S ratio. If, for example, there were no background then Eqn. (18b) becomes

$$\langle Y_2^0(\beta,\alpha)\rangle = \frac{|a_2|^2 - 2\sqrt{2}\,\mathrm{Re}(a_0 a_2^*)}{\sqrt{20\pi}\left[|a_0|^2 + |a_2|^2\right]} = 0$$

since D/S = 0 is a solution. In terms of the D/S ratio this can be written

$$\langle Y_2^0\rangle \rightarrow \frac{|D/S| - 2\sqrt{2}\,|D/S|^{\frac{1}{2}}}{\sqrt{20\pi}\left[1 + |D/S|\right]} = 0$$

which also has the solution $|D/S| = 8$. This solution will be modified by the presence of background, but the ambiguity still exists.

The initial conditions for the third solution were obtained by setting the D/S ratio to 8 and interchanging the S-wave and D-wave background phases in the second solution. The mass, width, and D/S ratio were determined to be

$$E_R = 1.256 \text{ GeV}$$

$$\Gamma^R = 0.155 \text{ GeV}$$

and $$\Gamma_2^R/\Gamma_0^R = 200.0$$

from a fit with $\chi^2_{min} = 42.57$ and 58 degrees of freedom. The solution parameters are summarized in Table (4).

Although there is now a large D-wave resonance contribution to $\langle Y_2^0(\beta,\alpha)\rangle$ (Eqn. 16b), this is nearly equalled by a negative contribution from the resonance-background interference. The phases

of the S-wave and D-wave background were interchanged so that the D-wave resonance-background interference in this solution is the same as the S-wave resonance-background interference in Solution II.

Solution IV: The initial conditions for the fourth solution were obtained by setting the D/S ratio to 8 and interchanging the S-wave and D-wave background amplitudes of the first solution. The D-wave background phase was chosen so that the S-wave and D-wave background interference would contribute negatively to $\langle Y_2^0(\beta,\alpha)\rangle$ and equal the contribution from the D-wave resonance amplitude. The mass, width, and D/S ratio were determined to be

$$E_R = 1.255 \text{ GeV}$$

$$\Gamma^R = 0.152 \text{ GeV}$$

and $$\Gamma_2^R/\Gamma_0^R = 23.4$$

from a fit with $\chi^2_{min} = 42.71$ and 58 degrees of freedom. The solution parameters are summarized in Table (4).

In this solution, although the S-wave resonance is small, the S-wave background is quite large and the S-wave resonance-background interference peaks below the resonance mass and requires it to increase. The D-wave background phase is approximately -38° and the D-wave resonance-background interference, while having little effect below the resonance, peaks above the resonance mass to account for

the minimum in the $\langle Y_2^0(\beta,\alpha)\rangle$ distribution.

D. PRODUCTION CROSS SECTION

The production cross section for the reaction $\pi^+ p \rightarrow B^+(1235)\, p$ at 7.1 GeV/c was determined with the assumption that $\omega\pi$ is the only decay mode of the B(1235). The number of observed events from this reaction was found by fitting an S-wave Breit-Wigner, with mass $E_R = 1.243$ GeV and width $\Gamma^R = 0.134$ GeV, and a polynomial background of degree three to the (4π) mass distribution for events with at least one $(3\pi)^0$ pion triplet in the ω mass region and $M(\omega\pi^+) \leqslant 1.750$ GeV.[29]

It was found that 1163^{+118}_{-219} $B^+(1235)$ events are observed in the region $M(\omega\pi^+) \leqslant 1.750$ GeV from a fit with $\chi^2_{min} = 78.65$ and 79 degrees of freedom. This number must be corrected for (a) the mass cut, and (b) experimental detection inefficiencies.

From fitting the $(3\pi)^0$ mass distribution in the region $0.725 \leqslant M(3\pi)^0 \leqslant 0.845$ GeV with a relativistic Breit-Wigner amplitude and quadratic background it was found that $77\pm1\%$ of the ω signal is contained in the interval $0.765 \leqslant M(3\pi)^0 \leqslant 0.805$ GeV. The mass and width of the ω, which were allowed to vary, were determined to be $E_R = 0.7812$ GeV and $\Gamma^R = 0.0123$ GeV.

Three sources of detection inefficiency were considered: (1) scanning, (2) measurement, and (3) final state ambiguities. The scanning efficiency was determined for events with small momentum transfer squared to the proton ($-t_{p,p} < 0.02$ $(GeV/c)^2$) and found to be consistent with that for all four-prong events. The measurement efficiency for these events was examined by comparing the ratio

of the number of events passing on the second measurement to the number of events passing on the first measurement to the same ratio for all four-prong events. Results indicate that there is no significant change in the scanning and measurement efficiencies for events with small momentum transfer squared to the proton from reaction (7).

There may be final state ambiguities which result in a change in the number of events of a given reaction. Estimates of corrections to the number of events of the reaction $\pi^+ p \rightarrow \pi^+\pi^+ p\pi^-\pi^0$ as a result of several possibly ambiguous reaction hypotheses have been determined.

(a) $\pi^+ p \rightarrow \pi^+ p\pi^+\pi^-\pi^0$ (track ambiguity): It was found that pion-proton track ambiguities are negligible. This is primarily the result of the change in ionization density chi-square when the pion and proton tracks are interchanged. Most events are peripherally produced and the proton is slow and easily recognized.

(b) $\pi^+ p \rightarrow \pi^+\pi^+ p\pi^-$ + missing mass: Ambiguities involving this reaction are also negligible when at least one ($\pi^+\pi^-$ missing mass) triplet is required to be in the ω mass region.

(c) $\pi^+ p \rightarrow \pi^+\pi^+\pi^+\pi^- n$: Two methods were used to estimate the correction for ambiguities involving this reaction. In the first method, events from reactions (7) and (8) were generated according to peripheral phase space and fitted using a modified version of the Alvarez Group program SIOUX. It was found that $8\pm8\%$ of the $\pi^+\pi^+ p\pi^-\pi^0$ events and $20\pm13\%$ of the $\pi^+\pi^+\pi^+\pi^- n$ events fit the ambiguous reaction. However, no ionization density information

is used to discriminate between hypotheses, the result of which is a large uncertainty in the ambiguity measurement. At this energy one might expect a change in ionization density of three to five when a proton is assumed to be a pion and conversely in these reactions. This method, therefore, is not very useful.

A second method involves changes in the missing mass distribution when an event is assigned an incorrect reaction hypothesis. For example, the missing mass distribution of events from reaction (7) is not the same as the missing mass distribution of events from reaction (8) which have reaction (7) as a prime hypothesis (lowest sum of kinematic and ionization density chi-squares), and the apparent missing mass distribution is some linear combination of the missing mass distribution for events from reaction (7) and the missing mass distribution of ambiguous events from reaction (8). With the assumption that the actual missing mass distribution is that for events which have reaction (7) as a prime hypothesis and which do not have reaction (8) as a secondary hypothesis, and that the ambiguous distribution is that for events which have reaction (8) as a prime hypothesis but which also have reaction (7) as a secondary hypothesis, it was determined that $4\pm1\%$ of the $\pi^+\pi^+ p\pi^-\pi^0$ events, and, similarly, $9\pm4\%$ of the $\pi^+\pi^+\pi^+\pi^- n$ events are actually events from the ambiguous reaction. The apparent number of events from reaction (7) is 2.6 ± 0.2 times the apparent number of events from reaction (8).

(d) Degenerate vee four-prongs: Events which were assigned a vee four-prong event type by the scanner may degenerate into a four-

prong event type if the vee is found to be unassociated with the vertex. The number of such events which have reaction (7) as a prime hypothesis and which are not included in the sample is equivalent to $1.5\pm0.5\%$ of the apparent number of events from reaction (7).

With corrections to the observed number of B(1235) events for the $(3\pi)^0$ mass cut and for experimental detection inefficiencies the production cross section is given by

$$\sigma^{B(1235)}_{production} = \frac{N_0\, E_A\, E_N}{E_\omega E_S\, E_M\, \lambda}$$

where N_0 is the number of observed events, E_A is the correction for final state ambiguities, E_N is the correction for unseen decay modes of the ω, E_ω is the correction for the $(3\pi)^0$ mass cut, E_S and E_M are the scanning and measurement efficiencies, and λ is the pathlength. This becomes

$$\sigma^{B(1235)}_{production} = \frac{(1163^{+118}_{-219})\ (1.01\pm0.02)\ (1.10\pm0.04)}{(0.77\pm0.01)\ (0.982\pm0.001)\ (0.947\pm0.014)\ (42.8\pm1.0)}\ \mu b$$

$$= 42^{+4}_{-7}\ \mu b$$

where the scanning and measurement efficiencies for HEAVY events has been used.

E. BRANCHING RATIOS

If the spin-parity of the B(1235) is $J^P = 1^+$ it cannot decay into $\pi\pi$, $\eta\pi$, or $K\bar{K}$ channels through strong interactions because parity would not be conserved. In addition, the quark model predicts that the $\phi\pi/\omega\pi$ branching ratio vanishes since $\phi = \lambda\bar{\lambda}$ would result in a disallowed duality diagram. We will show that these branching ratios are consistent with zero and determine an upper limit for each channel with a 90% confidence level.

(a) $B^+(1235) \rightarrow \pi^+\pi^0$: The $(\pi^+\pi^0)$ mass distribution for events from the reaction $\pi^+ p \rightarrow \pi^+ p\pi^0$ (Fig. 28) shows that the $\pi\pi/\omega\pi$ branching ratio is consistent with zero. We would be able to detect 220 events above background, and including a correction for scanning and measurement inefficiencies the branching ratio

$$B \rightarrow \pi\pi/B \rightarrow \omega\pi < 0.15$$

and is consistent with zero.

(b) $B^+(1235) \rightarrow \eta\pi^+$: The $(\eta\pi^+)$ mass distribution from the reaction $\pi^+ p \rightarrow \pi^+\pi^+ p\pi^-\pi^0$, where at least one pion triplet is required to be in the ω mass region $0.525 \leqslant M(3\pi)^0 \leqslant 0.550$ GeV, is shown in Fig. (29) with Δ^{++} removed. There is no evidence for $B \rightarrow \eta\pi$ and we estimate that we could detect 60 events above background. With corrections for neutral decays of the η and scanning and measurement inefficiencies, the branching ratio

$$B \rightarrow \eta\pi/B \rightarrow \omega\pi < 0.15$$

and is consistent with zero.

(c) $B^+(1235) \rightarrow K^+ \bar{K}^0$: The $(K^+ \bar{K}^0)$ mass distribution for events from the reaction $\pi^+ p \rightarrow K^+ p \bar{K}^0$, where the $\bar{K}^0$ is required to decay visibly in the chamber, does not give any evidence for $B \rightarrow K\bar{K}$ (Fig. 30). We estimate that we could detect 40 events above background. With corrections for unseen decays of the $\bar{K}^0$ and scanning and measurement inefficiencies the branching ratio

$$B \rightarrow K\bar{K}/B \rightarrow \omega\pi < 0.08$$

and is consistent with zero.

(d) $B^+(1235) \rightarrow \phi\pi^+$: The $(K^+ K^-\pi^+)$ mass distribution for the reaction $\pi^+ p \rightarrow \pi^+ K^+ p K^-$, where the $(K^+ K^-)$ mass is required to be in the $\phi(1019)$ mass region $0.944 \leqslant M(K^+ K^-) \leqslant 1.044$ GeV, is shown in Fig. (31). There is no evidence for $B \rightarrow \phi\pi$ and we could detect 20 events above background. With corrections for other decay modes of the $\phi(1019)$ and scanning and measurement inefficiencies we find that

$$B \rightarrow \phi\pi/B \rightarrow \omega\pi < 0.025$$

and is consistent with zero.

VI. DISCUSSION

The reaction $\pi^+ p \rightarrow \pi^+\pi^+ p\pi^-\pi^0$ at 7.1 GeV/c provides a satisfactory final state from which to determine the properties of the $B^+(1235)$ meson. There are no Dalitz plot anomalies nor any interference effects with baryon resonances which have been reported in $\pi^\pm p$ interactions at 3 to 4 GeV/c. Final states produced in proton-antiproton interactions have difficulties related to crossing ω bands, background, and poor signal to noise ratios. In this reaction we can determine to some extent the $\Delta^{++}(1236)\pi^+\pi^-\pi^0$ production channel interference effects, which appear to be negligible, since nearly all of the Δ^{++} is produced with the bachelor pion in the backward direction relative to the incident pion beam in the $\omega\pi$ center of mass, and the $\cos\beta$ distribution for events with the bachelor pion in the forward direction is theoretically the same as that for B(1235) events without a selection on the bachelor pion direction. Obviously this relies on the peripherality of the interaction and may not be useful at lower energies, while at higher energies the production cross section is smaller.

A Chung and Berman-Jacob analysis of the $\omega\pi$ angular distributions as a function of $(\omega\pi^+)$ mass shows that (a) the spin-parity of the B(1235) is $J^P = 1^+$ or 2^+, 3^-, ..., and (b) the spin-parity of the $\omega\pi$ background may contain J^P normal components. In a Chung analysis one first determines the spin-parity series of the decaying resonance using properties of the $G(\ell m;LM)$ functions. If the spin

is non-zero then $J(J+1)$ can be calculated directly using the $G(\ell m;LM)$ weighted averages (Eqn. B-5). However, in this experiment we found that the spin-parity series of the B(1235) could not be determined using these properties (Eqns. B-3,4). A determination of the spin-parity series from ω-polarization information was not possible since $\omega\pi$ background could account for longitudinal polarization of the ω if the spin-parity of the B(1235) were J^P normal.

In the determination of the mass, width, and D/S ratio of the B(1235) we found four related solutions to Eqns. (17) and (18b) which describe the $(\omega\pi^+)$ mass distribution and $\langle Y_2^0(\beta,\alpha)\rangle$ moments. Solutions III and IV follow from Solutions I and II and the behavior of Eqn. (18b) as a function of the D/S ratio. We attempted to eliminate these solutions, which have a large D/S ratio, by looking for inconsistencies in the $\cos\theta$ distribution, but without success. A solution with a large D/S ratio contradicts the result of an analysis by Werbrouck et al which indicated that the D/S ratio should be small[7], while an S-wave decay is preferred because of the orbital angular momentum potential barrier, although quantitatively this depends on the radius of interaction. We assume, therefore, that D/S $\simeq$ 0 is the physically correct solution.

Solutions I and II are related by an ambiguity in the S-wave and P-wave backgrounds. In the first solution the S-wave background vanishes while the P-wave background is quite large at threshold and nearly constant over the region of interest. Although this may be possible physically it is not very probable; orbital angular

momentum zero is usually dominant at threshold due to the centrifugal barrier potential and the small amount of kinetic energy available. In the second solution, however, the S-wave background is large near threshold and the P-wave background is small but non-vanishing. This solution is in agreement with ω-polarization information and results of the spin-parity analysis for the interval $M(\omega\pi^+) \leq 1.055$ GeV which indicated that J^P abnormal is dominant in this region.

We have determined improved upper limits for the branching ratios of the $\pi\pi$ and $\eta\pi$ channels relative to $\omega\pi$. The $\pi\pi$, $\eta\pi$, $K\bar{K}$, and $\phi\pi$ mass distributions are consistent with results for the branching ratios of the B(1235) meson determined by previous experiments - no evidence for decay channels other than $\omega\pi$ has been reported. If the spin-parity of the B(1235) is $J^P = 1^+$ it cannot decay into $\pi\pi$, $\eta\pi$, or $K\bar{K}$ if the decay is the result of strong interactions since parity must be conserved. The measured branching fractions of these possible decay modes provide a physical test of the spin-parity determination.

The B(1235) production cross section for the reaction $\pi^+ p \rightarrow \pi^+\pi^+ p\pi^-\pi^0$ at 7.1 GeV/c, determined to be $\sigma = 42^{+4}_{-7}$ μb, is in agreement with other experiments. Fig. (32) shows a compilation of the B(1235) production cross section as a function of incident beam momenta for $\pi^\pm$ p interactions by T. Ferbel.[2]

A summary of the properties and quantum numbers of the B(1235) meson is presented in Table (5).

ACKNOWLEDGEMENTS

I am very grateful to many physicists in the Alvarez Group including Stanley M. Flatté, Margaret Alston-Garnjost, Angela Barbaro-Galtieri, Gerry R. Lynch, Arthur H. Rosenfeld, Ronald R. Ross, and Frank T. Solmitz for their instruction, encouragement, and friendship, not only in reference to this thesis, but throughout my years of graduate study, and to my wife Suzie without whose understanding and support this work would have been much more difficult.

APPENDIX A

DECAY ANGULAR DISTRIBUTION OF THE B(1235)

The decay of the B(1235) meson is a two-step process in which the decay of the B(1235) into $\omega(784)\pi$ is followed by the decay of the ω into $\pi^+\pi^-\pi^0$. Except for a coupling constant, the rate of this two-step process is determined by the production mechanism of the B(1235) and the amplitudes of the first step of this process. The production mechanism, which may involve the exchange of Regge trajectories such as the π or ω, is not well known, and it is not our purpose to resolve this question. However, kinematic information from each step of the decay process allows one to determine several intrinsic properties of the B(1235) meson.[22]

One can write the 2J+1 pure state vectors of the B(1235) as a superposition of the total angular momentum eigenstates $|JM\rangle$ where J is the intrinsic spin of the B(1235) and M is the spin projection along the quantization axis in its rest frame

$$|B(1235),\alpha\rangle = \sum_M c_M^{\alpha}\,|JM\rangle \qquad \text{(A-1)}$$

for $\alpha = 1, 2, \ldots, 2J+1$. Since the dynamical state of the B(1235) is incompletely known, one can determine only the probability P(M) that the B(1235) is produced in a state $|JM\rangle$. It is convenient to describe this statistical mixture of states using the density operator ρ defined by

$$\begin{aligned}\rho &= \sum_{\alpha,\alpha'} |B(1235),\alpha\rangle\langle B(1235),\alpha'| \qquad \text{(A-2)}\\ &= \sum_{\alpha,\alpha'}\sum_{M,M'} c_M^{\alpha}\, c_{M'}^{\alpha'*}\,|JM\rangle\langle JM'|\\ &= \sum_{M,M'} \rho_{M,M'}\,|JM\rangle\langle JM'|\end{aligned}$$

where $\rho_{M,M'}$ is the B(1235) density matrix. The probability P(M) is given by

$$P(M) = \sum_{\alpha} |c_M^{\alpha}|^2 = \rho_{M,M} \qquad \text{(A-3)}$$

In the B(1235) center of mass let $\bar{P}(\theta,\phi)$ be the three-momentum of the ω where θ and ϕ are the polar and azimuthal angles of the ω momentum direction in the Jackson coordinate system in which the Z-axis is along the incident π^+ beam direction, and the Y-axis is along the production normal (Fig. 11). The relationship between a state $|JM\rangle$, which is an eigenstate of total angular momentum, and a state $|P,\theta,\phi,\lambda\rangle$, which describes the two-particle decay system with relative three-momentum $2\bar{P}(\theta,\phi)$ and helicity λ in the rest frame of the decaying particle, is given by the Wigner formula

$$|JM\rangle = \left[\frac{2J+1}{4\pi}\right]^{\frac{1}{2}} \int D^{(J)*}_{M,\lambda}(\phi,\theta,0)\,|P,\theta,\phi,\lambda\rangle \sin\theta\, d\theta\, d\phi \qquad \text{(A-4)}$$

Then the transition matrix element $T^{(1)}_{\lambda,M}$ which describes the decay of the B(1235) in a pure state $|JM\rangle$ into the two-particle state $\omega\pi$ in a pure state $|P,\theta,\phi,\lambda\rangle$ is given by

$$T^{(1)}_{\lambda,M} = \langle \omega(784)\pi; P,\theta,\phi,\lambda | T | B(1235); JM\rangle \qquad \text{(A-5)}$$

$$= \left[\frac{2J+1}{4\pi}\right]^{\frac{1}{2}} g_\lambda \, D^{(J)*}_{M,\lambda}(\phi,\theta,0)$$

where the helicity amplitudes are defined by

$$g_\lambda = \langle \omega(784)\pi; P,\theta,\phi,\lambda | T | B(1235); \text{helicity}=\lambda\rangle \qquad \text{(A-6)}$$

for $\lambda = -1, 0, +1$ where T is the usual transition operator.

In the ω center of mass let $\hat{n}(\beta,\alpha)$ be the normal to the $\pi^+\pi^-\pi^0$ decay plane where β and α are the polar and azimuthal angles of the decay plane normal in the ω-helicity rest frame in which the Z'-axis is along the direction of the ω in the center of mass of the B(1235) and the Y'-axis is along Z x Z' (Fig. 11). In this reference frame the spin projection of the ω along the Z' axis is just its helicity λ, and the transition matrix element $T^{(2)}_{0,\lambda}$ which describes the decay of the ω in a pure state $|j=1\ m=\lambda\rangle$ into the three-particle state $\pi^+\pi^-\pi^0$ in a pure state $|\hat{n}(\beta,\alpha);$ helicity=0$\rangle$ is given by

$$T^{(2)}_{0,\lambda} = \langle \pi^+\pi^-\pi^0; \hat{n}(\beta,\alpha),0 | T | \omega(784); 1\lambda\rangle \qquad \text{(A-7)}$$

$$= \left[\frac{3}{4\pi}\right]^{\frac{1}{2}} f_0 \, D^{(1)*}_{\lambda,0}(\beta,\alpha,0)$$

where the helicity amplitude f_0 is a coupling constant.

The transition matrix element $T_{0,M}$ for the two-step decay of

the B(1235) in a pure state $|JM\rangle$ into $(\pi^+\pi^-\pi^0)\pi^+$ in a pure state with helicity zero is the product of the transition matrices for each step of the process, and, therefore

$$\underset{\sim}{T} = \underset{\sim}{T}^{(2)} \underset{\sim}{T}^{(1)} \qquad \text{(A-8)}$$

or $$T_{0,M} = \left[\frac{3(2J+1)}{16\pi^2}\right]^{\frac{1}{2}} f_0 \sum_\lambda g_\lambda \, D^{(J)*}_{M,\lambda}(\phi,\theta,0)\, D^{(1)*}_{\lambda,0}(\beta,\alpha,0)$$

For systems specified by a density operator ρ the expectation value of any function F(A) of the observables A is the trace of $\rho F(A)$

$$\langle F(A)\rangle = \text{Trace}\ \rho F(A)$$

Then the decay angular distribution of the two-step decay of the B(1235) is given by

$$W(\beta,\alpha;\theta,\phi) = \text{Trace}\ \rho |T|^2 \qquad \text{(A-9)}$$

$$= \left[\frac{3(2J+1)}{16\pi^2}\right] |f_0|^2 \sum_{\lambda,\lambda'} \sum_{M,M'} \rho_{M,M'}\, g_\lambda g^*_{\lambda'}$$

$$\times\ D^{(J)*}_{M,\lambda}(\phi,\theta,0)\, D^{(J)}_{M',\lambda'}(\phi,\theta,0)\, D^{(1)*}_{\lambda,0}(\alpha,\beta,0)\, D^{(1)}_{\lambda',0}(\alpha,\beta,0)$$

The density matrix $\rho_{M,M'}$ depends on the production mechanism of the B(1235). By integrating over the angles θ, ϕ, and α and using the orthogonality properties of the D-functions and the trace

normalization of the density matrix

$$\sum_M \rho_{M,M} = 1$$

one obtains an angular distribution $I(\beta)$ given by

$$I(\beta) = \int W(\beta,\alpha;\theta,\phi)\ \sin\theta\ d\theta\ d\phi\ d\alpha \qquad \text{(A-10)}$$

$$= 3/2\ |f_0|^2 \sum_\lambda |g_\lambda|^2 \left[d^{(1)}_{\lambda,0}(\beta)\right]^2$$

which is independent of $\rho_{M,M'}$ explicitly. If parity is conserved then $|g_1|^2 = |g_{-1}|^2$ and hence

$$I(\beta) = 3/2\left[|g_0|^2 \cos^2\beta + |g_1|^2 \sin^2\beta\right] \qquad \text{(A-11)}$$

where f_0 has been set equal to one.

APPENDIX B

CHUNG SPIN-PARITY ANALYSIS

The spin-parity of a boson resonance which decays into a spin-1 and a spin-0 particle may be determined directly from experimentally measurable averages.[24]

Let θ and ϕ be the polar and azimuthal angles of the spin-1 particle momentum direction in the Jackson rest frame of the decaying spin-J boson resonance, and let β and α be the polar and azimuthal angles of the spin-1 particle decay indicator in the spin-1 particle helicity reference frame. (See Appendix A and Fig. 11)

The measurable averages

$$G(\ell\, m; LM) = \left[\frac{(2\ell+1)(2L+1)}{3}\right]^{\frac{1}{2}} \langle r^m_\ell(\theta,\phi) D^{(L)*}_{M,m}(\theta,\phi,0)\rangle \qquad \text{(B-1)}$$

are used directly to determine the spin-parity of the decaying boson resonance where the r^m_ℓ are multipole expansion parameters of the spin-1 particle density matirx

$$r^m_\ell(\theta,\phi) = -\left[\frac{4\pi}{3}\right]^{\frac{1}{2}} \frac{\langle Y^m_\ell(\beta,\alpha)\rangle_{\theta,\phi\ \text{fixed}}}{(1\ 0\ 1\ 0\ |\ \ell\ 0)} \qquad \text{(B-2)}$$

where the average is taken for fixed θ and ϕ, and $(1\ 0\ 1\ 0\ |\ \ell\ 0)$ is the usual Clebsch-Gordon coefficient.[25] The parameters L and M are related to a multipole expansion of the density matrix of the spin-J resonance in the Jackson rest frame.

To determine the parity, suppose

(a) $J = 0$: All $G(\ell m;LM)$ vanish except $G(00;00) = \sqrt{1/3}$ and $G(20;00) = -\sqrt{2/3}$ since only one orbital angular momentum $\ell_J = 1$ is possible.

(b) $J \geqslant 1$: If the parity is such that $\ell_J = J$ then

$$G(21;LM) = 0 \text{ for L even } (\geqslant 2) \text{ and L odd} \qquad \text{(B-3)}$$

and

$$G(00;LM) = \sqrt{2}\, G(20;LM) \text{ for L even } (\geqslant 2) \qquad \text{(B-4)}$$

However, if the parity is such that $\ell_J = J \pm 1$ one may have $G(21;LM) \simeq 0$ if $\ell_J = J-1$ dominates over $\ell_J = J+1$ so that (B-3) is a strong test only for L even ($\geqslant 2$).

To determine the spin J of the boson resonance directly, one uses the relation

$$J(J+1) = \frac{L(L+1)\, G(22;LM)}{\eta\left[2L(L+1)/3(L-1)(L+2)\right]^{\frac{1}{2}}\left[\sqrt{2}\, G(00;LM) + G(20;LM)\right] + 2\, G(22;LM)} \qquad \text{(B-5)}$$

where L is even ($\geqslant 2$) and $\eta = \pm 1$. If the orbital angular momentum ℓ_J of the two-particle decay system satisfies $\ell_J = J \pm 1$ (J) then $\eta = 1$ (-1). The functions $G(\ell m;LM)$ may be determined from the relations

$$G(00;LM) = \left[\frac{4\pi}{3}\right]^{\frac{1}{2}} \langle Y_L^M(\theta,\phi)\rangle \qquad \text{(B-6)}$$

and

$$G(2m;LM) = -\left[\frac{10\pi(2L+1)}{3}\right]^{\frac{1}{2}} \langle Y_2^m(\beta,\alpha) D_{M,m}^{(L)*}(\phi,\theta,0)\rangle \qquad \text{(B-7)}$$

Eqn. (B-5) is correct for both real and imaginary parts of $G(\ell m;LM)$ separately. To determine the minimum value of J consistent with the data one uses the condition $G(\ell m;LM) = 0$ if $L > 2J$ which is a result of conservation of angular momentum in the multipole parameter expansion. If L_{max} is the largest value of L for which the $G(\ell m;LM)$ are non-vanishing, there are $L_{max}(L_{max}+4)/4$ independent tests of (B-5).

APPENDIX C

BERMAN-JACOB SPIN-PARITY ANALYSIS

Using the results for the angular distribution of the B(1235) two-step decay one can express the density matrix $\rho'_{\lambda,\lambda'}$ of the ω with respect to the ω-helicity reference frame in terms of the helicity amplitudes g_λ and the density matrix $\rho_{M,M'}$ of the B(1235) in the Jackson coordinate system. From quantum mechanics one finds that

$$\underset{\sim}{\rho}' = \underset{\sim}{T}^{(1)} \underset{\sim}{\rho} \underset{\sim}{T}^{(1)} \qquad \text{(C-1)}$$

where $\underset{\sim}{T}^{(1)}$ is the transition matrix for the decay B(1235)$\rightarrow\omega\pi$. This becomes

$$\rho'_{\lambda,\lambda'} = \frac{2J+1}{4\pi} \sum_{M,M'} g_\lambda g^*_{\lambda'} \rho_{M,M'} \qquad \text{(C-2)}$$

$$\times D^{(J)*}_{M,\lambda}(\phi,\theta,0)\, D^{(J)}_{M',\lambda'}(\phi,\theta,0)$$

Using this relation it is possible to show by direct computation that

$$\frac{2\int \rho'_{1,-1}(\theta,\phi)\sin^2\theta\, d\Omega}{\int\left[\rho'_{1,1}(\theta,\phi) + \rho'_{-1,-1}(\theta,\phi)\right](3\cos^2\theta - 1)\, d\Omega} = \frac{(-1)^J\varepsilon\, J(J+1)}{3 - J(J+1)} \qquad \text{(C-3)}$$

where $d\Omega = \sin\theta\, d\theta\, d\phi$ and ε is the relative ω-B parity, and

$$\rho'_{1,-1}(\theta,\phi) = -\frac{3}{4\pi|f_0|^2}\int W(\beta,\alpha;\theta,\phi)\cos 2\alpha\, \sin\beta\, d\beta\, d\alpha \qquad \text{(C-4)}$$

and

$$\rho'_{1,1}(\theta,\phi) + \rho'_{-1,-1}(\theta,\phi) = \qquad \text{(C-5)}$$

$$\frac{3}{\varepsilon\pi|f_0|^2}\int W(\beta,\alpha;\theta,\phi)\,(3 - 5\cos^2\beta)\sin\beta\, d\beta\, d\alpha$$

And, therefore

$$\frac{4\,\langle\sin^2\theta\cos 2\alpha\rangle}{\langle(3\cos^2\theta - 1)(3 - 5\cos^2\beta)\rangle} = \frac{(-1)^J\varepsilon\, J(J+1)}{3 - J(J+1)} \qquad \text{(C-6)}$$

Explicit dependence on $\rho_{N,N'}$ has been eliminated by taking ratios of moments. Eqns. (C-3,4,5) were derived by Berman and Jacob to be used directly in the determination of the spin-parity of a decaying boson resonance.[23] Moreover, it can be shown using Eqn. (A-9) that

$$R^2_M = \frac{\langle \mathrm{Re}\, D^2_{M,-2}(\phi,\theta,\alpha)\rangle + \langle \mathrm{Re}\, D^2_{M,2}(\phi,\theta,\alpha)\rangle}{2\,\langle \mathrm{Re}\, D^2_{M,0}(\phi,\theta,\alpha)\,(5/2\sin^2\beta - 1)\rangle} \qquad \text{(C-7)}$$

$$= \sqrt{3/8}\;\frac{(-1)^J\varepsilon\, J(J+1)}{3 - J(J+1)}$$

for M = 0 and 2. R^2_M is independent of the production mechanism of the B(1235) and depends only on the decay kinematics. Table (3) gives values of R^2_M for several spin-parity assignments.

APPENDIX D

WEIGHTED AVERAGES AND STATISTICAL ERRORS

1. NORMALLY DISTRIBUTED VARIABLES

In computing the sample mean of some function F(A) of the kinematical variables A of the decay, events with one pion in the ω mass region are given weight one and counted once while events with both pion triplets in the ω mass region are given weight one-half and counted as separate events.

$$\langle F(A)\rangle = \sum_{i=1}^{N'} w_i\, F(A_i) \Big/ \sum_{i=1}^{N'} w_i \qquad \text{(D-1)}$$

$$= \frac{1}{N} \sum_{i=1}^{N'} w_i\, F(A_i)$$

where $F(A_i)$ is any function of the kinematical variables A_i of the i'th event, $w_i = 1$ or $1/2$ is the weight function, N is the number of events with at least one pion triplet in the ω mass region, and $N' = N$ + the number of events with both pion triplets in the ω mass region.

The statistical errors are approximated by the expression

$$\sigma^2\left[F(A)\right] = \frac{1}{N^2}\left[\sum_{i=1}^{N'} w_i^{\,2}\right] \qquad \text{(D-2)}$$

$$\times\left[\frac{1}{N}\sum_{i=1}^{N'} w_i\, F^2(A_i) - \left(\frac{1}{N}\sum_{i=1}^{N'} w_i\, F(A_i)\right)^2\right]$$

2. NON-NORMALLY DISTRIBUTED VARIABLES

The variables R_M^2 and $J(J+1)$ given by Eqns. (C-7) and (B-5) are not normally distributed. However, for each hypothesis of such variables one can calculate a chi-square and different hypotheses can be compared using a liklihood ratio or confidence level. Suppose one has n equations of the form

$$R = \langle F_k\rangle / \langle G_k\rangle \qquad \text{(D-3)}$$

for k = 1, 2, ..., n where $\langle F_k\rangle$ and $\langle G_k\rangle$ are expectation values of n functions of the kinematical variables A which are approximated by

$$\langle F_k\rangle = \sum_{i=1}^{N'} w_i\, F_k(A_i) \Big/ \sum_{i=1}^{N'} w_i \qquad \text{(D-4)}$$

$$= \frac{1}{N}\sum_{i=1}^{N'} w_i\, F_k(A_i)$$

and

$$\langle G_k\rangle = \frac{1}{N}\sum_{i=1}^{N'} w_i\, G_k(A_i)$$

where $w_i = 1$ or $1/2$ is the weight function, N is the number of events with at least one pion triplet in the ω mass region, and $N' = N$ + the number of events with both pion triplets in the ω mass region.

The equations to be satisfied by the parameter can be written

$$\langle F_k \rangle - R\langle G_k \rangle = 0 \quad k = 1, 2, \ldots, n \qquad \text{(D-5)}$$

and for each value of R one can calculate a chi-square given in matrix notation by

$$\chi^2(R) = \left[\langle \bar{F}(A)\rangle - R\langle \bar{G}(A)\rangle\right] \underset{\sim}{E}^{-1} \left[\langle \bar{F}(A)\rangle - R\langle \bar{G}(A)\rangle\right] \qquad \text{(D-6)}$$

where $\langle \bar{F}(A)\rangle = (\langle F_1(A)\rangle, \langle F_2(A)\rangle, \ldots, \langle F_n(A)\rangle)$ and $\underset{\sim}{E}(R)$ is an error matrix given by

$$E_{jk}(R) =$$

$$\frac{1}{N^3}\left[\sum_{i=1}^{N'} w_i^2\right]\left[\sum_{i=1}^{N'}\left[F_j(A_i) - RG_j(A_i)\right]\left[F_k(A_i) - RG_k(A_i)\right]^*\right] \qquad \text{(D-7)}$$

For the Chung spin-parity analysis we have (with L = 2 and M = 0, 1, 2)

$$R = J(J+1)$$

$$\langle F_k \rangle = 6\ G(22;2\ k-1)$$

and $\langle G_k \rangle = \eta\left[\sqrt{2}\ G(00;2\ k-1) + G(20;2\ k-1)\right] + 2\ G(22;2\ k-1)$

for k = 1, 2, 3.

For the Berman-Jacob spin-parity analysis we have (with M = 0 and 2)

$$R = \sqrt{3/8}\ \frac{J(J+1)}{J(J+1) - 3}$$

$$\langle F_k \rangle = \langle \mathrm{Re}\ D^{(2)}_{2k-2,-2}(\phi,\theta,\alpha)\rangle + \langle \mathrm{Re}\ D^{(2)}_{2k-2,2}(\theta,\phi,\alpha)\rangle$$

and $\langle G_k \rangle = 2\ \langle \mathrm{Re}\ D^{(2)}_{2k-2,0}(\theta,\phi,\alpha)\ (5/2\sin^2\beta - 1)\rangle$

for k = 1, 2.

FOOTNOTES AND REFERENCES

1. P. Soding, J. Bartels, A. Barbaro-Galtieri, J. E. Enstrom, A. Rittenberg, A. H. Rosenfeld, T. Trippe, N. Barash-Schmidt, C. Bricman, V. Chaloupka, and M. Roos, Review of Particle Properties, Lawrence Berkeley Laboratory Report LBL-100, April 1972.
2. T. Ferbel, in Meson Spectroscopy, W. A. Benjamin, New York and Amsterdam, 1968, p. 372.
3. R. Bizzari, M. Foster, Ph. Gavillet, G. Labrosse, L. Montanet, R. Salmeron, P. Villemoes, C. Ghesquière and E. Lillestøl, Nuc. Phys. B14, 169 (1969).
4. C. Baltay, J. C. Severiens, N. Yeh, D. Zanello, Phys. Rev. Letters 18, 93 (1967).
5. G. Ascoli, H. B. Crawley, D. W. Mortara and A. Shapiro, Phys. Rev. Letters 20, 1411 (1968).
6. D. D. Carmony, R. L. Lander, C. Rindfleisch, N. Xuong, and P. Yager, Phys. Rev. Letters 12, 254 (1964).
7. A. Werbrouck, G. Rinaudo, R. T. Van de Walle, D. J. Schöntanus, C. L. Pols, N. Steif, G. Gidal, and D. Brown, Nuovo Cimento IV, 1267 (1970).
8. S. Flatté, Manual for K82 Beam Watchers, Lawrence Berkeley Laboratory Group A Physics Memo 646, 1968 (unpublished).
9. S. Flatté, Beam Averaging for the SLAC C-K Beam, Lawrence Berkeley Laboratory Group A Physics Memo 664, 1968 (unpublished).
10. S. Protopopescu, M. Alston-Garnjost, and M. Bogdanski, Pathlength for π82, Lawrence Berkeley Laboratory Group A Physics Memo 750, 1972 (unpublished).
11. S. Derenzo, S. Flatté, and M. Rabin, Experiment 32 Scanning Instructions, Lawrence Berkeley Laboratory Group A Physics Memo 680, 1969 (unpublished).
12. A conflict scan is a third scan in which the conflict scanner decides which of the first two scans is correct if there is a discrepancy.

13. J. S. Danburg and G. R. Lynch, BUBBLE - A Program to Utilize the Spiral Reader Measurements of Track Brightness, Lawrence Berkeley Laboratory Group A Programming Note P-160, 1967 (unpublished).

14. M. Alston-Garnjost, Event Types for K82 Experiment 30 and for PI82 Experiment 32, Lawrence Berkeley Laboratory Group A Programming Note P-170, 1970 (unpublished).

15. The corresponding missing mass calculation to reaction (7) is a zero-constraint reaction hypothesis in which the mass of the missing neutral (π^0) is allowed to vary while the particle identification of the visible tracks is unchanged from the one-constraint hypothesis.

16. W. T. Eadie, D. Dryard, F. E. James, M. Roos, and B. Sadoulet, Statistical Methods in Experimental Physics, North-Holland Publishing Company, Amsterdam and London, 1971, p. 11.

17. G. Goldhaber, S. Goldhaber, J. A. Kadyk, and B. C. Shen, Phys. Rev. Letters 15, 118 (1965).

18. This definition of λ is an energy invariant generalization of that used by Goldhaber et al (Reference 17).

19. S. U. Chung, O. I. Dahl, J. Kirz, and D. H. Miller, Phys. Rev. 165, 1491 (1968).

20. The $t'_{p,p}$ distribution for the interval $1.085 \leqslant M(\omega\pi^+) \leqslant 1.385$ GeV (not shown) indicates there is strong forward-peaking for $-t'_{p,p} < 0.04$ $(GeV/c)^2$.

21. The ω mass region is defined to be the interval $0.765 \leqslant M(3\pi)^0 \leqslant 0.805$ GeV, and the Δ^{++} mass region is the interval $M(\pi^+ p) = 1.236 \pm 0.120$ GeV.

22. We will use the same phase convention as Berman and Jacob (Reference 23).

23. S. M. Berman and M. Jacob, Spin and Parity Analysis in Two-Step Decay Processes, Stanford Linear Accelerator Center Report 43, 1965 (unpublished).

24. S. U. Chung, Phys. Rev. 138, B1541 (1968).

25. G. Grayer, B. Hyams, C. Jones, P. Schlein, W. Blum, J. Meissburger, W. Ochs, U. Stierlin, and P. Weilhammer, Phys. Letters 35B, 610 (1971).
J. A. J. Matthews, J. D. Prentice, T. S. Yoon, J. T. Carrol, M. W. Firebaugh, and W. D. Walker, Nuc. Phys. B33, 1 (1971).
For references concerning the determination of the mass and width of the g(1680) see Reference (1).

26. K. W. J. Barnham, D. C. Colley, M. Jobes, I. R. Kenyon, P. Pathak, L. Riddiford, P. M. Watkins, I. Griffiths, I. S. Hughes, J. W. P. McCormick, I. McLaren, C. D. Proctor, R. M. Turnbull, and I. R. White, Phys. Rev. Letters 24, 1083 (1970).

27. M. Alston-Garnjost, A. Barbaro-Galtieri, W. F. Buhl, S. E. Derenzo, L. D. Epperson, S. M. Flatte, J. H. Flatte, J. H. Friedman, G. R. Lynch, R. L. Ott, S. D. Protopopescu, M. S. Rabin, and F. T. Solmitz, Phys. Letters 33B, 607 (1970).

28. S. Derenzo, MINF68 - A General Minimizing Routine, Lawrence Berkeley Laboratory Group A Programming Note P-190, 1969 (unpublished).

29. In the determination of the production cross section the kinematic confidence level requirement is changed to 10^{-5} and there is no selection on missing mass.

30. There is an additional detection efficiency correction of 97.8% for two-prongs because of steep or overlapping tracks.

TABLE 1. SCANNING EFFICIENCIES

TWO-PRONG EVENTS[a]

Efficiency X	HEAVY	LIGHT	Total
N_A	1185	507	1692
N_B	52	30	82
N_C	65	15	80
$N_{C'}$[b]	72	18	90
N_D	7	1	8
E_S^*	93.8±0.7%	96.4±0.8%	94.5±0.6%

* $f = 0.0047 \pm 0.0010$

FOUR-PRONG EVENTS[c]

Efficiency X	HEAVY	LIGHT	Total
N_A	21978	14354	36332
N_B	445	382	827
N_C	471	334	805
$N_{C'}$[b]	478	342	820
N_D	16	13	29
E_S^*	98.2±0.1%	98.1±0.1%	98.2±0.1%

* $f = 0.20 \pm 0.01$

VEE TWO-PRONG EVENTS

Efficiency X	HEAVY	LIGHT	Total
N_A	1913	2087	4000
N_B	339	256	595
N_C	163	123	286
$N_{C'}$[b]	181	137	318
N_D	17	17	34
E_S^*	92.2±0.6%	94.3±0.5%	93.3±0.4%

* $f = 0.20 \pm 0.01$

(a) Scanning efficiency computed from five rolls (See Footnote 30).

(b) Corrected for second measurement of failing events which were not remeasured.

(c) Scanning efficiency computed from 10% of the sample.

TABLE 2. MEASUREMENT EFFICIENCIES

TWO-PRONG EVENTS[a]

Correction for unmeasurable events = 0.97±0.01

HEAVY	First Measurement	Second Measurement
Passing events	1241	1309
Failing events	131	63

Measurement efficiency = 93.3±3.8%

LIGHT	First Mesurement	Second Measurement
Passing events	529	552
Failing events	56	33

Measurement efficiency = 93.2±5.7%

Total	First Measurement	Second Measurement
Passing events	1770	1861
Failing events	187	96

Measurement efficiency = 93.2±3.4%

FOUR-PRONG EVENTS[b]

Correction for unmeasurable events = 0.95±0.01

HEAVY	First Measurement	Second Measurement
Passing events	21467	23106
Failing events	3926	2287

Measurement efficiency = 94.7±1.4%

LIGHT	First Measurement	Second Measurement
Passing events	14073	15206
Failing events	2691	1558

Measurement efficiency = 94.4±1.6%

Total	First Measurement	Second Measurement
Passing events	35540	38312
Failing events	6617	3845

Measurement efficiency = 94.6±1.3%

VEE TWO-PRONG EVENTS

HEAVY	First Measurement	Second Measurement	Third Measurement
Passing events	10143	11421	11489
Failing events	3029	1751	1683

Measurement efficiency = 94.8±1.6%

LIGHT	First Measurement	Second Measurement	Third Measurement
Passing events	11093	12667	12736
Failing events	3531	1957	1888

Measurement efficiency = 94.7±1.6%

Total	First Measurement	Second Measurement	Third Measurement
Passing events	21236	24088	24225
Failing events	6560	3708	3571

Measurement efficiency = 94.7±1.3%

(a) Failing events from only five rolls were remeasured.

(b) Measurement efficiency computed from 10% of the sample.

TABLE 3. R_M^2 FOR SEVERAL J^P ASSIGNMENTS

J^P	$0^{\pm}$	1^+	1^-	2^+	2^-	3^+	3^-	∞^N	∞^A
R_M^2	0	-1.22	1.22	-1.22	1.22	0.82	-0.82	0.61	-0.61

TABLE 4. SUMMARY OF PARAMETERS - DETERMINATION OF THE MASS, WIDTH, AND D/S RATIO OF THE B(1235)

Solution	I	II
E_R	1.235 ± 0.005 GeV	1.252 ± 0.006 GeV
Γ^R	0.147 ± 0.021 GeV	$0.156^{+0.021}_{-0.018}$ GeV
Γ_2^R/Γ_0^R	$0.00^{+0.05}_{-0.00}$	$0.00^{+0.06}_{-0.00}$
$\lvert B_0\rvert^2$	0	30.05 - 16.16M
δ_0	0	0.995
K_0	0	0.882
$\lvert B_1\rvert^2$	27.62 - 12.31M	-4.44 + 4.67M
$\lvert B_2\rvert^2$	-1.45 + 7.05M	-21.87 + 23.88M
δ_2	1.920	1.591
K_2	0.585	0.696
Γ_P	8.33 Q/Q_R	4.62 Q/Q_R
χ^2 (NDF)	45.95 (58)	42.95 (58)

Solution	III	IV
E_R	1.256 GeV	1.255 GeV
Γ^R	0.155 GeV	0.152 GeV
Γ^R_2/Γ^R_0	200.0	23.37
$\lvert B_0\rvert^2$	37.96 - 16.72M	-4.75 + 12.14M
δ_0	1.333	1.295
K_0	1.000	0.735
$\lvert B_1\rvert^2$	-2.23 + 1.88M	15.67 - 4.78M
$\lvert B_2\rvert^2$	-23.03 + 24.02M	1.11 + 0.61M
δ_2	0.322	-0.657
K_2	0.647	0.963
Γ_p	5.99 Q/Q_R	8.59 Q/Q_R
χ^2 (NDF)	42.57 (58)	42.71 (58)

TABLE 5. PROPERTIES OF THE B(1235) MESON

Property or Quantum Number	Determined Value	Evidence or Method of Determination
Mass	$1.252^{+}_{-}0.006$ GeV	Fit to $(\omega\pi^+)$ mass distribution and moments
Width	$0.156^{+0.021}_{-0.018}$ GeV	Fit to $(\omega\pi^+)$ mass distribution and moments
D/S Ratio	$0.00^{+0.06}_{-0.00}$	Fit to $(\omega\pi^+)$ mass distribution and moments
Spin-Parity	$J^P = 1^+$ or $2^+, 3^-, \ldots$	Chung and Berman-Jacob spin-parity analyses
Isospin G-Parity	$I^G = 1^+$	$B(1235) \rightarrow \omega(784)\pi$
Charge Conjugation Eigenvalue	$C_n = -1$	$C_n = (-1)^I G$
Decay Modes	$\omega(784)\pi$	Mass distribution
Branching Ratios	$\pi\pi/\omega\pi < 0.15$ $\eta\pi/\omega\pi < 0.15$ $K\bar{K}/\omega\pi < 0.08$ $\phi\pi/\omega\pi < 0.025$	Mass distributions with corrections for unseen decay modes and detection inefficiencies
Production Cross Section $\pi^+ p \rightarrow B^+(1235)\, p$ at 7.1 GeV/c	$42^{+4}_{-7}\ \mu b$	$\omega\pi$ mass distribution with corrections for $(3\pi)^c$ mass cut and detection inefficiencies

FIGURE CAPTIONS

Fig. 1. Structure of the Stanford Linear Accelerator 18 GeV/c primary electron beam.

Fig. 2. Schematic of the secondary beam optics configuration from the primary electron beam target to the 82" hydrogen bubble chamber.

Fig. 3. Two pion mass distribution for $\pi^+ p \rightarrow \pi^+\pi^+ p\pi^-\pi^0$: (a) $M(\pi^+\pi^-)$ (two combinations), (b) $M(\pi^+\pi^0)$ (two combinations), and (c) $M(\pi^-\pi^0)$.

Fig. 4. $(\pi^+\pi^-\pi^0)$ mass distribution (two combinations) for $\pi^+ p \rightarrow \pi^+\pi^+ p\pi^-\pi^0$: (a) all events, (b) $\lambda \geqslant 0.006$ (inner Dalitz plot region) with Δ^{++} removed, and (c) $\lambda \leqslant 0.006$ (outer Dalitz plot region) with Δ^{++} removed.

Fig. 5. Four pion mass distribution for $\pi^+ p \rightarrow \pi^+\pi^+ p\pi^-\pi^0$: (a) all events, (b) events with at least one pion triplet in the ω mass region, (c) events with at least one pion triplet in the ω mass region and with Δ^{++} removed, and (d) events with both pion triplets in the ω mass region and with Δ^{++} removed.

Fig. 6. (πp) mass distribution for $\pi^+ p \rightarrow \pi^+\pi^+ p\pi^-\pi^0$: (a) $M(\pi^+ p)$ (two combinations), (b) $M(\pi^+_b p)$ where the $(\pi^+_a\pi^-\pi^0)$ mass is in the ω mass region, (c) $M(\pi^- p)$, and (d) $M(\pi^0 p)$.

Fig. 7. Normalized three pion Dalitz plot with $X = (T_+ - T_-)/\sqrt{3}\,Q$ and $Y = T_0/Q$ where T_+, T_-, and T_0 are the kinetic energies of the π^+, π^-, and π^0 in their center of mass and Q is their total kinetic energy for $\pi^+ p \rightarrow \pi^+\pi^+ p\pi^-\pi^0$ with Δ^{++} removed: (a) all events, (b) $\lambda \geqslant 0.006$ (inner Dalitz plot region), and (c) $\lambda \leqslant 0.006$ (outer Dalitz plot region).

Fig. 8. $(\omega\pi^+)$ mass distribution for $\pi^+ p \rightarrow \pi^+\pi^+ p\pi^-\pi^0$ with Δ^{++} removed: (a) $\lambda \geqslant 0.006$ (inner Dalitz plot region), and (b) $\lambda \leqslant 0.006$ (outer Dalitz plot region).

Fig. 9. Dalitz plot of $M^2(\omega\pi^+_a)$ against $M^2(\pi^+_b p)$ for $\pi^+ p \rightarrow \pi^+\pi^+ p\pi^-\pi^0$.

Fig. 10. Distribution of momentum transfer squared to the proton for $\pi^+ p \rightarrow \pi^+\pi^+ p\pi^-\pi^0$ for three $(\omega\pi^+)$ mass regions below, centered on, and above the mass of the B(1235): (a) $M(\omega\pi^+) \leqslant 1.085$ GeV, (b) $1.085 \leqslant M(\omega\pi^+) \leqslant 1.385$ GeV, and (c) $1.385 \leqslant M(\omega\pi^+) \leqslant 1.535$ GeV.

Fig. 11. Definition of the angles used to describe the two-step decay of the B(1235) where the Z-axis is along the incident beam direction, the Y-axis is along the production normal, and θ and ϕ are the polar and azimuthal angles of the ω direction in the B(1235) center of mass (Jackson coordinate system); in the ω rest frame this direction is the Z'-axis, Y' = Z x Z', and β and α are the polar and azimuthal angles of the normal $\hat{n}(\beta,\alpha)$ to the $\pi^+\pi^-\pi^0$ decay plane (ω helicity rest frame).

Fig. 12 - 15. $\cos\theta$, ϕ, $\cos\beta$, and α distributions for $\pi^+ p \rightarrow \pi^+\pi^+ p\pi^-\pi^0$ with at least one pion triplet in the ω mass region for three $(\omega\pi^+)$ mass regions below, centered on, and above the mass of the B(1235): (a) $M(\omega\pi^+) \leqslant 1.085$ GeV, (b) $1.085 \leqslant M(\omega\pi^+) \leqslant 1.385$ GeV, and (c) $1.385 \leqslant M(\omega\pi^+) \leqslant 1.535$ GeV. Subfigures (d,e,f) are the same distributions for events which, in addition, have Δ^{++} removed.

Fig. 16. $\cos\theta$ distribution for $\pi^+ p \rightarrow \pi^+\pi^+ p\pi^-\pi^0$ with $M(\pi^+_a\pi^-\pi^0)$ in the ω mass region and (a) $M(\pi^+_b p) < 1.4$ GeV, and (b) $M(\pi^+_b p) > 1.4$ GeV.

Fig. 17. $\cos\beta$ distribution for $\pi^+ p \rightarrow \pi^+\pi^+ p\pi^-\pi^0$ with at least one pion triplet in the ω mass region and with $\cos\theta < 0$ for three $(\omega\pi^+)$ mass regions below, centered on, and above the mass of the B(1235): (a) $M(\omega\pi^+) < 1.085$ GeV, (b) $1.085 \leqslant M(\omega\pi^+) \leqslant 1.385$ GeV, and (c) $1.385 \leqslant M(\omega\pi^+) \leqslant 1.535$ GeV.

Fig. 18. $G(\ell m;LM)$ weighted averages for $\pi^+ p \rightarrow \pi^+\pi^+ p\pi^-\pi^0$ with at least one pion triplet in the ω mass region and with Δ^{++} removed as a function of $(\omega\pi^+)$ mass: (a) G(20;00), (b) G(00;22), and (c) G(20;20).

Fig. 19. Distribution of chi-square as a function of J(J+1) in the Chung analysis (with L = 2) for J^P normal for six 120 MeV $(\omega\pi^+)$

mass intervals: (a) $M(\omega\pi^+) \leqslant 1.055$ GeV, (b) $1.055 \leqslant M(\omega\pi^+) \leqslant 1.175$ GeV, (c) $1.175 \leqslant M(\omega\pi^+) \leqslant 1.295$ GeV, (d) $1.295 \leqslant M(\omega\pi^+) \leqslant 1.415$ GeV, (e) $1.415 \leqslant M(\omega\pi^+) \leqslant 1.535$ GeV, and (f) $1.535 \leqslant M(\omega\pi^+) \leqslant 1.655$ GeV.

Fig. 20. Distribution of chi-square as a function of $J(J+1)$ in the Chung analysis (with $L = 2$) for J^P abnormal for six 120 MeV $(\omega\pi^+)$ mass intervals: (a) $M(\omega\pi^+) \leqslant 1.055$ GeV, (b) $1.055 \leqslant M(\omega\pi^+) \leqslant 1.175$ GeV, (c) $1.175 \leqslant M(\omega\pi^+) \leqslant 1.295$ GeV, (d) $1.295 \leqslant M(\omega\pi^+) \leqslant 1.415$ GeV, (e) $1.415 \leqslant M(\omega\pi^+) \leqslant 1.535$ GeV, and (f) $1.535 \leqslant M(\omega\pi^+) \leqslant 1.655$ GeV.

Fig. 21. Plot of the parameter

$$R = \sqrt{3/8}\,\frac{\mathcal{E}\,J(J+1)}{J(J-1) - 3}$$

as a function of spin J for J^P normal (dashed curve) and J^P abnormal (solid curve).

Fig. 22. Distribution of chi-square as a function of R_M^2 in the Berman-Jacob spin-parity analysis for six 120 MeV $(\omega\pi^+)$ mass intervals (a) $M(\omega\pi^+) \leqslant 1.055$ GeV, (b) $1.055 \leqslant M(\omega\pi^+) \leqslant 1.175$ GeV, (c) $1.175 \leqslant M(\omega\pi^+) \leqslant 1.295$ GeV, (d) $1.295 \leqslant M(\omega\pi^+) \leqslant 1.415$ GeV, (e) $1.415 \leqslant M(\omega\pi^+) \leqslant 1.535$ GeV, and (f) $1.535 \leqslant M(\omega\pi^+) \leqslant 1.655$ GeV.

Fig. 23. $\langle Y_\ell^0(\beta,\alpha)\rangle$ moments of the decay angular distribution for $\pi^+ p \rightarrow \pi^+\pi^+ p\pi^-\pi^0$ with at least one pion triplet in the ω mass region and with Δ^{++} removed as a function of $(\omega\pi^+)$ mass: (a) $\langle Y_1^0(\beta,\alpha)\rangle$, (b) $\langle Y_2^0(\beta,\alpha)\rangle$, (c) $\langle Y_3^0(\beta,\alpha)\rangle$, and $\langle Y_4^0(\beta,\alpha)\rangle$.

Fig. 24. $\langle Y_\ell^0(\beta,\alpha)\rangle$ moments of the decay angular distribution for the backward hemisphere ($\cos\theta < 0$) for $\pi^+ p \rightarrow \pi^+\pi^+ p\pi^-\pi^0$ with at least one pion triplet in the ω mass region as a function of $(\omega\pi^+)$ mass: (a) $\langle Y_1^0(\beta,\alpha)\rangle$, (b) $\langle Y_2^0(\beta,\alpha)\rangle$, (c) $\langle Y_3^0(\beta,\alpha)\rangle$, and (d) $\langle Y_4^0(\beta,\alpha)\rangle$.

Fig. 25. Four pion mass resolution function for $\pi^+ p \rightarrow \pi^+\pi^+ p\pi^-\pi^0$ with at least one pion triplet in the ω mass region and with Δ^{++} removed.

Fig. 26. Several terms in the amplitude squared for Solution I as a function of $(\omega\pi^+)$ mass: (a) total amplitude squared, (b) S-wave resonance squared, (c) P-wave background squared, (d) D-wave background squared, and (e) S-wave resonance and D-wave background interference.

Fig. 27. Several terms in the amplitude squared for Solution II as a function of $(\omega\pi^+)$ mass: (a) total amplitude squared, (b) S-wave resonance squared, (c) S-wave resonance-background interference, (d) S-wave background squared, (e) P-wave background squared, (f) D-wave background squared, (g) S-wave resonance and D-wave background interference, and (h) S-wave and D-wave background interference.

Fig. 28. Two pion mass distribution for $\pi^+ p \rightarrow \pi^+ p\pi^0$.

Fig. 29. $(\omega\pi^+)$ mass distribution for $\pi^+ p \rightarrow \pi^+\pi^+ p\pi^-\pi^0$ with Δ^{++} removed.

Fig. 30. $(K^+ \bar{K}^0)$ mass distribution for $\pi^+ p \rightarrow K^+ p \bar{K}^0$.

Fig. 31. $(\phi(1019)\pi^+)$ mass distribution for $\pi^+ p \rightarrow K^+\pi^+ p K^-$.

Fig. 32. B(1235) production cross section as a function of incident pion laboratory momentum in $\pi^\pm p$ interactions (Reference 2).

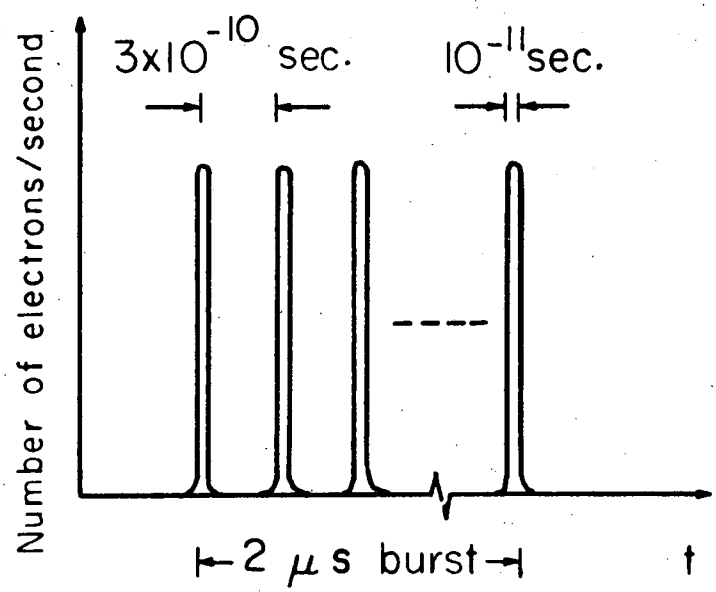

Figure 1

XBL727- 3402

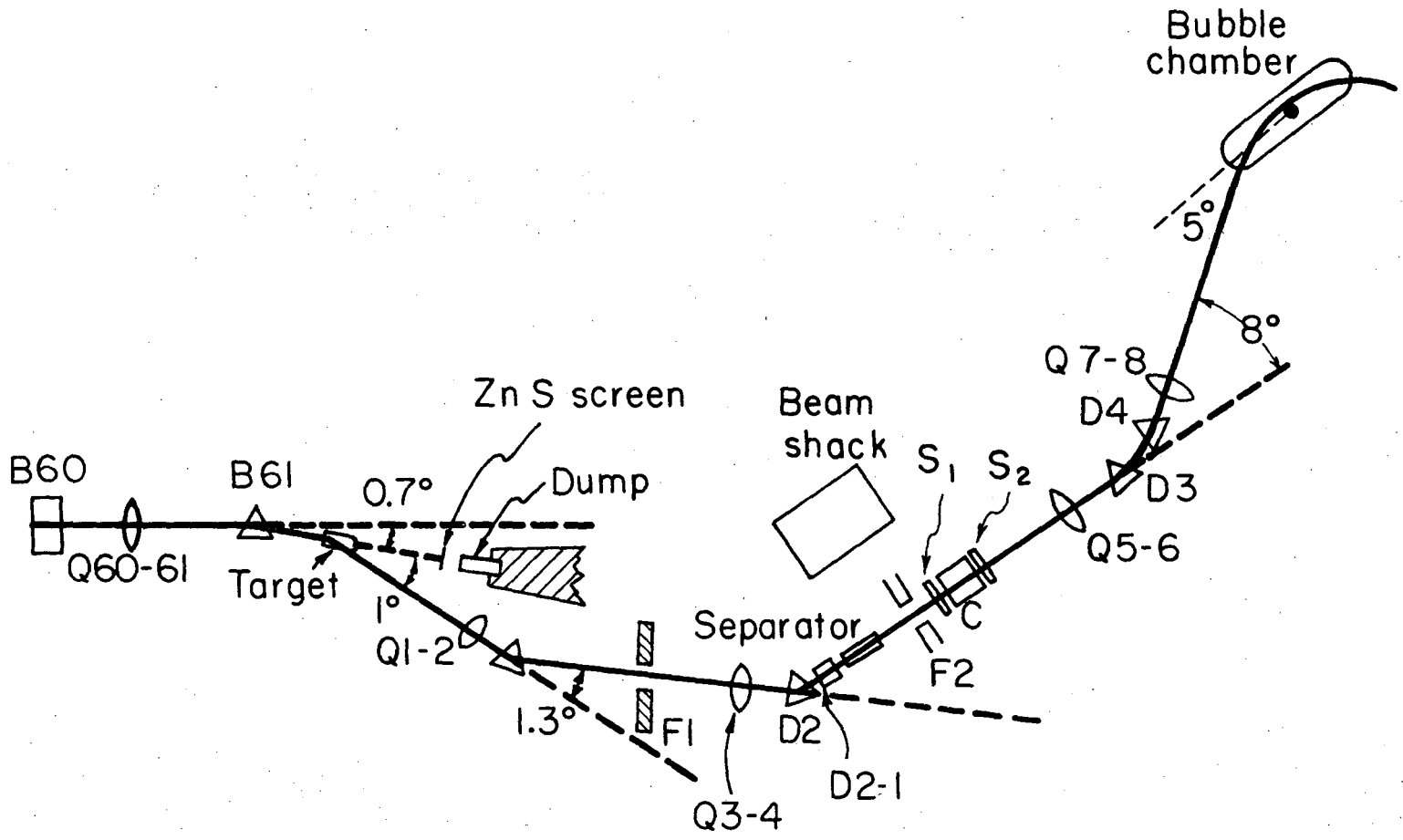

Figure 2

XBL727-3403

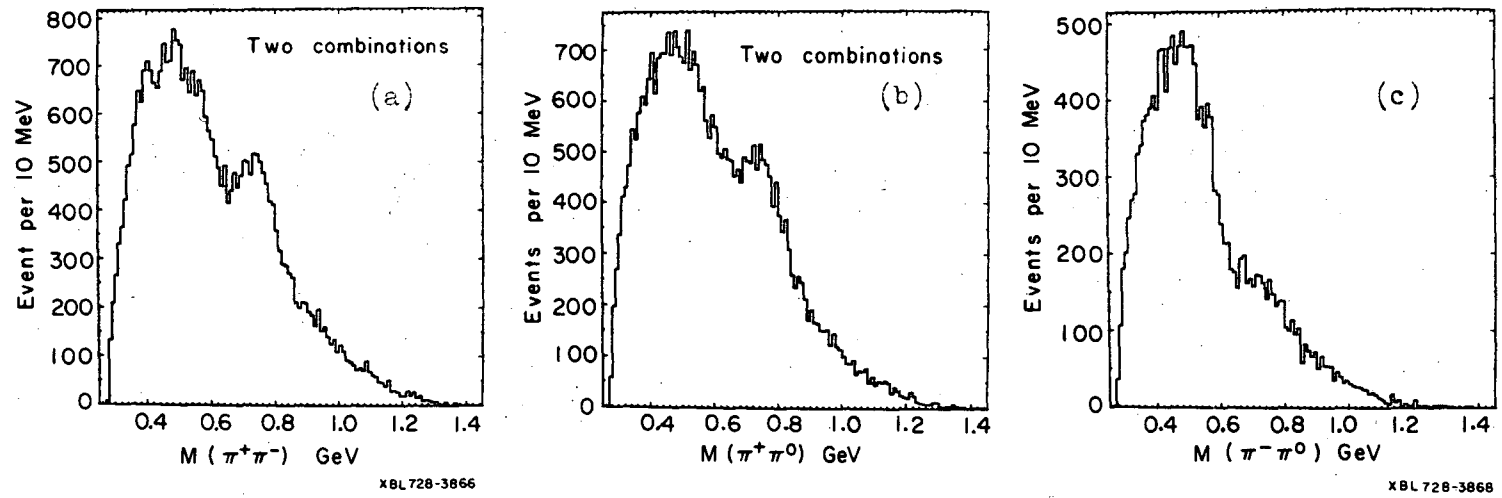

Figure 3

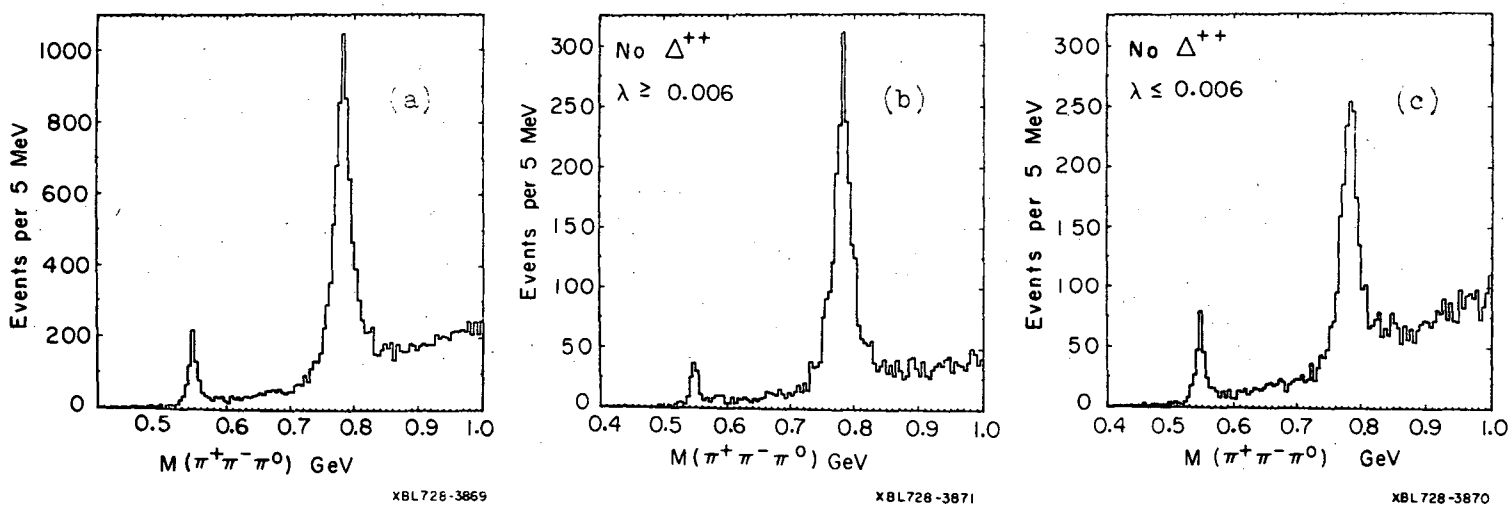

Figure 4

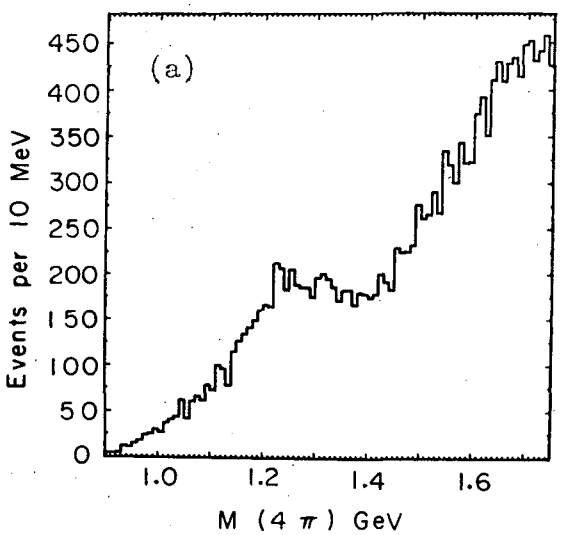
(a)
Events per 10 MeV
M (4 π) GeV
XBL728-3872

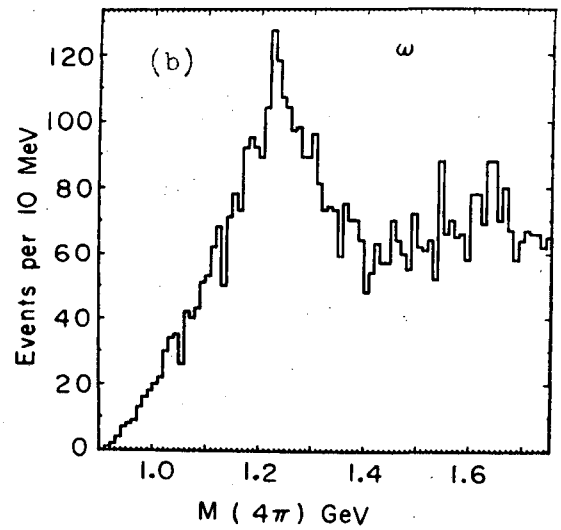
(b)
ω
Events per 10 MeV
M (4π) GeV
XBL728-3873

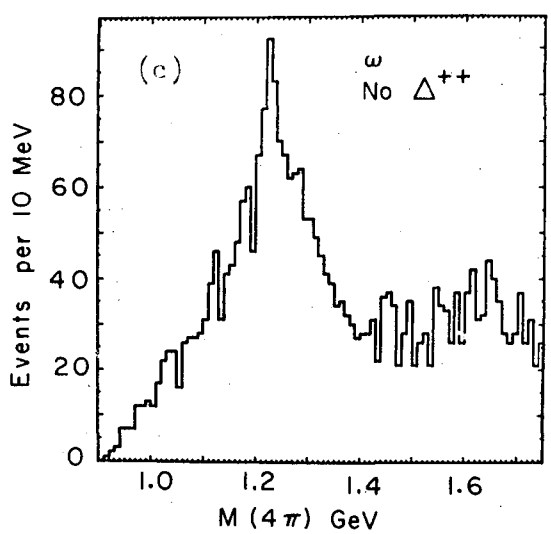
(c)
ω
No Δ++
Events per 10 MeV
M (4π) GeV
XBL728-3874

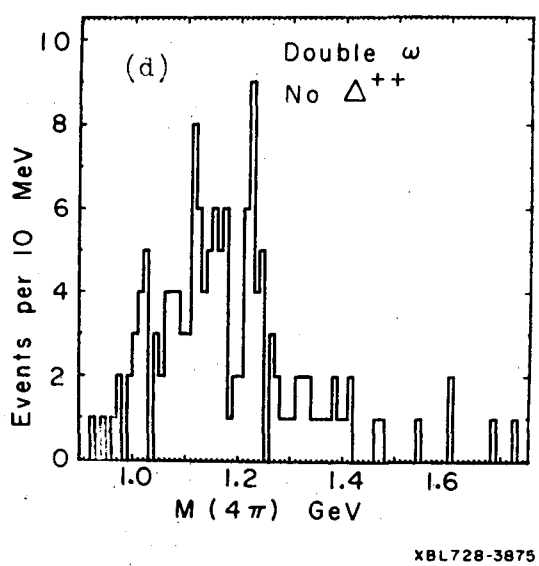
(d)
Double ω
No Δ++
Events per 10 MeV
M (4π) GeV
XBL728-3875

Figure 5

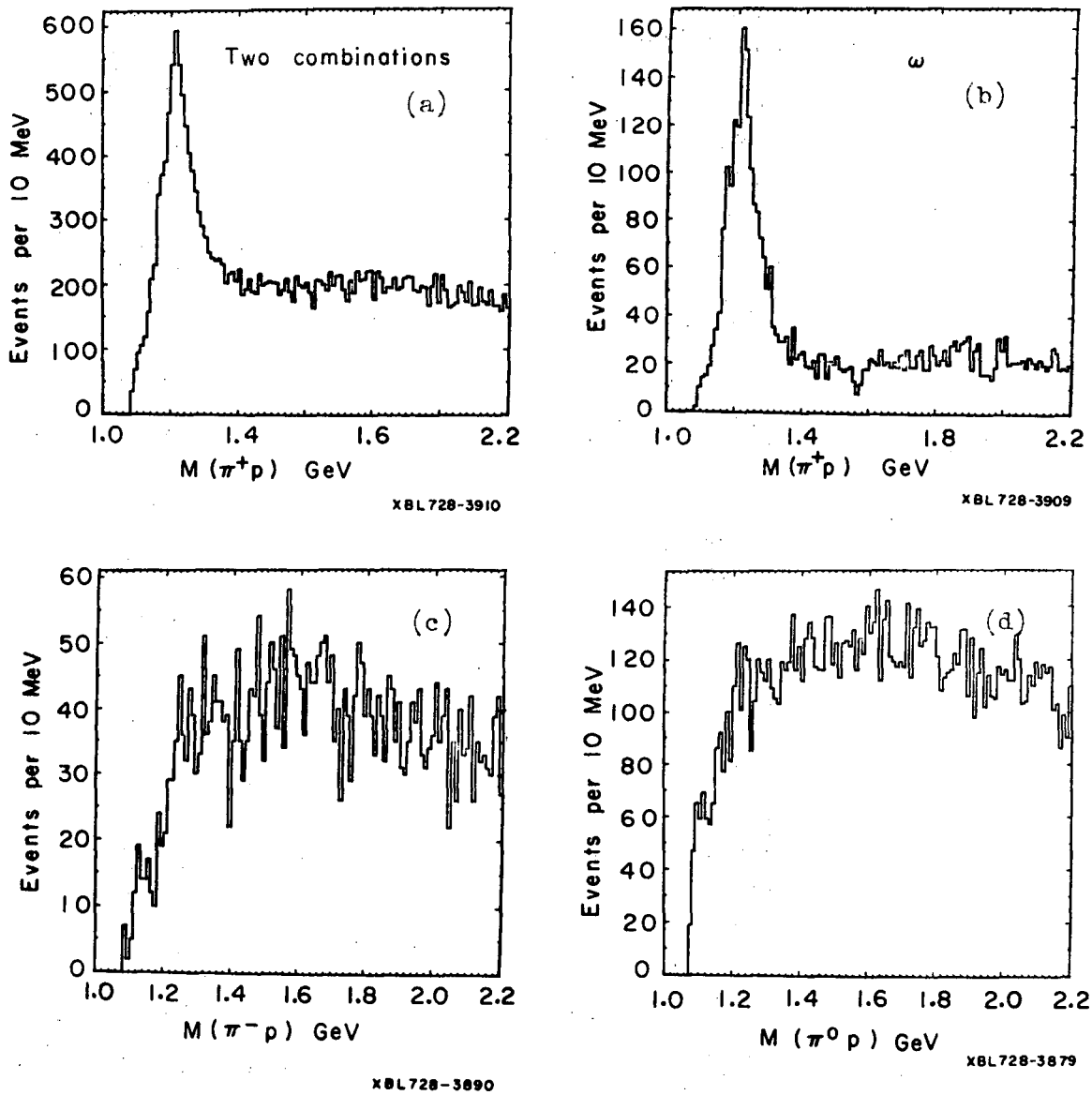
Two combinations
(a)
Events per 10 MeV
M (π^+p) GeV
XBL728-3910
ω
(b)
Events per 10 MeV
M (π^+p) GeV
XBL728-3909
(c)
Events per 10 MeV
M (π^-p) GeV
XBL728-3890
(d)
Events per 10 MeV
M (π^0p) GeV
XBL728-3879

Figure 6

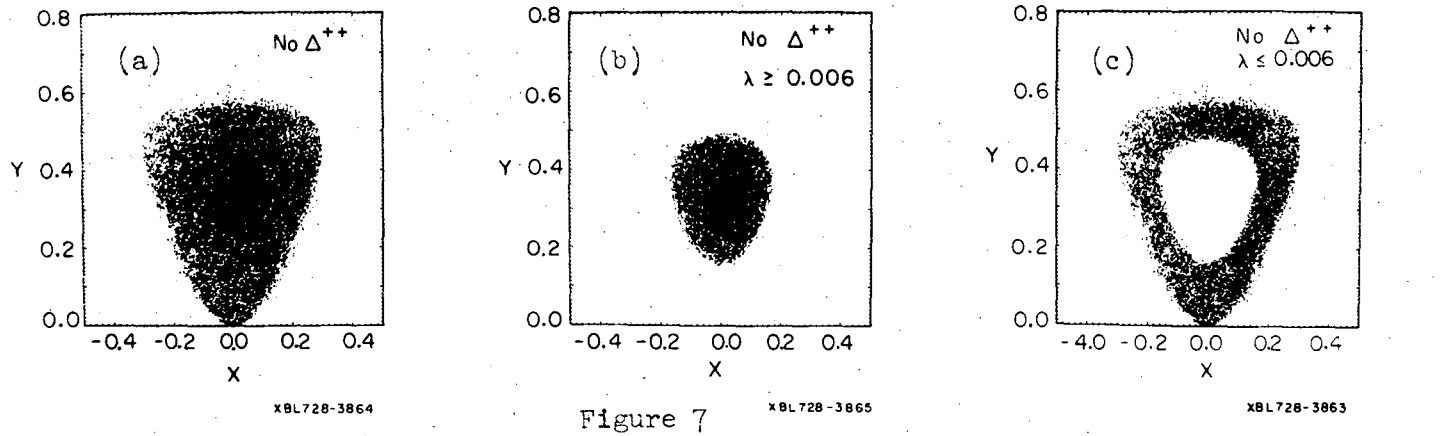

Figure 7

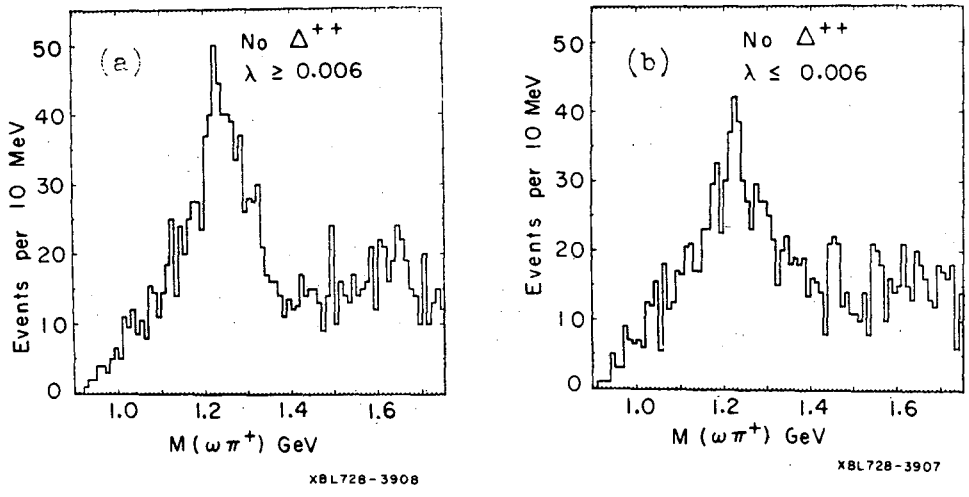

Figure 8

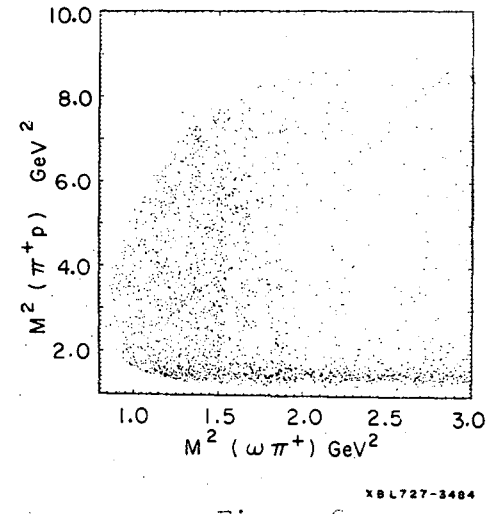

Figure 9

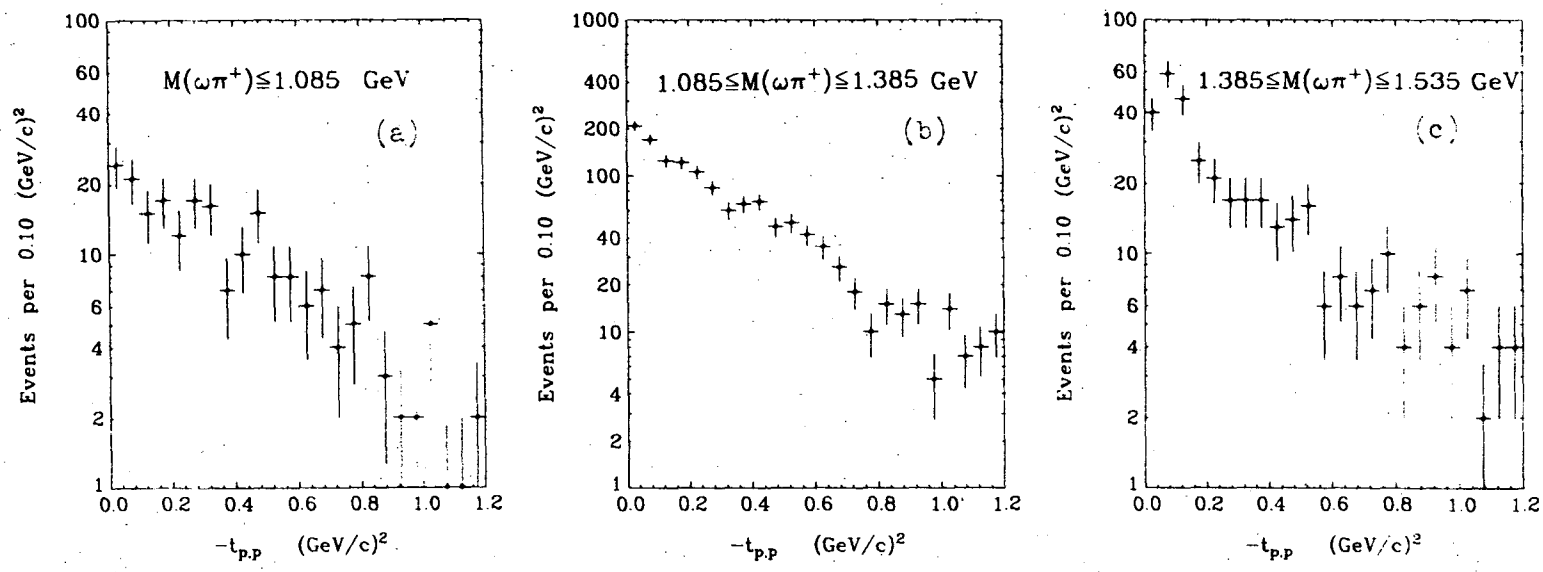

XBL 728-1607

Figure 10

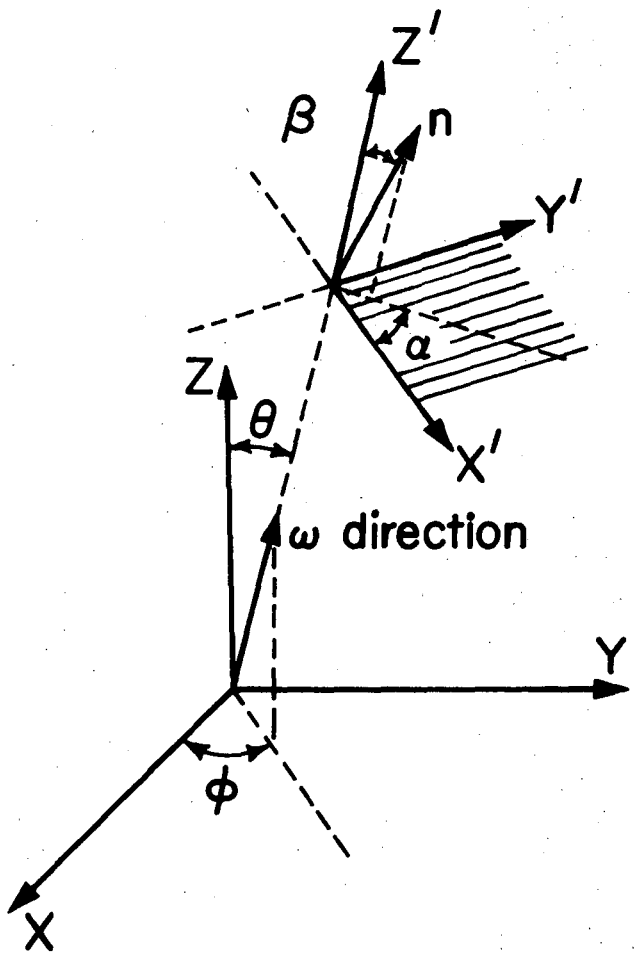

XBL729-3970

Figure 11

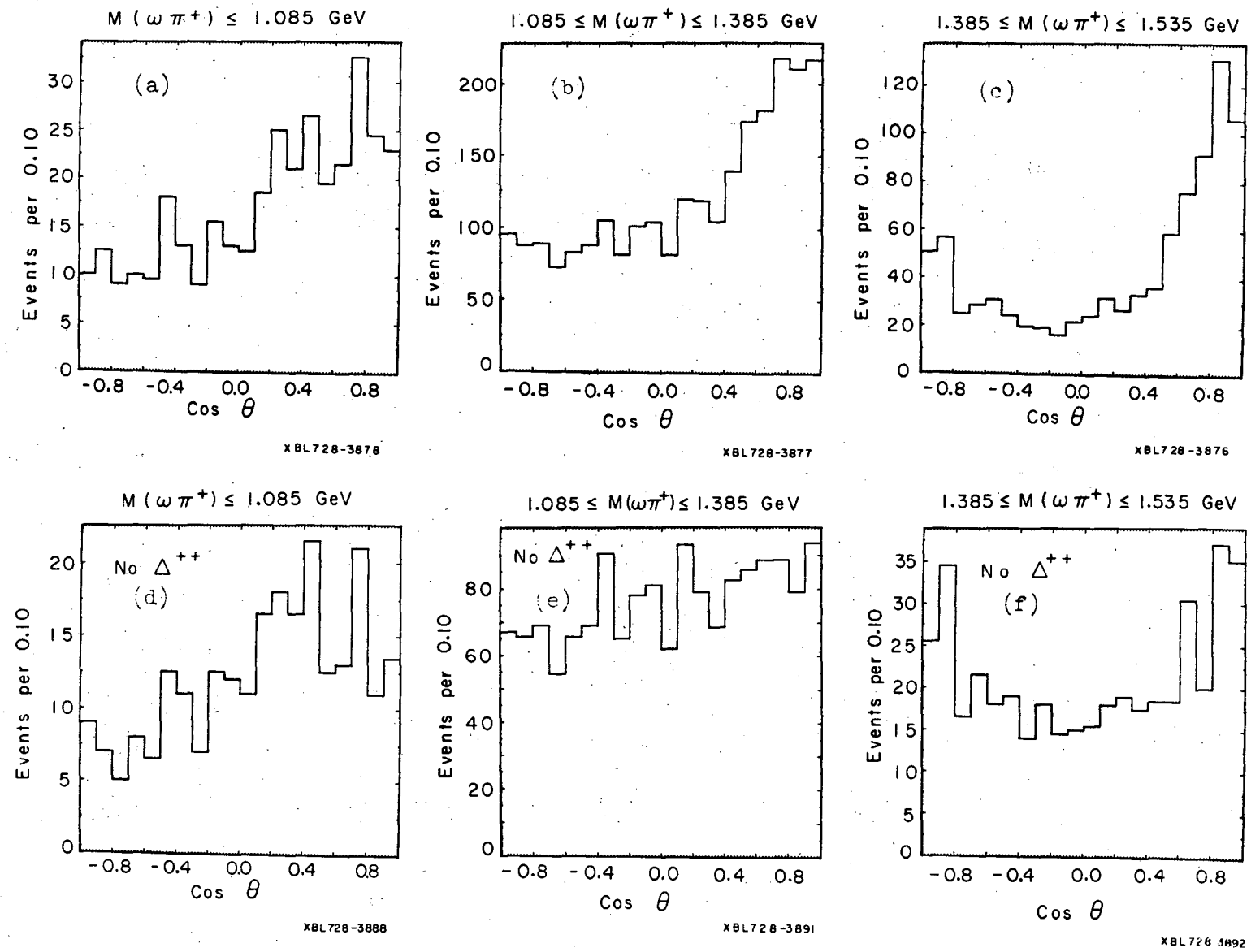
M (ω π+) ≤ 1.085 GeV
(a)
Events per 0.10
Cos θ
XBL728-3878
1.085 ≤ M (ωπ+) ≤ 1.385 GeV
(b)
Events per 0.10
Cos θ
XBL728-3877
1.385 ≤ M (ωπ+) ≤ 1.535 GeV
(c)
Events per 0.10
Cos θ
XBL728-3876
M (ω π+) ≤ 1.085 GeV
No Δ++
(d)
Events per 0.10
Cos θ
XBL728-3888
1.085 ≤ M(ωπ+) ≤ 1.385 GeV
No Δ++
(e)
Events per 0.10
Cos θ
XBL728-3891
1.385 ≤ M (ω π+) ≤ 1.535 GeV
No Δ++
(f)
Events per 0.10
Cos θ
XBL728-3892

Figure 12

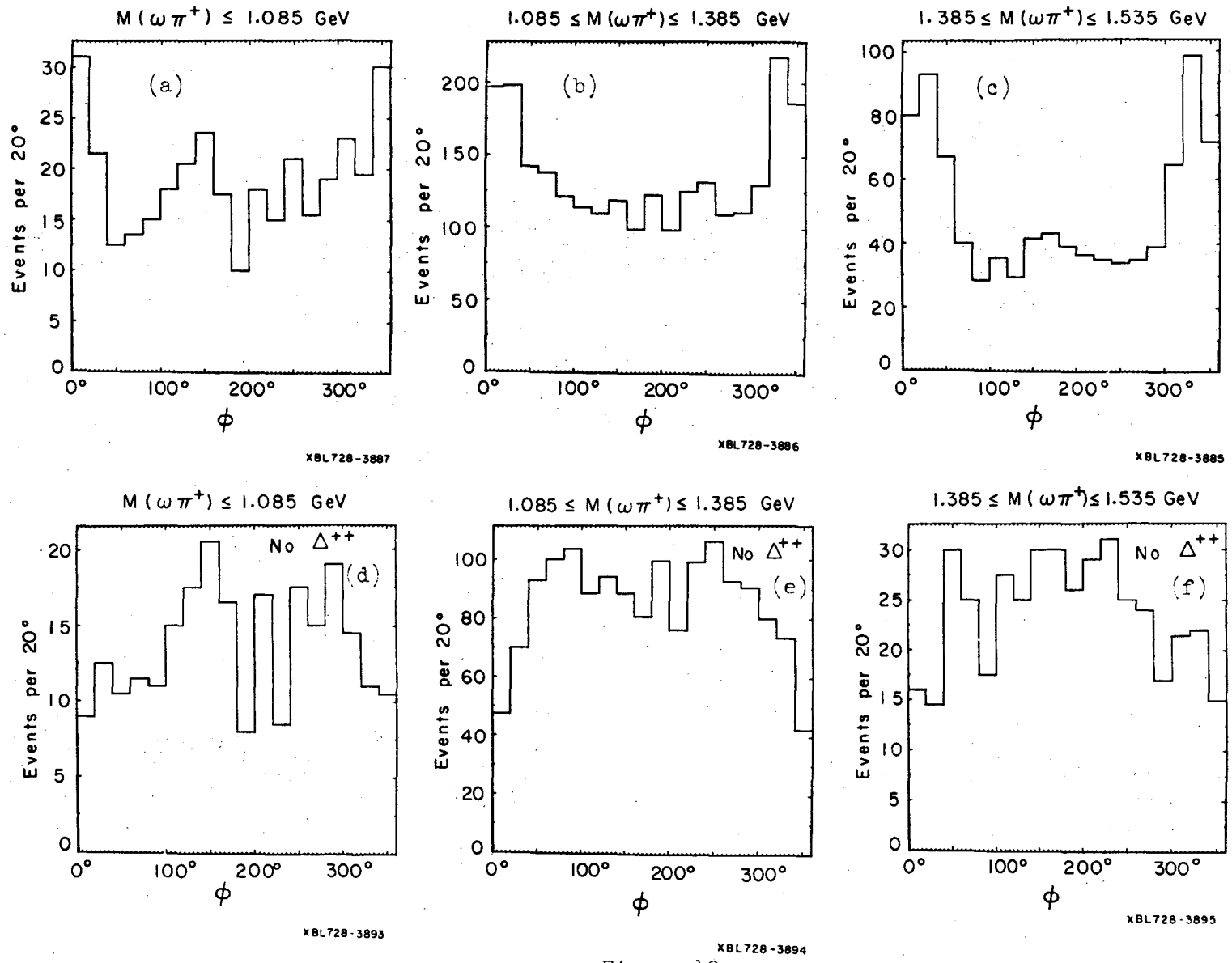
M (ω π+) ≤ 1.085 GeV
(a)
Events per 20°
φ
XBL728-3887
1.085 ≤ M (ωπ+) ≤ 1.385 GeV
(b)
XBL728-3886
1.385 ≤ M (ωπ+) ≤ 1.535 GeV
(c)
XBL728-3885
No Δ++
(d)
XBL728-3893
(e)
XBL728-3894
(f)
XBL728-3895

Figure 13

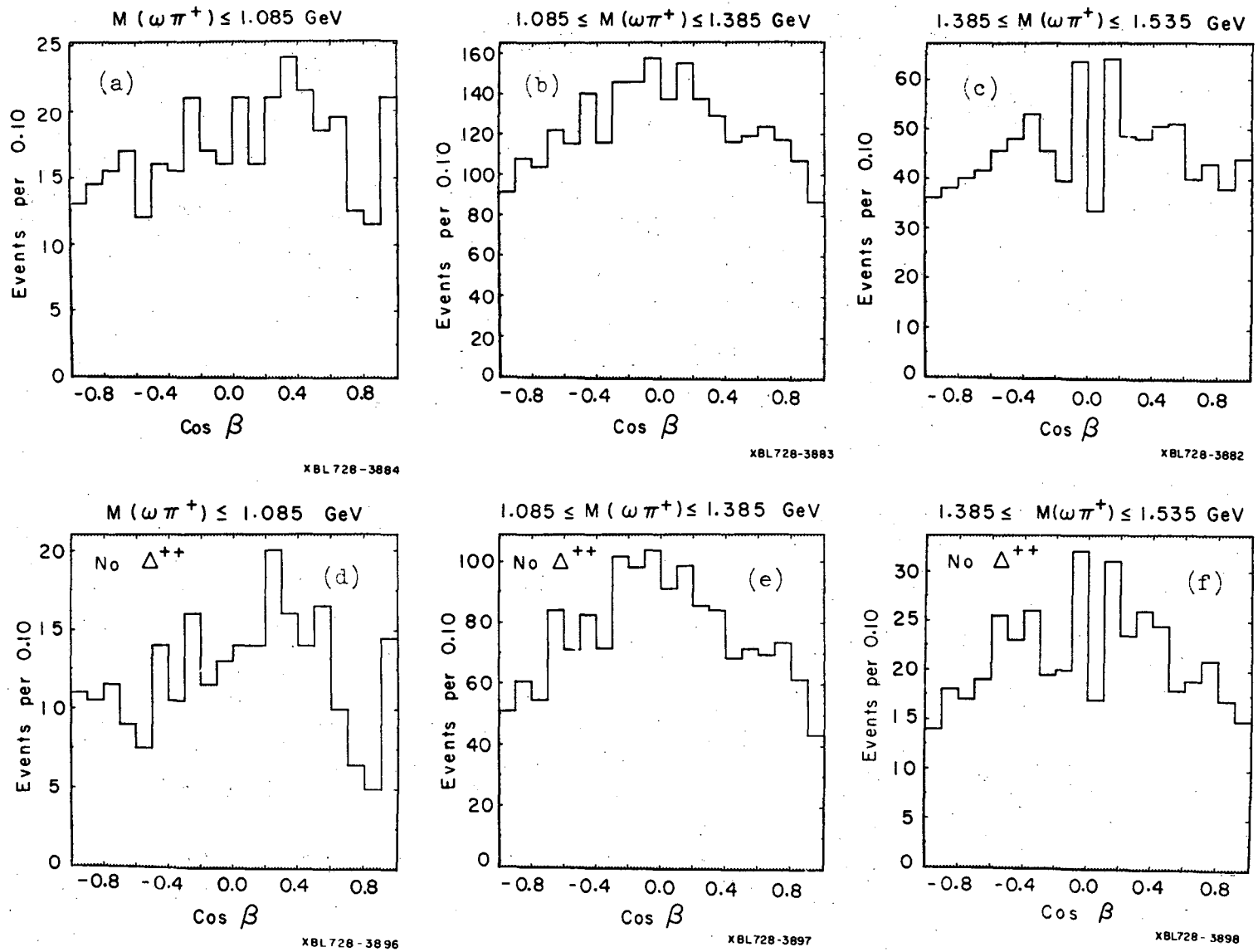
M ($\omega\pi^+$) ≤ 1.085 GeV
(a)
Events per 0.10
Cos β
XBL728-3884
1.085 ≤ M ($\omega\pi^+$) ≤ 1.385 GeV
(b)
Events per 0.10
Cos β
XBL728-3883
1.385 ≤ M ($\omega\pi^+$) ≤ 1.535 GeV
(c)
Events per 0.10
Cos β
XBL728-3882
M ($\omega\pi^+$) ≤ 1.085 GeV
No Δ^{++}
(d)
Events per 0.10
Cos β
XBL728-3896
1.085 ≤ M ($\omega\pi^+$) ≤ 1.385 GeV
No Δ^{++}
(e)
Events per 0.10
Cos β
XBL728-3897
1.385 ≤ M($\omega\pi^+$) ≤ 1.535 GeV
No Δ^{++}
(f)
Events per 0.10
Cos β
XBL728-3898

Figure 14

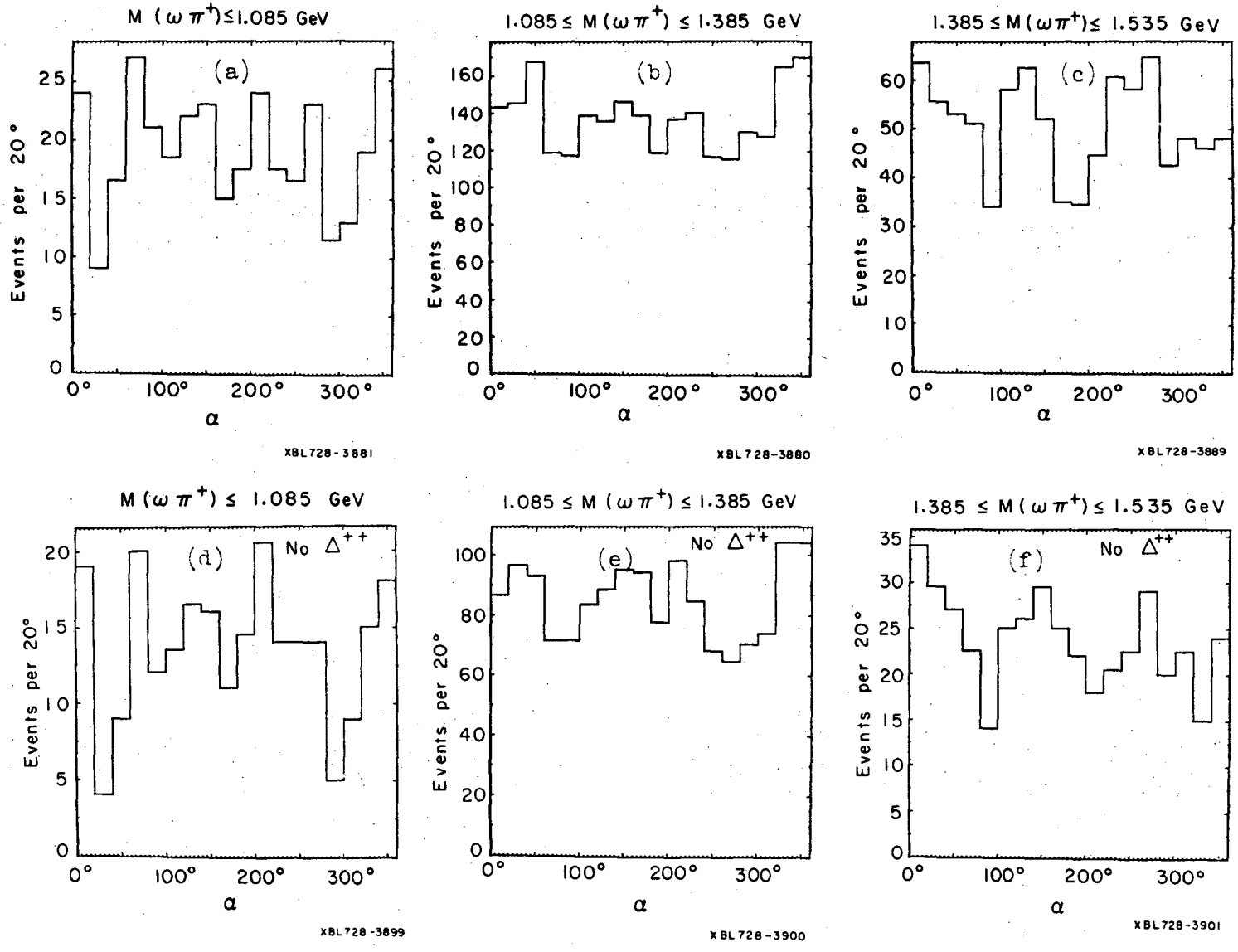
M (ω π+) ≤ 1.085 GeV
(a)
Events per 20°
α
XBL728-3881
1.085 ≤ M (ω π+) ≤ 1.385 GeV
(b)
XBL728-3880
1.385 ≤ M (ω π+) ≤ 1.535 GeV
(c)
XBL728-3889
M (ω π+) ≤ 1.085 GeV
(d)
No Δ++
XBL728-3899
1.085 ≤ M (ω π+) ≤ 1.385 GeV
(e)
No Δ++
XBL728-3900
1.385 ≤ M (ω π+) ≤ 1.535 GeV
(f)
No Δ++
XBL728-3901

Figure 15

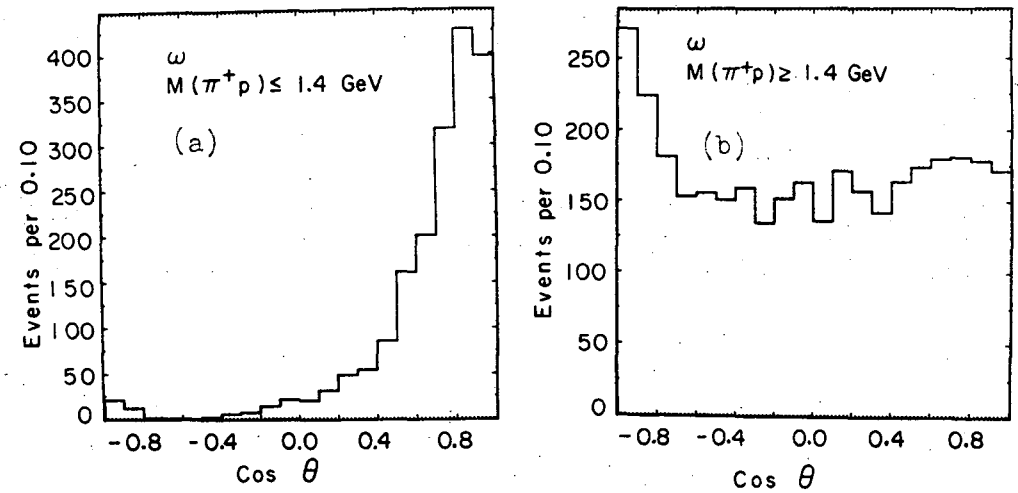

Figure 16

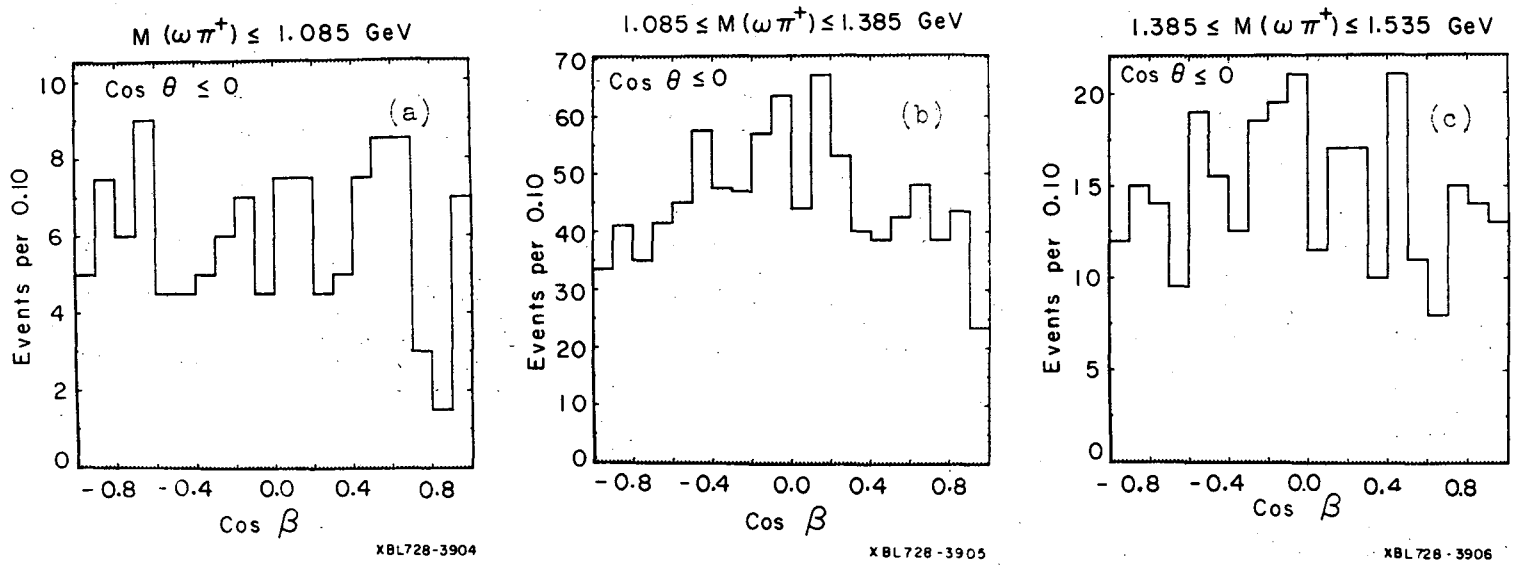

Figure 17

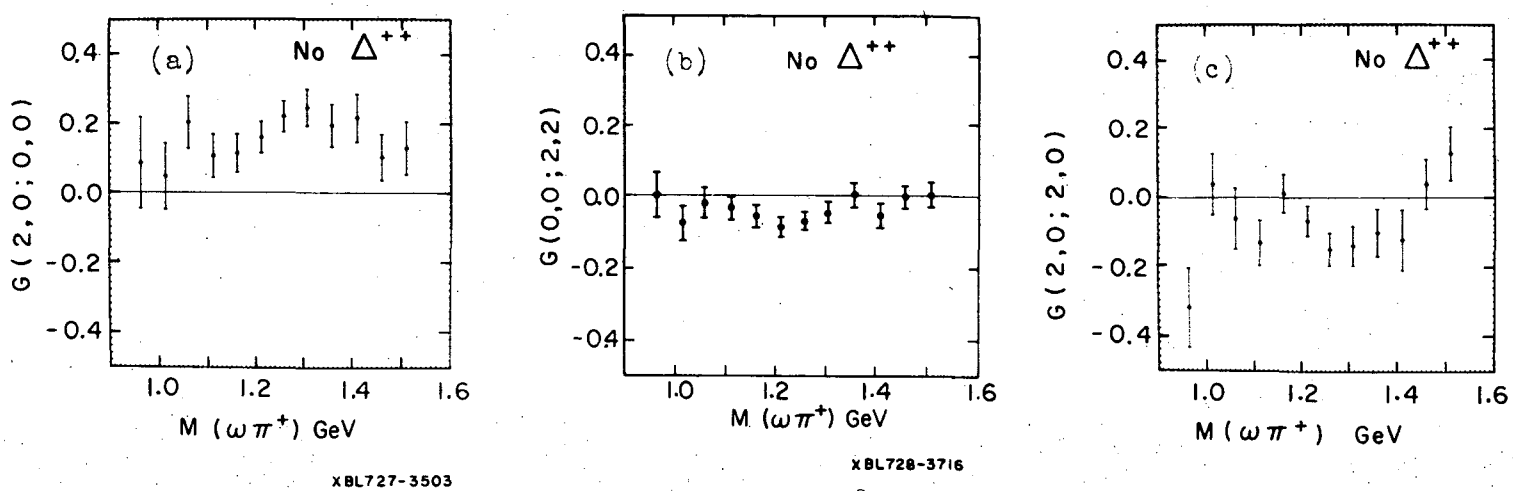
(a)
No Δ^{++}
G(2,0;0,0)
0.4
0.2
0.0
-0.2
-0.4
1.0
1.2
1.4
1.6
M ($\omega\pi^+$) GeV
XBL727-3503
(b)
No Δ^{++}
G(0,0;2,2)
M ($\omega\pi^+$) GeV
XBL728-3716
(c)
No Δ^{++}
G(2,0;2,0)
M ($\omega\pi^+$) GeV
XBL727-3502

Figure 18

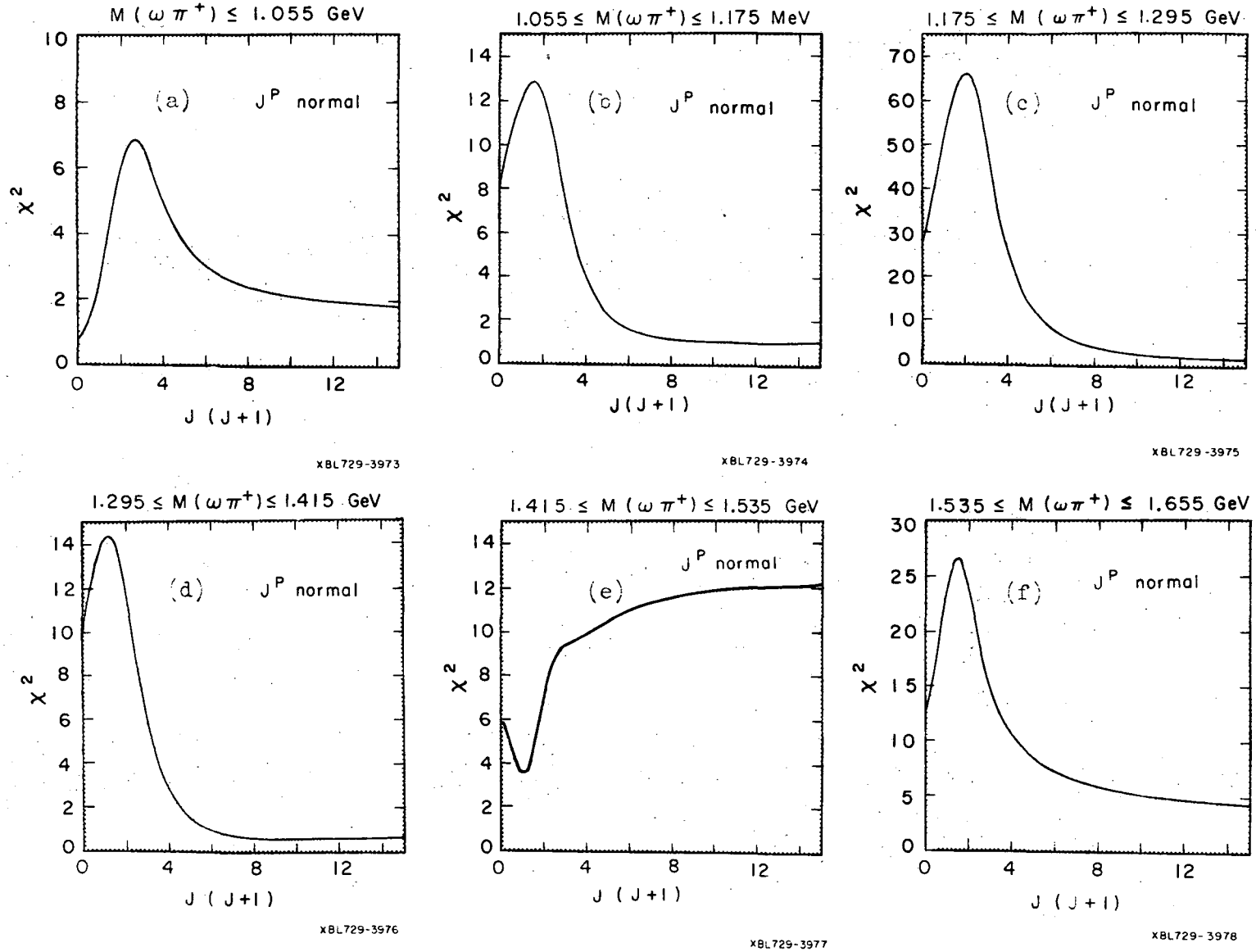
M (ω π+) ≤ 1.055 GeV
(a)
J^P normal
χ²
J (J+1)
XBL729-3973
1.055 ≤ M (ω π+) ≤ 1.175 MeV
(b)
J^P normal
χ²
J(J+1)
XBL729-3974
1.175 ≤ M (ω π+) ≤ 1.295 GeV
(c)
J^P normal
χ²
J(J+1)
XBL729-3975
1.295 ≤ M (ω π+) ≤ 1.415 GeV
(d)
J^P normal
χ²
J (J+1)
XBL729-3976
1.415 ≤ M (ω π+) ≤ 1.535 GeV
(e)
J^P normal
χ²
J (J+1)
XBL729-3977
1.535 ≤ M (ω π+) ≤ 1.655 GeV
(f)
J^P normal
χ²
J (J+1)
XBL729-3978

Figure 19

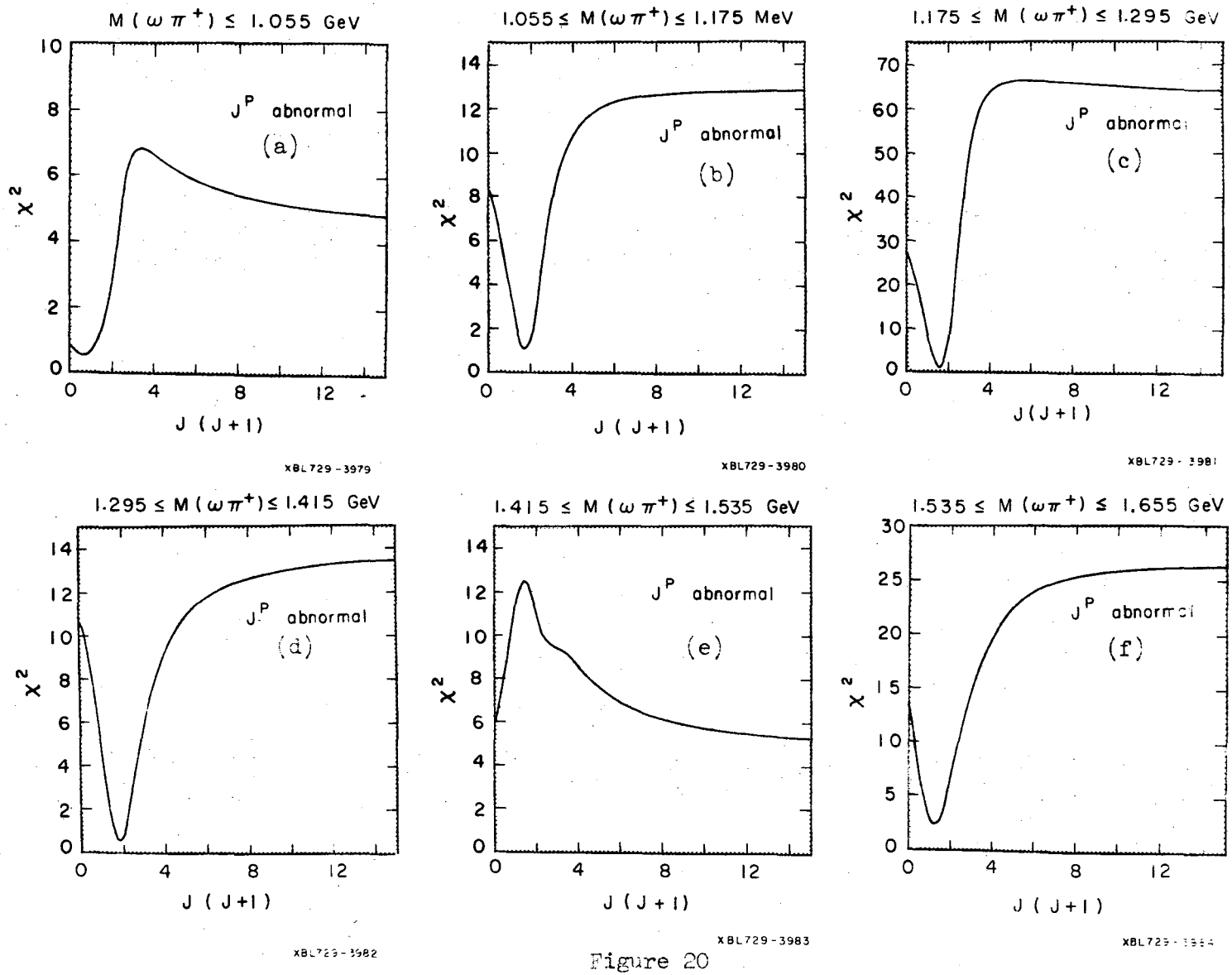
M (ω π+) ≤ 1.055 GeV
J^P abnormal
(a)
χ²
J (J+1)
XBL729-3979
1.055 ≤ M(ωπ+) ≤ 1.175 MeV
J^P abnormal
(b)
χ²
J (J+1)
XBL729-3980
1.175 ≤ M (ωπ+) ≤ 1.295 GeV
J^P abnormal
(c)
χ²
J(J+1)
XBL729-3981
1.295 ≤ M(ωπ+) ≤ 1.415 GeV
J^P abnormal
(d)
χ²
J (J+1)
XBL729-3982
1.415 ≤ M (ω π+) ≤ 1.535 GeV
J^P abnormal
(e)
χ²
J (J+1)
XBL729-3983
1.535 ≤ M (ωπ+) ≤ 1.655 GeV
J^P abnormal
(f)
χ²
J (J+1)

Figure 20

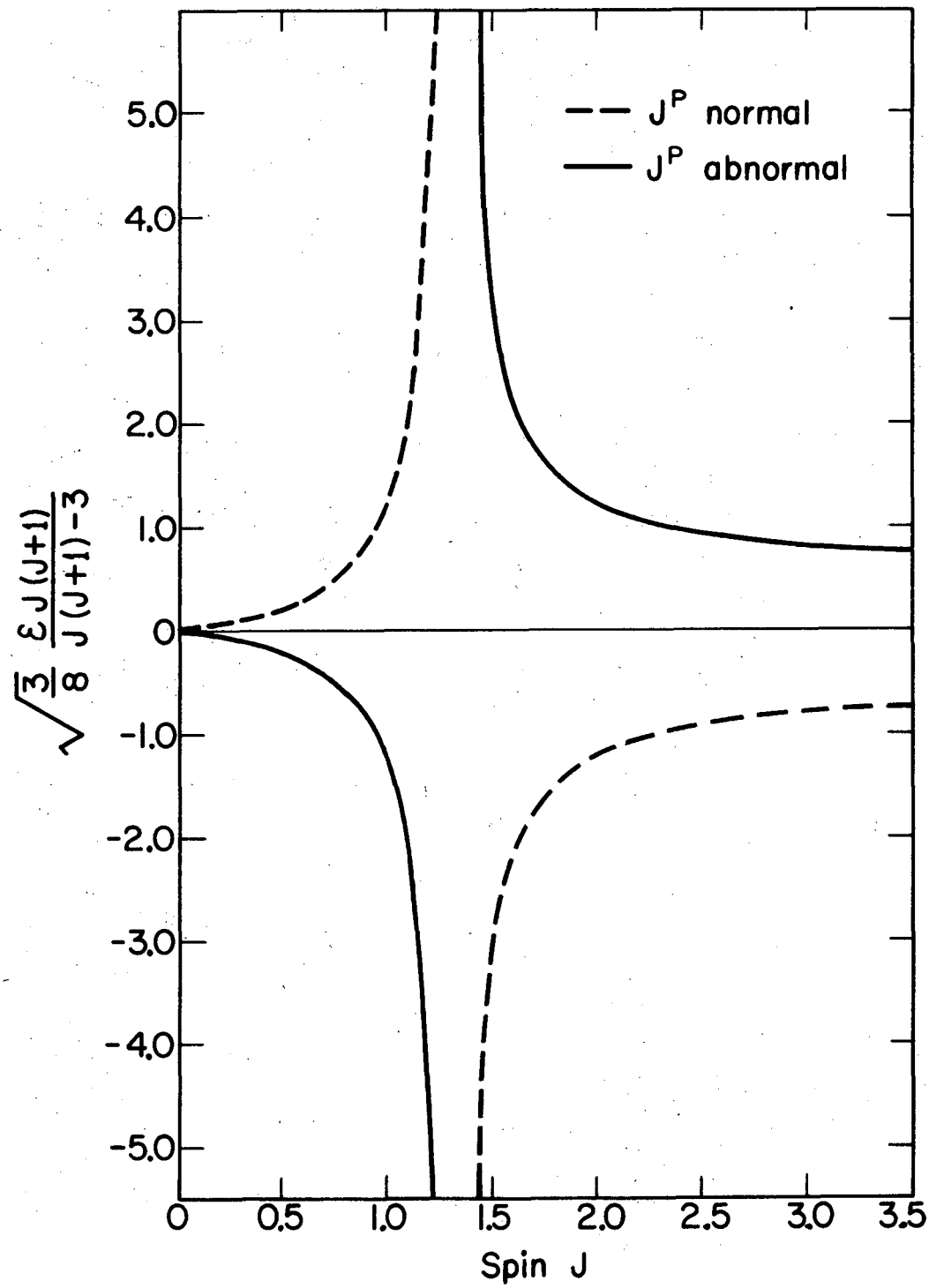

XBL729-3969

Figure 21

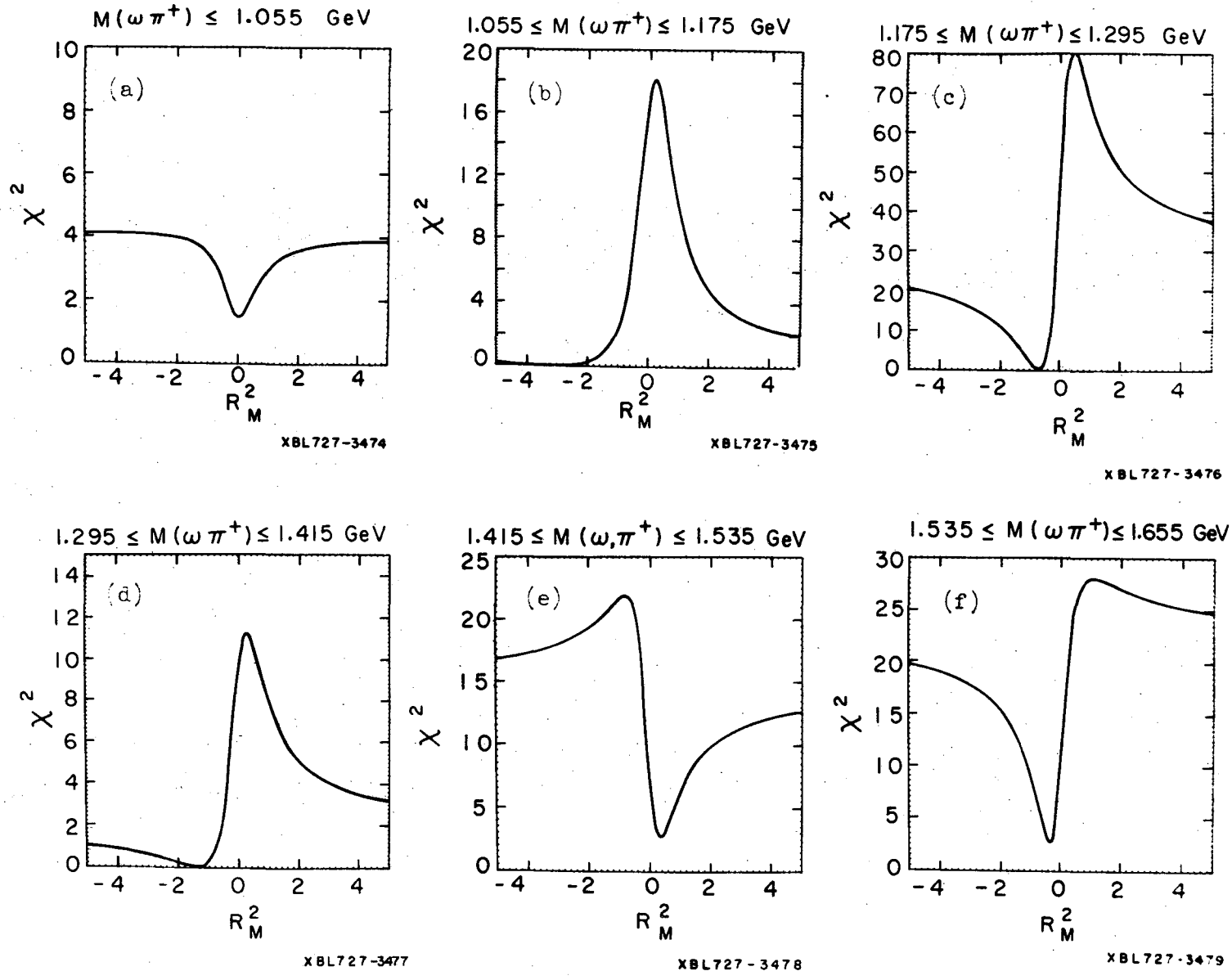
M(ωπ+) ≤ 1.055 GeV
(a)
XBL727-3474
1.055 ≤ M(ωπ+) ≤ 1.175 GeV
(b)
XBL727-3475
1.175 ≤ M(ωπ+) ≤ 1.295 GeV
(c)
XBL727-3476
1.295 ≤ M(ωπ+) ≤ 1.415 GeV
(d)
XBL727-3477
1.415 ≤ M(ω,π+) ≤ 1.535 GeV
(e)
XBL727-3478
1.535 ≤ M(ωπ+) ≤ 1.655 GeV
(f)
XBL727-3479
χ2
R2M

Figure 22

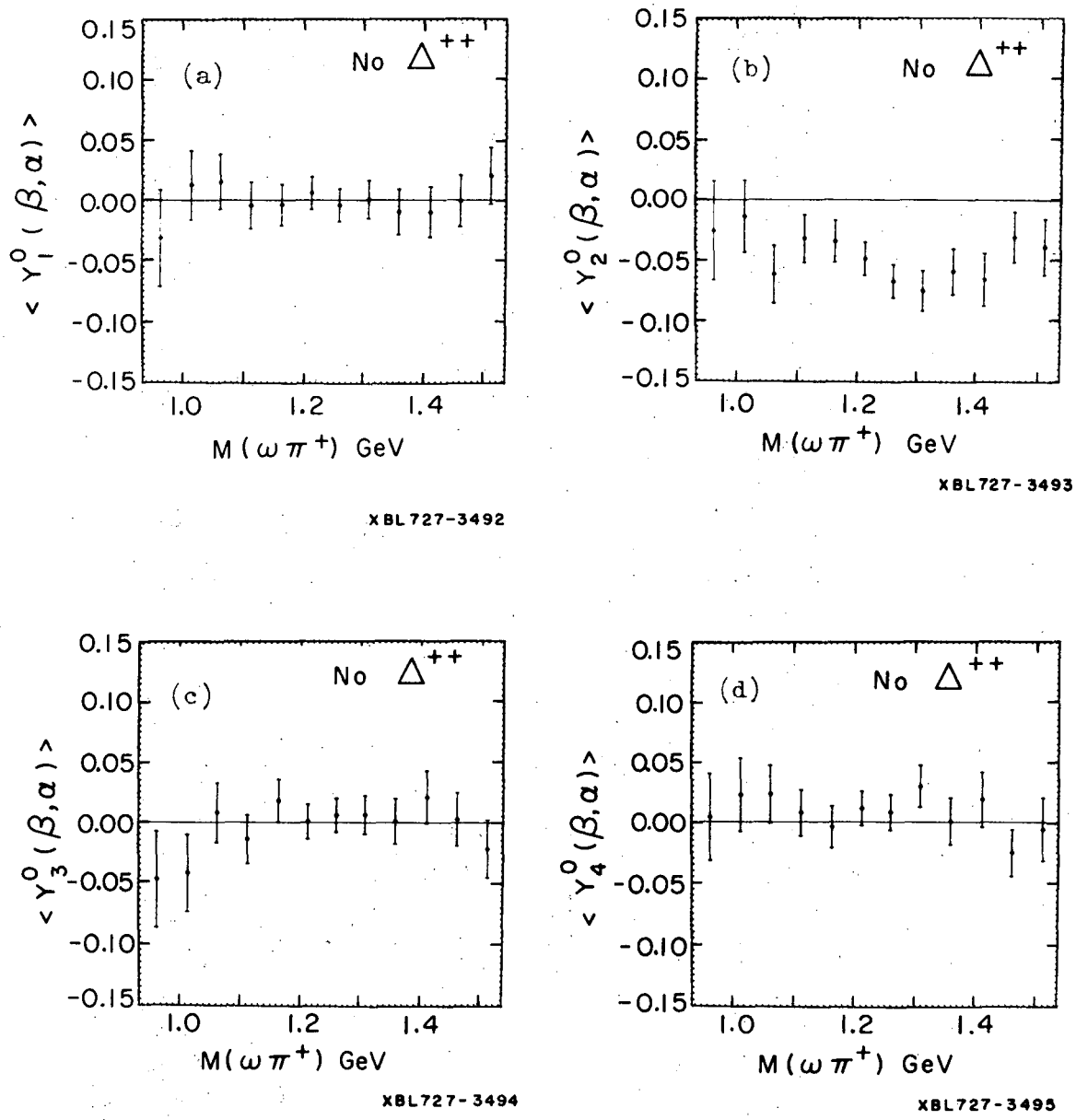
(a)
No Δ^{++}
$< Y_1^0(\beta,\alpha) >$
M ($\omega\pi^+$) GeV
XBL727-3492
(b)
No Δ^{++}
$< Y_2^0(\beta,\alpha) >$
M ($\omega\pi^+$) GeV
XBL727-3493
(c)
No Δ^{++}
$< Y_3^0(\beta,\alpha) >$
M ($\omega\pi^+$) GeV
XBL727-3494
(d)
No Δ^{++}
$< Y_4^0(\beta,\alpha) >$
M ($\omega\pi^+$) GeV
XBL727-3495

Figure 23

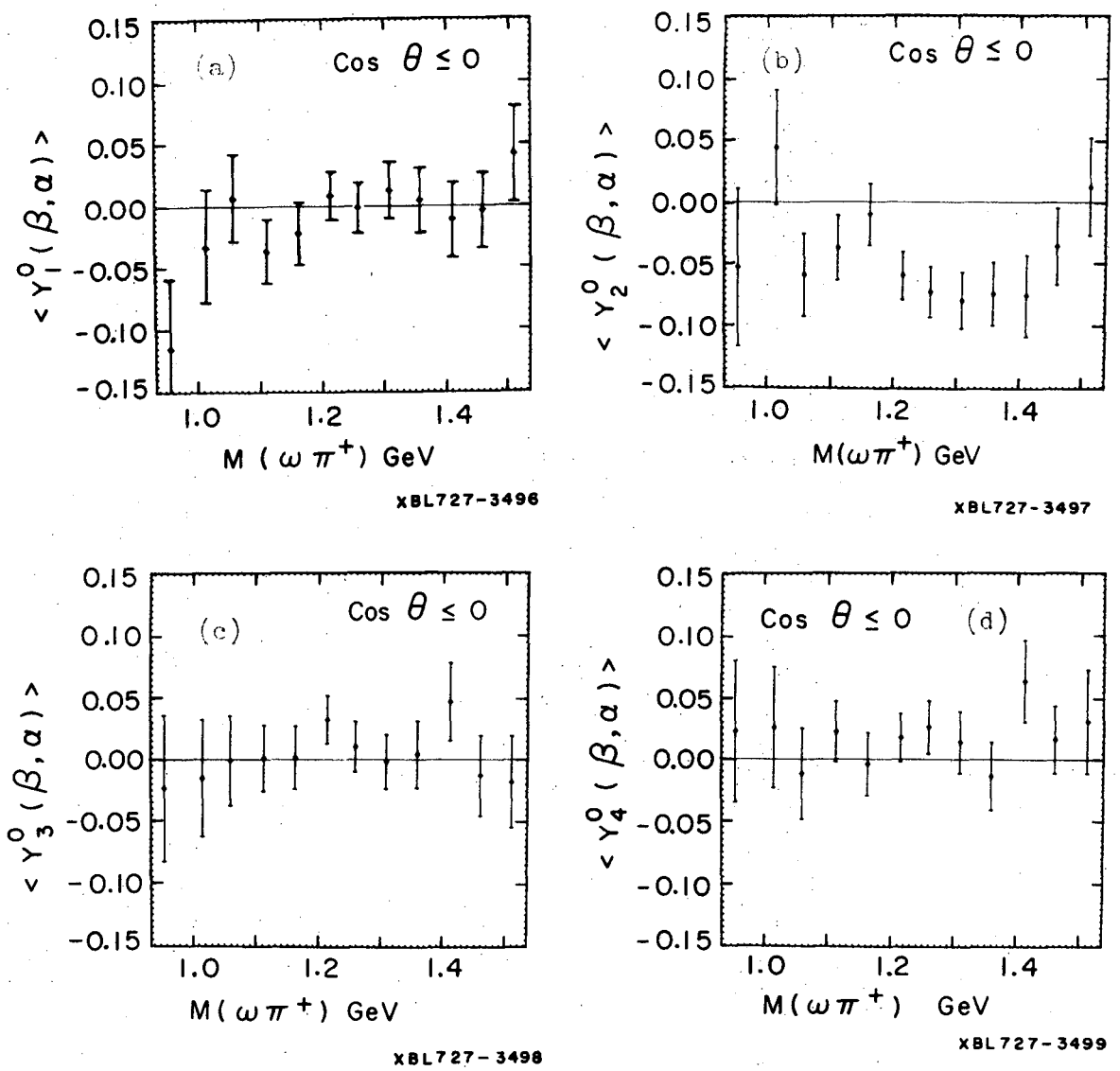
(a)
Cos θ ≤ 0
< Y₁⁰ (β, α) >
M (ω π⁺) GeV
XBL727-3496
(b)
Cos θ ≤ 0
< Y₂⁰ (β, α) >
M(ωπ⁺) GeV
XBL727-3497
(c)
Cos θ ≤ 0
< Y₃⁰ (β, α) >
M(ω π⁺) GeV
XBL727-3498
Cos θ ≤ 0
(d)
< Y₄⁰ (β, α) >
M(ω π⁺) GeV
XBL727-3499

Figure 24

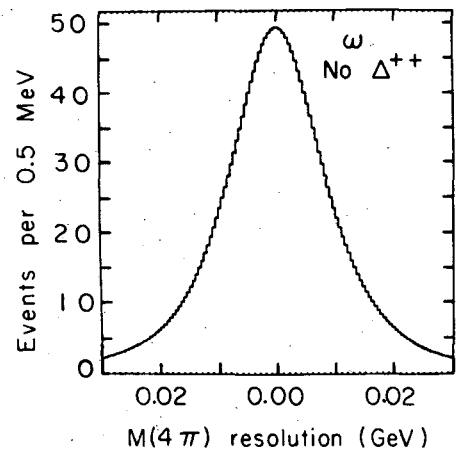

Figure 25

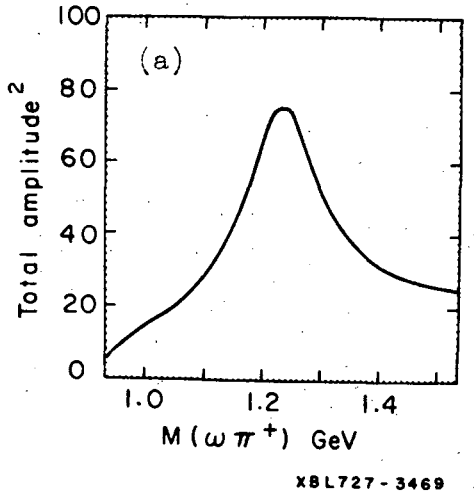

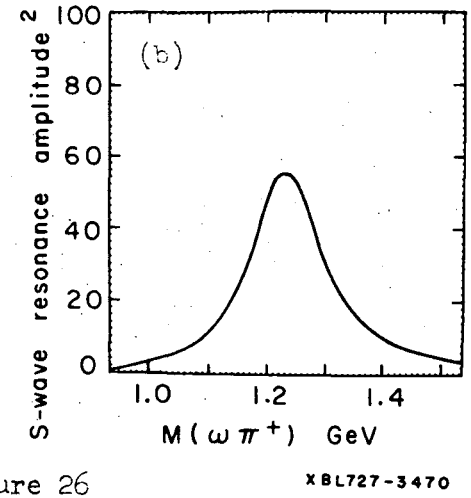

Figure 26

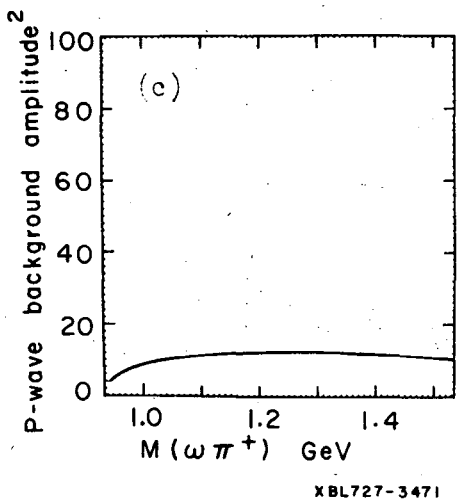

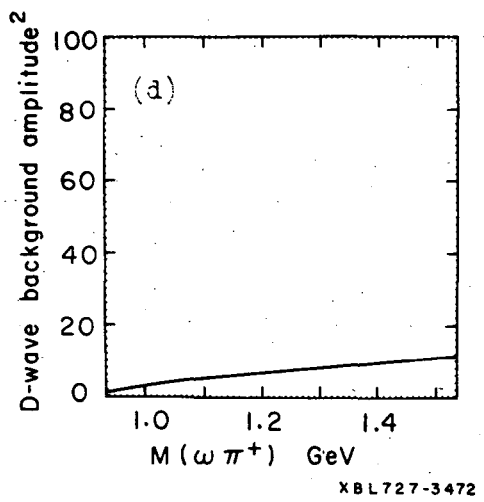

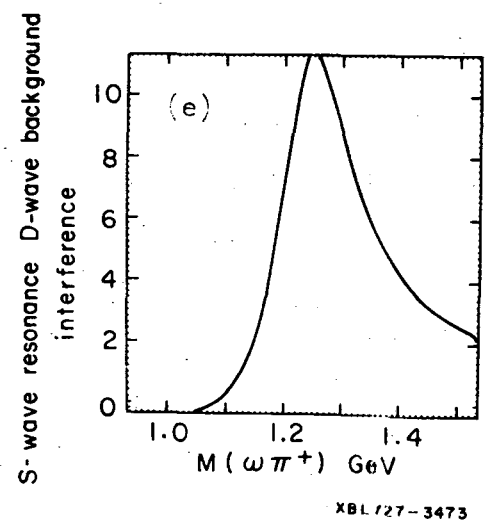

Figure 26

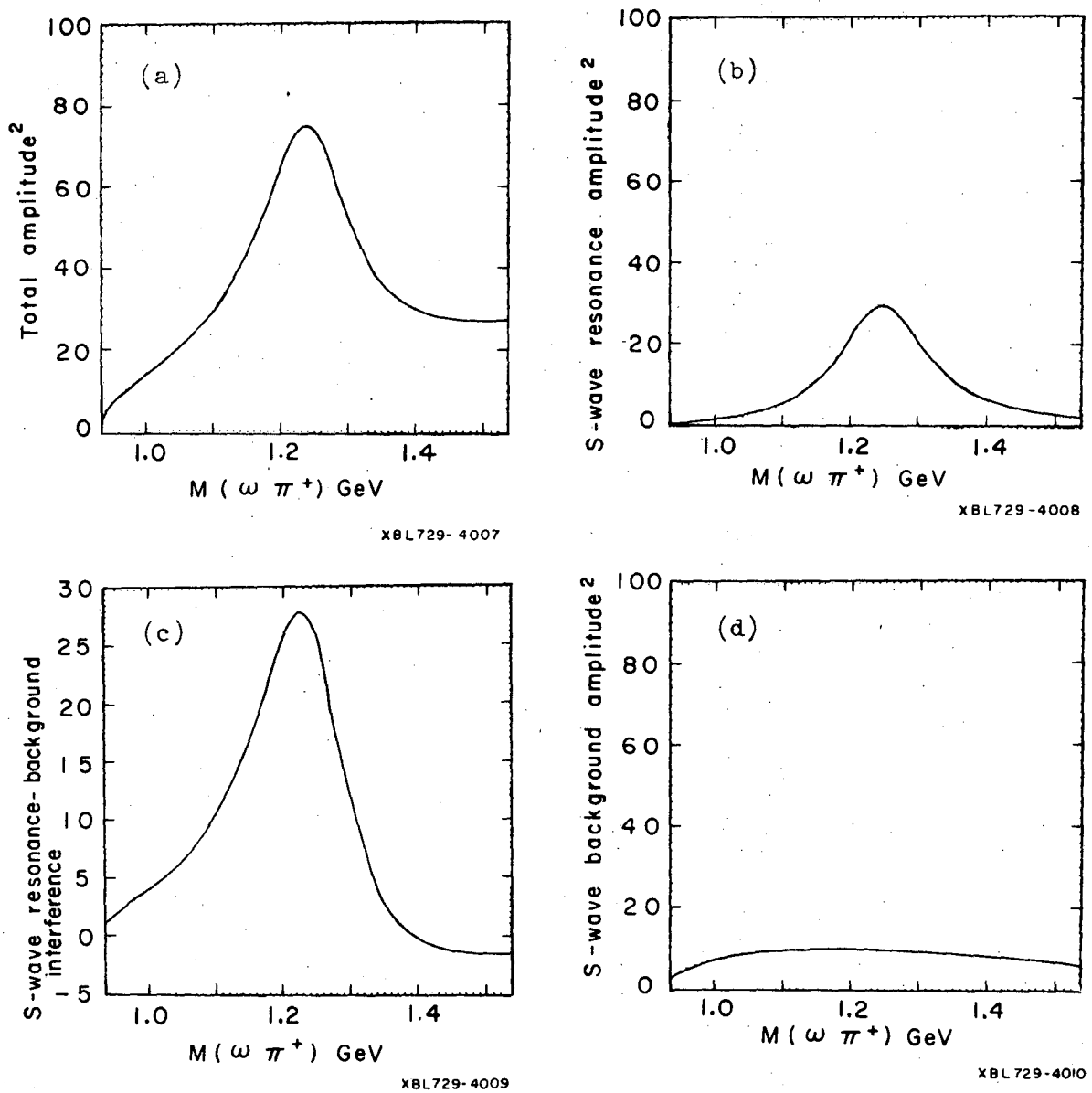
(a)
Total amplitude²
M (ω π⁺) GeV
XBL729-4007
(b)
S-wave resonance amplitude²
M (ω π⁺) GeV
XBL729-4008
(c)
S-wave resonance-background interference
M (ω π⁺) GeV
XBL729-4009
(d)
S-wave background amplitude²
M (ω π⁺) GeV
XBL729-4010

Figure 27

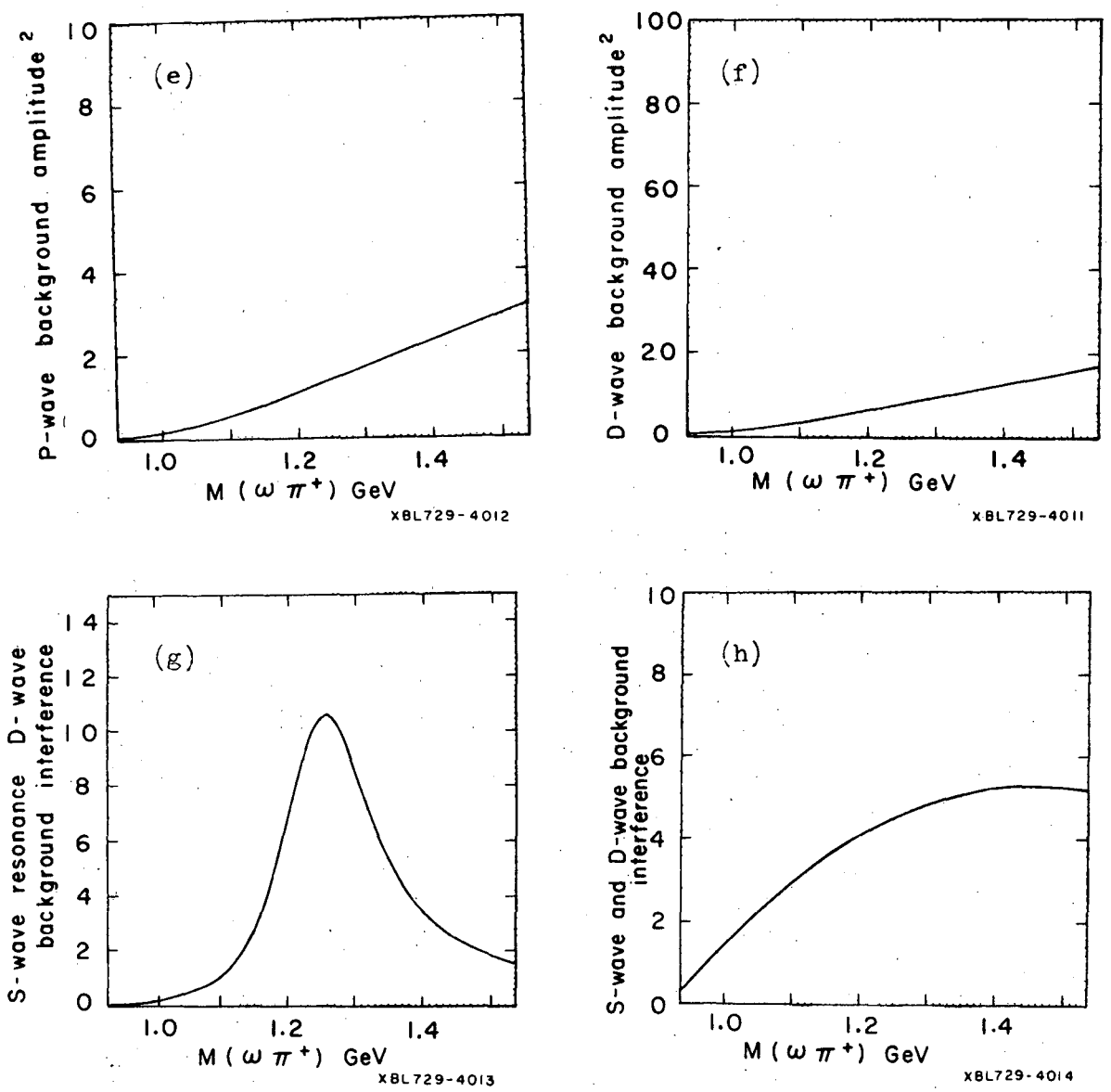
(e)
P-wave background amplitude²
M (ω π⁺) GeV
XBL729-4012
(f)
D-wave background amplitude²
M (ω π⁺) GeV
XBL729-4011
(g)
S-wave resonance D-wave background interference
M (ω π⁺) GeV
XBL729-4013
(h)
S-wave and D-wave background interference
M (ω π⁺) GeV
XBL729-4014

Figure 27

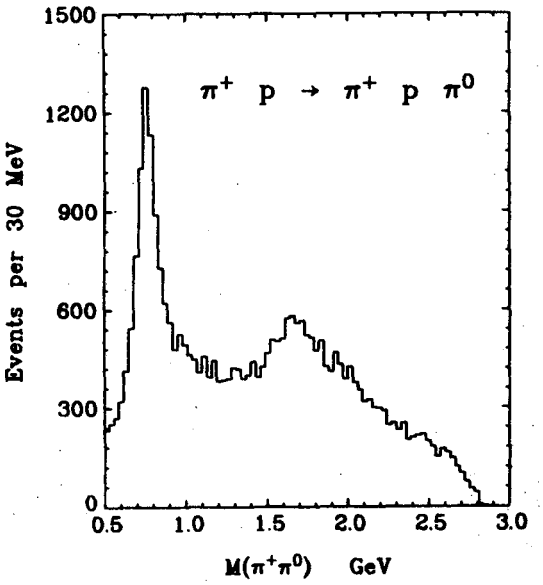

Figure 28

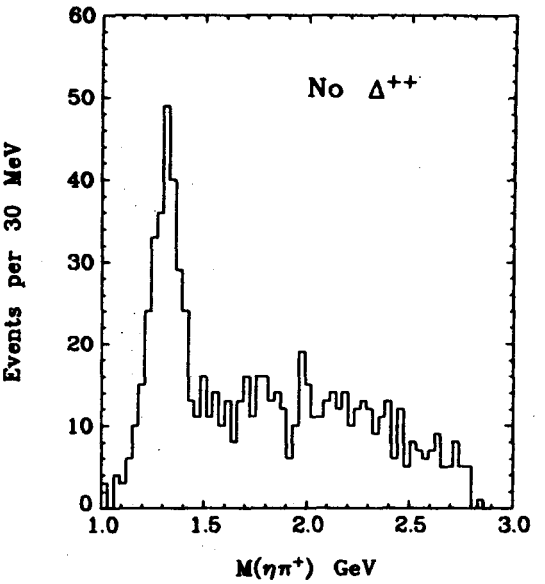

Figure 29

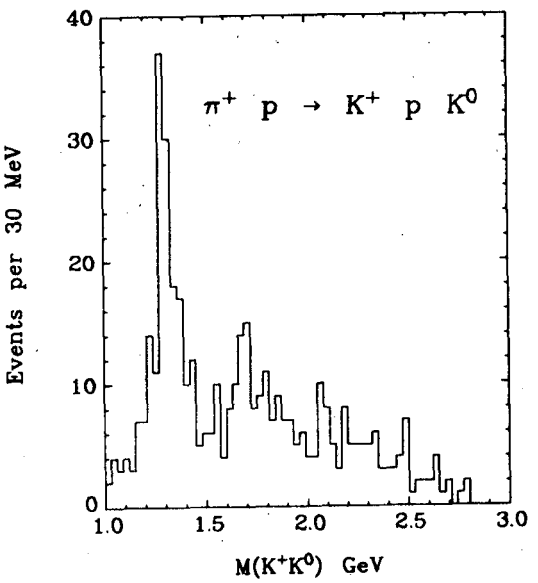

Figure 30

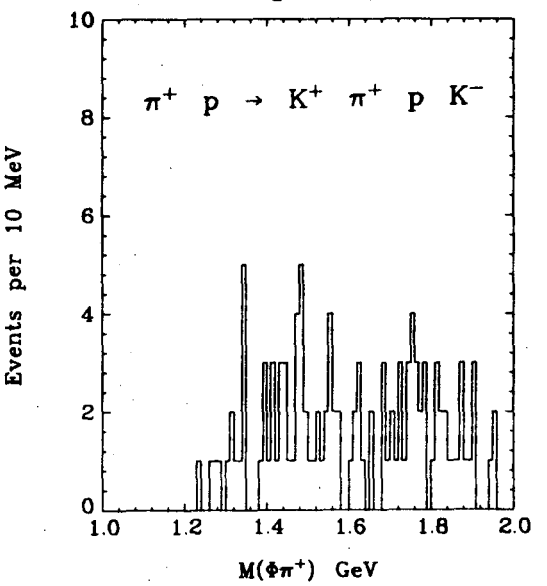

Figure 31 XBL 728-1606

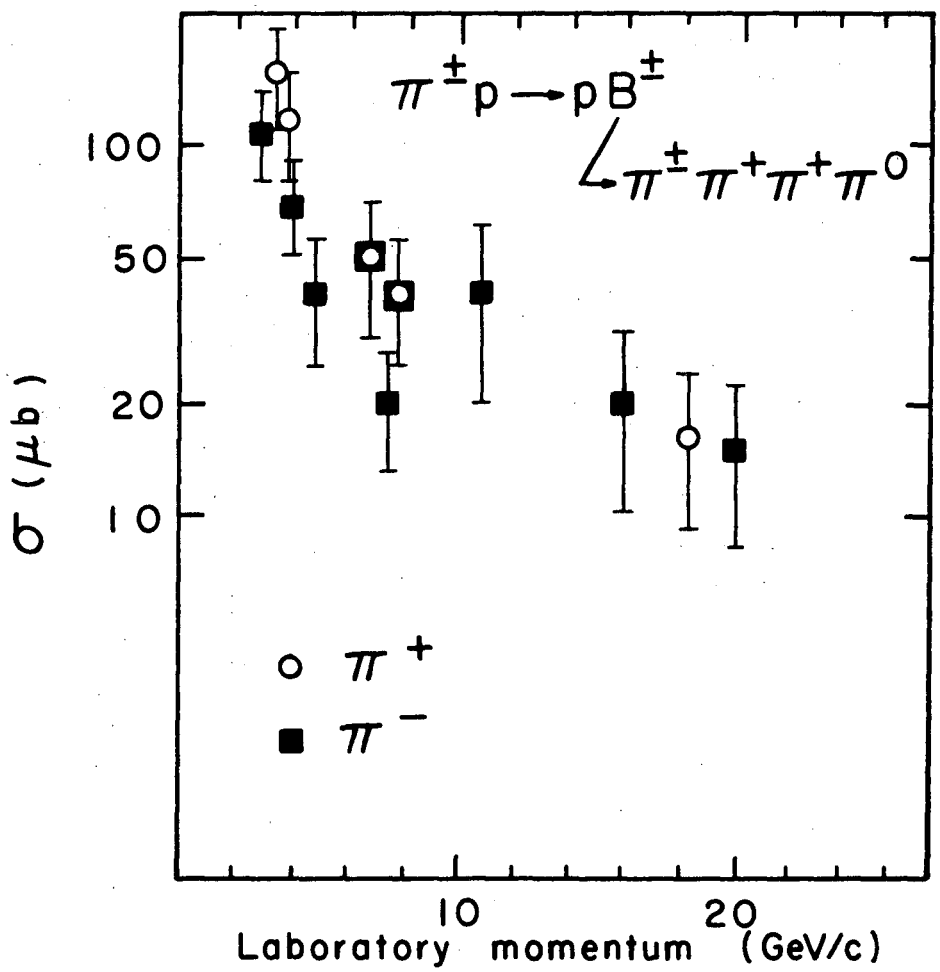

Figure 32

XBL729-3989

LEGAL NOTICE

This report was prepared as an account of work sponsored by the United States Government. Neither the United States nor the United States Atomic Energy Commission, nor any of their employees, nor any of their contractors, subcontractors, or their employees, makes any warranty, express or implied, or assumes any legal liability or responsibility for the accuracy, completeness or usefulness of any information, apparatus, product or process disclosed, or represents that its use would not infringe privately owned rights.

TECHNICAL INFORMATION DIVISION
LAWRENCE BERKELEY LABORATORY
UNIVERSITY OF CALIFORNIA
BERKELEY, CALIFORNIA 94720